Photoelectron Spectroscopy of Ionic Liquid-Based Interfaces

Kevin R. J. Lovelock,[†] Ignacio J. Villar-Garcia,[†] Florian Maier,[‡] Hans-Peter Steinrück,*[,‡] and Peter Licence*[,†]

School of Chemistry, The University of Nottingham, Nottingham NG7 2RD, U.K., and Lehrstuhl für Physikalische Chemie II, Friedrich-Alexander-Universität Erlangen-Nürnberg, Egerlandstrasse 3, D-91058 Erlangen, Germany

Received April 14, 2010

Contents

1. Introduction 5158
1.1. Role of This Review 5158
1.2. Principles of Photoelectron Spectroscopy 5159
1.2.1. Vacuum Environment 5160
1.2.2. Surface Sensitivity 5160
1.2.3. Sample Charging and Charge Neutralization 5161
1.2.4. Chemical State Analysis 5161
1.2.5. Surface Composition 5162
1.3. Photoelectron Spectroscopy of Liquids 5162
1.4. Introduction to Ionic Liquids 5162
1.4.1. What is an Ionic Liquid? 5162
1.4.2. Properties of Ionic Liquids 5163
1.4.3. Applications of Ionic Liquids 5164
2. Study of Ionic Liquid Interfaces 5164
2.1. Simple Primary Ionic Liquids 5165
2.1.1. Element and Chemical State Analysis 5165
2.1.2. Valence Band Structure 5172
2.1.3. Surface Composition 5174
2.1.4. Phase Change Detection 5174
2.2. Supported Ionic Liquid Layers 5175
2.2.1. Physisorbed Ionic Liquid Layers (PhILL) 5175
2.2.2. Chemisorbed Ionic Liquid Layers (ChILL) 5177
2.3. Mixtures and Solutions 5179
2.3.1. Ionic Liquid Mixtures 5179
2.3.2. Metal Catalysts/Complex Solutions 5179
2.4. Reaction Monitoring 5180
2.4.1. *Ex Situ* Analysis 5181
2.4.2. *In Situ* Analysis 5181
2.5. Materials-Based Applications 5182
2.5.1. Metal Nanoparticles 5182
2.5.2. Electrodes 5183
2.5.3. Membranes 5183
2.5.4. Lubricants 5184
3. Conclusions and Recommendations 5185
4. Acknowledgments 5187
5. References 5187

Kevin R. J. Lovelock (born 1981) graduated from the University of Nottingham with an M.Sci. in Chemistry in 2004. In 2008 he received his Ph.D. in chemistry under the supervision of Professor Rob Jones at the University of Nottingham. After conducting postdoctoral research in the group of Professor Hans-Peter Steinrück at the University of Erlangen-Nuremberg in Germany, Kevin returned to Nottingham, where he is currently a postdoctoral research fellow in the groups of Dr. Peter Licence and Dr. Darren Walsh. His research interests are focused on the physical properties of ionic liquids, particularly at the solid−ionic liquid and ionic liquid−vapor interfaces.

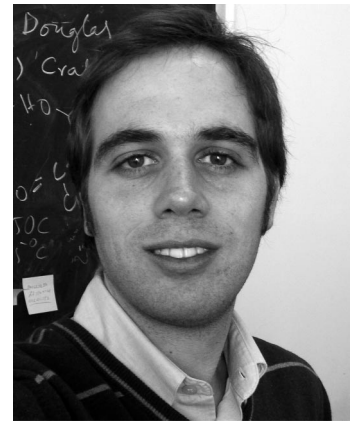

Ignacio J. Villar-Garcia (born 1979) obtained his Chemical Engineering Degree and Masters in Quality, Safety and Environmental Management from the University of Oviedo, Spain. In 2005, he joined the University of Nottingham as a Marie Curie Early Stage Researcher, where he completed doctoral studies under the supervision of Dr. Peter Licence. His Ph.D. research was focused on the study of ionic liquids and ionic liquid-based catalytic systems by XPS. Ignacio is currently Assistant Professor of Chemistry at the University of Addis Ababa, Ethiopia.

1. Introduction

1.1. Role of This Review

It has been made clear over the past 5 years that a fundamental understanding of the interfacial areas surrounding ionic liquids (ILs) will be crucial to the successful scale-up and application of IL-based processes. The study of both the IL−vacuum interface and the solid−IL interface is the subject of a rapidly expanding literature base. X-ray photoelectron spectroscopy (XPS) and ultraviolet photoelectron spectroscopy (UPS) have been shown to provide unique data

* To whom correspondence should be addressed. P.L.: e-mail, peter.licence@nottingham.ac.uk; telephone, +44 115 8466176. H.-P.S.: e-mail, steinrueck@chemie.uni-erlangen.de; telephone, +49 913 18527343.
[†] The University of Nottingham.
[‡] Friedrich-Alexander-Universität Erlangen-Nürnberg.

10.1021/cr100114t
Published on Web 07/02/2010

Florian Maier (born 1969) studied physics at the universities of Würzburg and of Grenoble (France). After finishing his Ph.D. studies in 2001 under the supervision of Prof. L. Ley at the University of Erlangen-Nuremberg on "Electronic Properties of Diamond Interfaces"—in particular, on the unique surface conductivity of hydrogenated diamond surfaces—he became a postdoc and, eventually, permanent assistant ("Akademischer Rat") at the chair Physical Chemistry II, led by Prof. H.-P. Steinrück. Presently, he is group leader of the "Ionic Liquid Surface Science" project in the DFG priority program SPP1191 on the "Ionic Liquids".

Hans-Peter Steinrück (born 1959 in Austria) studied physics at the TU Graz (Diploma in 1983; Ph.D. in 1985), was a postdoc at Stanford University (1985/1986), and received his Habilitation at the TU Munich in 1992. After a sabbatical at Rutgers University, he became Professor at the University of Würzburg in 1993; since 1998, he has held a chair of Physical Chemistry at the University of Erlangen-Nuremberg.

on chemical state identification, near surface composition, and valence band structure of primary ILs and those containing adsorbants/absorbants and solutes. For example, this data can reveal signpost information about IL−catalyst interactions and enrichment of ions/solutes at the IL−vacuum interface, potentially revolutionizing solution-based and supported IL phase (SILP) reactions. A recent review of the primary scientific literature using the keywords "ionic liquid*" reveals that ILs were featured in over 7000 publications during the period 2008−09. The research topics covered by these papers are incredibly diverse; however, many of these contributions could potentially benefit from the additional characterization capabilities of photoelectron spectroscopy. However, although XPS and related techniques are well established in the solid surface and materials communities, their application in solution-based studies is minimal. Consequently, the transfer of best practice between these diverse research communities and the development of rigorous experimental−analytical protocols has yet to be finalized. Consequently, there are a growing number of

Pete Licence (born 1973) obtained both his B.Sc. (1996) and subsequently his Ph.D. (2000) from the University of Wales (Bangor). After postdoctoral studies in the group of Martyn Poliakoff FRS CBE, Licence was awarded an Early Career Research Fellowship by the Leverhulme Trust, which he used to kick-off independent research on the topic of "ionic liquids in vacuo" in 2005. Pete is currently Associate Professor and Reader in Chemistry at the University of Nottingham, holder of an Advanced Research Fellowship (EPSRC), and Adjunct Professor in Chemistry at Addis Ababa University, Ethiopia.

inconsistencies appearing throughout the field of photoelectron spectroscopy applied to ILs.

It is our opinion that the field now requires a comprehensive review article to allow key strengths and also weaknesses to be highlighted for the healthy development of the field. The potential is incredible, and we believe that the entire IL field would benefit from this review, as many applications could potentially profit from XPS analysis capabilities. However, it is also important to set standards for both data presentation and the reviewing of future contributions. The critical review of this research field will have the effect of consolidating the excellent progress made over the past 5 years and minimizing the potential barriers that new researchers would encounter when entering the field, and, at the same time, it will be paramount for the dissemination of best-practice to obtain optimum results.

As a general comment, this review offers an overview of both the IL−vacuum interface and the solid−IL interface, which are readily investigated using photoelectron spectroscopy. Interestingly, a third type of interfacial region, the liquid−IL region, offers much information, particularly in liquid-based multiphase chemistries. However, investigation of this interface is much more problematic; consequently, little understanding has been achieved thus far.

1.2. Principles of Photoelectron Spectroscopy

Photoelectron spectroscopies (PES) are a class of surface analysis techniques that involve irradiating the sample *in vacuo* with photons and measuring the kinetic energy of the electrons emitted. PES analyses can provide quantitative (e.g., relative atomic percentage) and qualitative (e.g., oxidation states) information of the near surface region of a sample. Although the photoelectric effect was discovered by Hertz in 1887, it was not until the mid-1950s that the development of PES was able to really push forward. The advent of high quality, welded stainless steel vacuum chambers allowed the investigation of higher resolution PES using both X-ray sources and UV lamps. XPS, or ESCA (electron spectroscopy for chemical analysis) as the lead developer Kai Siegbahn preferred to call it, offered potential in determination of

composition, whereas UPS was independently developed by David W. Turner as a probe of molecular orbital structure in the gas phase. The first commercial instruments were introduced to the market in the early 1970s, and presently, XPS equipment is available in many laboratories throughout the world. Today, PES is a basic analytical tool in many research fields, such as microelectronics, metallurgy, heterogeneous catalysis, corrosion science, and polymer technology.[1,2] Siegbahn was later awarded the Nobel Prize for Physics for his developmental work in the field.

The photoelectric effect is the basic principle upon which PES operate; the sample is irradiated with photons, and the energy of the photoemitted electrons is analyzed. Incoming photons penetrate the sample in the order of micrometers. However, due to their significantly stronger interaction with matter, the excited electrons have a much shorter inelastic mean free path, which makes PES a surface sensitive technique. Only those electrons that originate within the uppermost few nanometers of the sample can leave the surface without energy losses; this so-called escape depth depends upon the measurement angle (see section 1.2.2).

Emitted electrons that do not undergo any inelastic scattering exhibit specific kinetic energies (KE) defined by the Einstein Equation, eq 1:

$$\mathrm{KE} = h\nu - \mathrm{BE} \quad (1)$$

where $h\nu$ is the energy of the incident photon and BE is the binding energy of the atomic orbital from which the excited electron originated. The binding energy can be regarded as the energy difference between the initial and final states after the photoelectron has left the atom. For solids the binding energy is commonly referenced to the highest occupied quantum level, the Fermi level, E_F, and, accordingly, eq 1 is rewritten:

$$\mathrm{KE} = h\nu - \mathrm{BE} - \Phi_{\mathrm{analyzer}} \quad (2)$$

where Φ_{analyzer} is the work function of the electron analyzer; note that the work function of the sample, Φ_{sample}, which is defined as the minimum energy required to remove an electron from the sample Fermi level to the sample vacuum level, does not enter eq 2. Electrons that escape from the surface without energy electron losses produce characteristic peaks in the PE spectrum whereas electrons that undergo inelastic processes before emerging from the surface contribute to the background at the high binding energy side of the corresponding peak in the spectrum.

1.2.1. Vacuum Environment

Ultrahigh vacuum (UHV) is generally required to analyze the emitted photoelectrons without interference from gas phase collisions. Electrons traveling from the sample surface toward the analyzer should encounter as few gas molecules as possible; otherwise, they will be scattered and lost to the analysis. Moreover, under UHV conditions, the impingement rate of molecules on the surface from the residual gas phase is very low; consequently, a freshly cleaned surface remains at a low contamination level for a sufficient time to measure a PE spectrum. While this aspect is very critical for reactive surfaces, it only plays a minor role in the case of inert substrates. Furthermore, under UHV conditions, dissolved gases and volatile impurities, including water, will vaporize to a large extent. As a general comment, chamber pressures in the 10^{-8} to 10^{-10} mbar range are required for PES analysis.

In terms of reliable sources of incident irradiating photons, there are three main sources that are commonly employed in the measurement of PES: laboratory-based fixed-energy X-ray sources, laboratory-based fixed-energy ultraviolet sources, and synchrotron radiation sources. Regarding sources that are used for XPS, the most commonly used laboratory-based fixed-energy X-ray sources have either Mg or Al anodes, yielding Mg Kα radiation at 1253.6 eV or Al Kα radiation at 1486.6 eV, respectively. The line width of the source can be reduced by employing an appropriate monochromation device prior to irradiation. Turning to UPS, the most commonly used laboratory-based fixed-energy ultraviolet source is He I (21.2 eV). He II (40.8 eV) is sometimes also used, although it has lower intensity and the presence of a significant He I component can complicate analysis of the spectra. Synchrotron radiation sources are much more flexible, as they provide high intensity photons that can be tuned across a broad range of energies, from UV to hard X-rays. Advantages of synchrotron-based PES experiments are higher energy resolution, well-defined polarization, higher photon flux, and a higher photoemission cross section (which may be achieved by tuning the irradiating energy to an energy just above that of the orbitals of interest). Furthermore, there are several techniques that can only be performed with synchrotron radiation, such as near-edge X-ray absorption fine structure (NEXAFS), normal incidence X-ray standing wave (NIXSW), and scanned energy photoelectron diffraction (PED).[3]

1.2.2. Surface Sensitivity

Principally there are two ways to influence the surface sensitivity of PES experiments. The first approach is based on the dependence of the inelastic mean free path, λ, of electrons on the kinetic energy, which shows a minimum at 50−100 eV; that is, the surface sensitivity is highest at these kinetic energies. Upon increasing the kinetic energy, the mean free path increases, making the spectra more and more sensitive to the bulk properties. The disadvantage of this approach is that it can only be performed at synchrotron radiation facilities, and at low kinetic energies (<500 eV), photoelectron diffraction effects (PED) can strongly influence the observed results and thereby hamper the quantitative analysis from XP spectra.[3]

The alternative, and much more commonly applied, approach to influence surface sensitivity, is achieved by variation of the detection angle of the emitted photoelectrons. For an analyzer with a sufficiently small acceptance angle (e.g., <±5°), the probe depth varies, mainly with $\cos(\theta)$, giving rise to angle resolved XPS (ARXPS) studies. In typical ARXPS experiments, successive spectra are recorded in the normal emission geometry, where $\theta = 0°$, and in a number of incremental grazing emission geometries, where θ is typically ≥70° (up to and including ∼85°). Typically, the inelastic mean free path, λ, of exiting photoelectrons in organic compounds is of the order of ∼3 nm; this is an excellent first approximation based upon findings on composition of the near-surface regions across a wide range of ILs. At a typical applied KE of between 800 and 1300 eV, the information depth (ID = 3λ) defines a region (where 95% of the signal originates) of experiments where $\theta = 0°$ is between 7 and 9 nm (dependent on KE). Similarly, at emission angles of 70° or 80°, the measured ID will be 2−3 nm or 1−1.5 nm, respectively. It is worth emphasizing that when the emission angle $\theta = 80°$, ≈65% of the XPS signal

intensity originates in the uppermost 0.3−0.5 nm of the sample; this is less than the width of a single molecule of many of the ILs studied.

After careful calibration of the experimental setup, a preferential increase of a particular core level intensity with increasing detection angle, and thus with increasing surface sensitivity, indicates a higher concentration of this element in the topmost layers as compared to the "bulk measurement" at 0°. The calibration procedure is absolutely essential and can be performed with a solid or liquid substrate of homogeneous chemical composition where contamination and/or surface enrichment effects are absent.

1.2.3. Sample Charging and Charge Neutralization

For conducting samples, charge compensation for emitted photoelectrons occurs by demand via the instrument sample stage earth connection. For nonconducting samples, including many ceramics, inorganic oxides, and organic polymers, no continuous electrical connection to earth occurs; consequently, the emitted photoelectrons leave a positively charged bias at the sample surface. Insulating samples can acquire a positively charged state of several volts as a consequence of the electron loss due to this emission. The immediate consequence is a dramatic shift to higher apparent binding energy (BE) and in most cases a broadening in all peaks in the XPS spectra due to differential charging across the sample surface.[4−7]

Charging (and also beam damage; see section 2.1.1.9) depends primarily upon the intensity of the photon flux impinging on the investigated sample per surface area. For charging, the number of photons per surface area is one of several decisive properties that can be influenced by experimental parameters. Measurements using high intensity synchrotron radiation, which normally operate with a small focus (diameter typically <500 μm) or with monochromated Al or Mg Kα radiation (focus depends on setup; typically on the order of 0.5 mm × 0.5 mm), have a higher photon flux per surface area than measurements conducted with standard Al or Mg anodes. This leads to the observation that in most cases only minor charging problems (shifts typically <0.5 eV) are encountered for most ILs (and also beam damage only plays a minor role) when using standard Al or Mg Kα anodes. In addition, there may be some charge compensation by secondary electrons from the Al window of the anode. As a general statement, charging can also be minimized by recording spectra with a reduced photon flux. This implies longer experiment (counting) times that, in turn, can lead to undesired enhanced surface contamination. To compensate for charging, a normal procedure when using monochromated sources is the use of a charge neutralization device that delivers low energy electrons to the area of analysis, stopping the development of uncontrollable positive charging. A charge neutralizer filament situated above the sample surface supplies a continuous flux of low energy electrons, providing uniform charge neutralization and contributing to reduce differential charging and sharpen spectral lines. However, after charge neutralization, the spectra usually appear slightly shifted to negative binding energy, due to overcompensation, meaning a charge correction for all peaks is required.

PES analyzers should generally be calibrated using a number of different core levels of well-defined substrates (e.g., atomically clean Ag and Au). The use of several levels instead of only one is recommended, since often the analyzers show deviations from the assumed linearity of the electronics involved. However, it is common practice that spectrometers are calibrated to only one well-known and commonly employed core level such as Au 4f (at 83.96 eV using monochromated Al Kα).[8] For conducting samples, if the calibration is known, then comparisons of peak BE are possible and relatively straightforward. For nonconducting or poorly conducting samples, a further charge correction is often required, especially in cases where the use of a charge neutralizer is required for the measurement of sharp PE spectra. Sometimes it is possible to use substrate signals as charge references for very thin, nonconducting films on conducting substrates. However, it is more common that nonconducting samples will charge differentially to the substrate, and hence, an internal reference standard is required. The most commonly used internal reference standard is C 1s aliphatic carbon, referenced to either 284.8 or 285.0 eV (the exact value does not matter, as long as the value is noted). Aliphatic carbon is often used, as typically samples contain an aliphatic carbon component or are contaminated by adventitious carbon in the near surface region.

1.2.4. Chemical State Analysis

XPS can be used to identify and quantify the different chemical environments of the same element within a given IL. Each individual element signal is a function of the chemical environment of the atoms of interest, i.e. the oxidation state, type of bonding, and nature of the neighboring atoms. Moreover, Auger peaks, shake up lines, and other energy loss features can also vary in terms of both shape and intensity. All these variations can be used to identify the chemical structure of the surface analyzed. In a simplified picture, the same atom exhibits higher binding energies (for all core levels) when it is positively charged or has a lower electron density than when it is negatively charged or has a high electron density. The chemical bonding within a molecule thus has a great influence on the electron binding energies obtained by XPS.[9] Consequently, XPS is able to distinguish between different oxidation states and local electronic environments affecting a particular element. While many attempts have been made to calculate absolute binding energies and chemical shifts, the factors involved are not yet perfectly understood, and one often must rely on experimental data from a range of standard materials.

The peak positions in an XP spectrum can be interpreted in terms of the chemical environment of the atoms from which they originate. This analysis is relatively straightforward for components originating from s-type orbitals, where a single peak usually indicates a single chemical state. For signals originating from orbitals of p-, d-, and f-type symmetry, the PE spectrum is observed as a doublet for every chemical state (for further discussion, see section 2.1.1.6). If this effect is not recognized, the complex nature of spin−orbit coupled peaks may be erroneously assigned to individual chemical species.

There are two contributions to the observed chemical shifts in XP spectra, i.e. initial and final state effects.[10,11] Initial state effects are those that affect the charge of the atom before the photon strikes and are described by calculations of the ground state of a particular system. The nature of the chemical bond or the oxidation state of the atom is such an effect. Final state effects are those that affect the peak position during or after the photon strikes. Typical effects

include inelastic processes such as electron−hole pairs and phonon excitations, a reduced lifetime of the excitation due to the coupling to the environment, extramolecular screening or by charge transfer from neighboring molecules, and multiplet splitting for systems with unpaired spins. Charging is often also seen as a final state effect, although strictly speaking it is an experimental artifact due to a shift of the reference level, which leads to a homogeneous shift of all peaks in the XP spectrum.[10,11]

1.2.5. Surface Composition

By analysis of the peak areas and by considering the sensitivity factors for the different elements, quantitative information on the overall stoichiometry of the investigated sample can be derived from the XP spectra. The common approach to account for the relative sensitivity factors (RSFs) is to use the literature values empirically developed by Wagner et al.,[12] which account for the cross sections of the elements and the particular orbitals from which the emitted electrons originate. However, this analysis does not account for the particular transmission function of a specific analyzer at a given pass energy and can yield deviations on the order of ±15%. To improve this situation, a careful calibration of the spectrometer is required. Ultraclean, well characterized ILs, namely $[C_2C_1Im][Tf_2N]$ and $[C_2C_1Im][EtOSO_3]$, are very well suited to determine accurate sensitivity factors. Due to their small size, when compared to the inelastic electron mean free path, molecular orientation effects are expected to be minimal, especially when measurements are performed at normal emission ($\theta = 0°$) when the information depth is large.

To determine the probed region of the analysis, the information depth, ID (which is three times the mean free path of the photoelectrons), has to be considered (see also section 1.2.2). XP measurements in the "bulk sensitive" geometry ($\theta = 0°$, ID = 7−9 nm) yield reliable information for the near surface region. If the analysis in this geometry and also in the "surface sensitive" geometry, $\theta = 70$ and 80°, ID 2−3 or 1−1.5 nm, respectively), yield identical results, one can conclude a homogeneous distribution of the involved elements, which then also presents the bulk composition. Depending on the cross section of the analyzed level of an element, the accuracy is on the order of 5−10%.

1.3. Photoelectron Spectroscopy of Liquids

Techniques that require UHV generally involve detection of a species that has a sufficient mean free path in the chamber to reach the detector without being scattered by gas molecules; examples of such probes are electrons or desorbing molecules/ions.[13] The ability to study any liquid at UHV would allow the use of a large variety of surface techniques, such as photoelectron spectroscopy, high resolution electron energy loss spectroscopy (HREELS), low and medium energy ion scattering (LEIS and MEIS, respectively), and temperature programmed desorption (TPD). These measurements provide detailed information on the electronic and vibrational structure, among other properties, that will complement previous studies at the macroscopic level, such as surface tension measurements. Moreover, under UHV conditions, the gas−liquid interface and also the vapor phase can be studied without interference from third-party entities such as water vapor.

Over the past 35 years, many attempts have been made to successfully apply UHV techniques to the study of the liquid−gas interface.[14−16] There are two methods for studying liquids at UHV: studying liquids with sufficiently low vapor pressure where sample loss through evaporation is insignificant, and modifying the apparatus to allow studies at elevated pressures, applying differential pumping stages. Examples of liquids with sufficiently low vapor pressures include liquid metals[17] and a small selection of hydrocarbons.[18] Many elegant experiments have been conducted on modified apparatus on a range of aqueous[19] and nonaqueous solutions.[20] Techniques developed include the introduction of liquid samples using continually moving, wetted wires,[21] rotating disks,[22] and free-flowing macroscopic jets.[23] Liquid-containing cells with X-ray permeable silicon nitride windows can also be used at UHV.[24]

Unfortunately, none of the aforementioned techniques have been demonstrated to be universally applicable. In the case of PES, for instance, the use of liquid jets and liquid-coated moving wires using instruments constructed around custom designed vacuum chambers has been successful with a limited range of low vapor pressure liquids. Furthermore, very precise adjustment of the jet/wire position relative to the spectrometer slit is required to ensure that the liquid surface spectrum is not convoluted with that representative of the rapidly expanding vapor phase.[22] In all cases, the key problem in the investigation of many traditional liquid samples is the extremely high evaporation rate. The residence time (the average time for a molecule to desorb at a given temperature) for bulk water at room temperature is ~1 μs.[25] This high evaporation rate places an unacceptably large load on the pumping system employed to maintain collision-free conditions within the analytical chamber. More recently, experiments coupling liquid microjets with *in vacuo* surface-specific or -sensitive probes have been shown to be more successful; as a result, reports detailing this type of interface are becoming much more common in the literature.[19,23,26,27]

The problem of high evaporation rates does not apply to a particular class of liquids, namely those that have vapor pressures that are comparable to or lower than the base pressures maintained within a typical UHV analytical chamber (10^{-8} to 10^{-10} mbar). A broad class of liquids that offer this property is ILs.

1.4. Introduction to Ionic Liquids

1.4.1. What is an Ionic Liquid?

ILs are composed solely of cations and anions: cations are generally organic compounds with low symmetry; anions are usually weak basic inorganic or organic compounds.[28,29] Common examples are given in Tables 1 and 2. A combination of one cation and one anion is referred to as a primary IL but is more commonly referred to more simply as an IL (and sometimes, confusingly and often incorrectly, as a pure IL).[30,31] There are at least 10^6 potential primary ILs.[32] Across this huge range of ILs, there are generic properties that are common to many but not all. The two defining properties common to all ILs are (i) that the substance is liquid (its glass transition temperature and/or melting point are <373 K) and (ii) that it contains ions and therefore exhibits ionic conductivity.[33] This definition excludes molten salts such as molten NaCl, which has a melting point of 1074 K. Solutions such as NaCl dissolved in molecular solvents and organic solutions are technically not excluded by this definition. A

Table 1. Commonly Studied Cations

Abbreviation	Structure	Name
$[C_nC_1Im]^+$	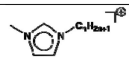	1-alkyl-3-methylimidazolioum
$[C_nC_1Pyrr]^+$		1-alkyl-1-methylpyrrolidinium
$[C_nPy]^+$		1-alkylpyridinium
$[N_{RR'R''R'''}]^+$		Tetraalkylammonium
$[P_{RR'R''R'''}]^+$		Tetraalkylphosphonium
$[S_{RR'R''}]^+$		Trialkylsulfonium

Table 2. Commonly Studied Anions

Abbreviation	Structure	Name
Cl^-		Chloride
Br^-		Bromide
I^-		Iodide
$[BF_4]^-$		Tetrafluoroborate
$[EtOSO_3]^-$		Ethylsulfate
$[(CF_3SO_2)_2N]^-$ or $[Tf_2N]^-$		Bis[(trifluoromethane)sulfonyl]imide
$[CF_3SO_3]^-$ or $[TfO]^-$		Trifluoromethanesulfonate
$[N(CN)_2]^-$		Dicyanamide
$[PF_6]^-$		Hexafluorophosphate
$[PF_3(C_2F_5)_3]^-$ or $[FAP]^-$		Tris(pentafluoroethyl)trifluorophosphate

third defining property could be "composed solely of ions". Synonyms for materials that meet this definition of ILs include room temperature molten salt (RTIL), low temperature molten salt, ambient temperature molten salt, ionic fluid, Coulombic fluid, and liquid organic salt.[34−36]

1.4.2. Properties of Ionic Liquids

ILs exhibit many unusual properties[37] compared to molecular liquids, which make them interesting to a wide range of researchers.[32] Aside from their low melting points and negligible vapor pressure, attractive macroscopic properties of many ILs include a very large liquid range, a wide electrochemical window, and the ability to solubilize a wide range of solutes.[38] This section will concentrate on IL properties which are most relevant to the research presented in this review. There are many reviews of IL properties available, several of which include a far broader summary than included here.[35,38−41]

1.4.2.1. Melting Point. The key property for all ILs is the melting point. Melting points of ILs have been found to be as low as 255 K.[42] The reasons for the low melting points exhibited by these salts are found in the nature of their ionic components. Cations are generally large and asymmetric and combine, most of the times, with bulky anions that have a high degree of charge delocalization. These characteristics contribute to lower the lattice energy and hence the negative free fusion energies exhibited by ILs.[43]

1.4.2.2. Vapor Pressure. The lack of detectable vapor pressure of ILs at atmospheric conditions has been a major driving force in ILs research.[44−48] Until recently, it had been assumed that aprotic ILs had no detectable vapor pressure.[49] The main breakthrough in the field came when Earle et al.[50] reported the distillation of a range of commonly used aprotic ILs at reduced pressure. However, this landmark paper offered no insights into the nature of ILs in the vapor phase. In so doing, it stimulated a completely new area of research to answer this open question, the study of the vapor phase.[51−53] Elegant studies including the mass spectroscopic confirmation of neutral ion pairs in the vapor phase and subsequent determination of thermodynamic properties including the heat of vaporization at 298 K, $\Delta_{vap}H_{298}$,[53] give an insight into IL-based systems in terms of physical organic characterization.[54−56] Unsurprisingly, the measurement of direct physical properties is not straightforward. To date, vapor pressures have been measured for only five ILs; room temperature vapor pressures for these ILs are estimated at $\sim 10^{-11}$ mbar.[57−59] As recognized by the work in this review, vapor pressures of ILs at room temperature are very low; ILs exhibit vapor pressures similar to those of metallic elements such as Zn and Na at 400 K,[57,60] allowing the analysis of these materials in the liquid state under the high vacuum conditions needed for PES analyses. It should be noted that many protic ILs have significant vapor pressures even at atmospheric pressure, and therefore, the liquid−vapor interface cannot be studied using high vacuum techniques at room temperature.[61,62]

1.4.2.3. Conductivity. Due to their composition, ILs conduct via ion mobility. Typical conductivity values for ILs are in the range 0.1−3 S m^{-1},[63] although ILs exhibiting conductivities up to 11 S m^{-1} have also been synthesized.[34,64] These values are comparable to those of the best nonaqueous electrolytes but are significantly lower than those of concentrated aqueous electrolytes.[65] Moreover, wet ILs usually exhibit higher conductivities than neat ILs themselves.[66,67] Possible explanations for the lower than expected conductivities exhibited by neat ILs are the hindered mobility of the normally bulky and asymmetric ions and related high viscosity exhibited by most ILs[68] and the existence of ion pairing.[34,69,70] ILs exhibit relatively high viscosities; values typically fall in the 10−500 cP range[71] (the viscosity of water is 0.890 cP at room temperature). By means of the Walden plot (log(molar conductivity) versus log(1/viscosity)), it has been shown that viscosity and conductivity are strongly coupled.[66,68] The further existence of ion pairing in ILs has been suggested in several research studies[29,72] and has been recently identified by Tokuda et al.[42,73,74] by comparing the diffusion coefficients of ions measured by NMR and by electrochemical methods: ion self-diffusion values measured by NMR that give a measure of the mobility of all ions, even if they are involved in ion pairing, are usually higher than electrochemically measured ones, which only measure ionic species. The increase in anion−cation interactions has been found to be one of the main factors controlling the amount of ion pairing in the liquid[70] and ion mobilities.[74] In general, cations exhibit higher transport numbers than anions.[42,73,74] An increase in the alkyl chain of the imidazolium cation usually results in a large decrease in conductivity.[74−76]

1.4.2.4. Effect of Impurities. Ultrapure ILs with minimal impurity levels are required for the determination of IL properties and structure and also for many applications, such as electrochemical deposition.[41,77−80] There are three broad categories of IL impurities—water, halides, and excess organics (which may be chromophoric)—carried over from synthesis including silicone grease.[80] An explanation of each category is given below along with the difficulties associated with removing impurities from ILs using the current methods.

The effect of the presence of water on IL properties has been known for some time.[77,81] Nonfunctionalized ILs are generally air- and water-stable, unlike many of the early $AlCl_3$-type ILs.[82] However, all ILs are hygroscopic to some extent.[77] Careful synthesis can reduce the amount of water present, but ILs will absorb water over time, so degassing is often required prior to use. Water is generally removed by heating to ~338 K "under vacuum" (a vague term that probably means using a rotary pump to reach pressures of $\sim 10^{-2}$ mbar).[80] However, there is no proof that this level of pumping removes all traces of water.[83,84]

The effect of the presence of halides on IL properties is also well-known.[77] The salt metathesis route has become the standard synthetic method for ILs.[85] The two steps involved are [cation]X synthesis followed by a salt metathesis that gives the IL and a water-soluble halide salt. Complete removal of the halide salt is difficult and generally requires multiple washes with water; this step wastes IL, obviously adds water that subsequently has to be removed, and is not always successful.[80]

1.4.3. Applications of Ionic Liquids

Aside from the negligible vapor pressure, attractive macroscopic properties of many ILs include a very large liquid range, a wide electrochemical window, and the ability to solubilize a wide range of solutes.[37] There is also the potential for IL−solute interactions and catalysis that is not possible when using molecular solvents.[86,87]

ILs were originally viewed as potential green solvents due to their negligible vapor pressure and the consequent prospect of replacing traditional molecular solvents.[88,89] The major issues for applications of ILs with respect to green chemistry are toxicity,[90,91] biodegradability,[92] and IL synthesis.[93] Many commonly used ILs are toxic and nonbiodegradable and are made from nonrenewable feedstocks, clearly in contradiction of many of the 12 Principles of Green Chemistry.[94] A much more subtle problem is the energy required for IL synthesis. Nontoxic and biodegradable ILs have been synthesized, and attempts have been made to determine quantitative structure property relationships and, hence, predict IL properties.[90,95] It is clear that ILs possess properties that can improve the sustainability of a process. However, to determine if using an application involving ILs is greener than a traditional method, a complete life-cycle assessment is required.[93,96]

Due to the interesting and tunable nature of IL properties, there are many potential applications, including solvent replacement, catalysis, electrodeposition, electrolytes in a range of devices, chromatography, and lubricants. The opportunities for industrial application are almost boundless; it is clear that ILs are certainly not yet being used to their full potential.[32]

The bulk of IL research conducted thus far has focused upon so-called nonfunctionalized ILs.[28] Such ILs are characterized by a relatively small range of anions (e.g., those given in Table 2) and cations containing R groups consisting only of aliphatic chains of the form C_nH_{2n+1}. However, a vast array of ILs have been synthesized that contain chemical functionality beyond those listed above. Such ILs are often referred to as task specific ILs (TSILs),[97,98] as the chemical functionality can be selected to match a property required of the ILs. This diversity of functionality and, therefore, properties has led to ILs being dubbed tunable, as, in theory, the properties can be tuned by subtly varying the functional substituents to meet the demand of the task. Functionalized ILs are of particular importance for studies at the solid−IL interface, especially with regard to surface attachment.

2. Study of Ionic Liquid Interfaces

If one considers chemical processes and materials-based devices that employ ILs, it becomes clear that phase boundaries, interfaces, and near-interfacial areas dominate both function and performance. In most cases, the determining factor is the interaction of a reactant, typically an organic liquid or a permanent gas, with the surface of the IL. For example, the initial step in gas separations where ILs act as absorbents[37,99,100] is the collision of the gaseous molecule of interest with the IL surface. Whether this molecule is absorbed is partly dependent on whether the molecule is adsorbed at the surface initially. In terms of synthetic strategy, the support of homogeneous catalysis within a surface adsorbed IL layer (i.e., SILP systems)[48] offers a wide variety of reaction systems where the advantages of homogeneous catalysis are retained, without the troublesome downstream problem of product catalyst separation.

Literature Selection Criteria and Review Structure

The following sections form a summative/critical review of the application of photoelectron spectroscopies in the characterization of interfacial regions of ionic liquid-based systems. At the outset of preparing this review, the authors agreed on two basic criteria that were considered when drawing up the bibliography and resulting discussion; these are noted below.

(i) That the primary focus of included studies was the investigation of the IL itself, as opposed to materials prepared in the IL.

(ii) That the IL/IL moiety remained chemically intact throughout the study, unless degradation or damage was observed as a direct result of the incident photon source.

The structure of the following sections is arranged arbitrarily in order of increasing complexity, running from simple primary ILs, where only one IL is present (i.e. one cation and one anion), to multicomponent systems that may include solutes, reactants, or even chemical reactions.

PES is one surface sensitive method among many others that have been applied to the analysis of IL interfaces. For more comprehensive reviews of other surface sensitive techniques, the reader is directed toward the excellent reviews of Baldelli[101,102] and a very topical perspectives article by Steinrück entitled "Surface science goes liquid!".[103] It should however be noted that, in both cases, only short sections of each manuscript were dedicated to PES; throughout this document, we aim to draw comparisons between the information available from PES and that available from other techniques. As a general comment, to date, most PES of ILs have focused upon laboratory-based XPS, rather than synchrotron studies or laboratory-based UPS. Consequently, laboratory-based XPS comprises the bulk of this review.

2.1. Simple Primary Ionic Liquids

As highlighted in section 1.4.2, ILs are defined, rather arbitrarily, as having a melting point of <100 °C.[33] XPS has been carried out on samples with melting points just above this temperature for more than 30 years.[104−108] For example, the $[Et_4N][TfO]$ salt, which has a melting point of 160 °C, was analyzed by Wagner et al. in 1980 using XPS.[107] With regard to the solid−IL interface, a number of XPS studies of monolayers of surfactants such as hexadecyltrimethylammonium halides, $[N_{1,1,1,16}]X$ (where X = Cl^-, Br^-, I^-), and dimethyldioctadecylammonium, $[N_{1,1,18,18}]X$, on mica have been carried out.[109,110]

In 2005, almost simultaneously, Smith et al.[111] and Caporali et al.[112] published the first work focused specifically on XPS of ILs at the liquid−vapor interface. Also in 2005, Fortunato et al.[113] published XPS analyses of supported IL membranes and Yoshimura et al. published UPS of ILs.[114] Together these publications triggered interest in the field, and since then, many research groups have analyzed ILs by XPS in the course of their investigations, and this work is the major focus of this review.

2.1.1. Element and Chemical State Analysis

In early work, it was observed that core level photoemissions are observed for each element within the samples investigated.[111−113] Therefore, it is possible to identify elements present in the IL sample. ILs normally contain carbon and nitrogen (and hydrogen, which cannot be observed using XPS) in the cation; XPS has also been carried out on functionalized ILs containing oxygen or sulfur in the cation.[115−117] The anions in ILs by their nature contain a far larger range of elements. Therefore, elements identified by XPS in ILs include C, N, O, F, P, B, S, Cl, Br, I, Fe, and Au. As well as element identification, oxidation state identification is also possible using XPS. The most important element in this regard is carbon, in particular for the cation. Carbon is present in the cation in all ILs investigated thus far with XPS, and also many of the anions. To accurately determine the binding energies of the different components, the development of a fitting procedure is common practice.

2.1.1.1. Charge Correction/Referencing. BE is the most important piece of information provided by XPS analyses. Therefore, obtaining absolute and comparable binding energies from all types of samples has been the subject of detailed study since the origins of XPS.[8,9,118] Without accurate and quantitative charge correction, i.e., calibration of the binding energy scale, comparisons of BE values from different measurements are very difficult and in many cases even impossible.

ILs emit a good photoelectron flux, and survey spectra are recorded with good resolution, as shown in Figure 1, for $[C_2C_1Im][Tf_2N]$.[119] High intensity photoelectron flux is possible due to the conducting nature of the IL samples. Moreover, the fact that the peaks are symmetrical and narrow indicates that the surface does not suffer from differential charging. The absence of differential charging also contributes to the high resolution achieved.

Initially, many groups considered that ILs could therefore be analyzed as normal metallic conductive samples and did not use any charge correction in the analysis of their spectra. Some groups used an instrument calibration, such as Au $4f_{7/2}$, as reference.[116,119] If ILs were perfect conductors, aliphatic carbon peaks would be expected to appear consistently at energies close to 285 eV.[2,11] However, Smith et al.[119] reported BE reproducibility problems which were initially related to differences in the grounding of the sample; similar reproducibility problems have been also observed by others.[116,120,121] It has been observed that peaks for different elements all shift approximately the same amount, indicating sample charging.[122] It thus appears that ILs, while conductors, are insufficiently conducting to compensate for the emitted photoelectrons. This effect certainly depends on the photon flux per surface area (see section 1.2.3). Maier et al., for example, quoted a reproducible BE of ±0.15 eV when using a nonmonochromated source. Villar-Garcia, using a monochromated source, quoted far larger BE variations, indicating that, for the nonmonochromated source, electrons from the anode provide a level of compensation for the emitted photoelectrons.[122]

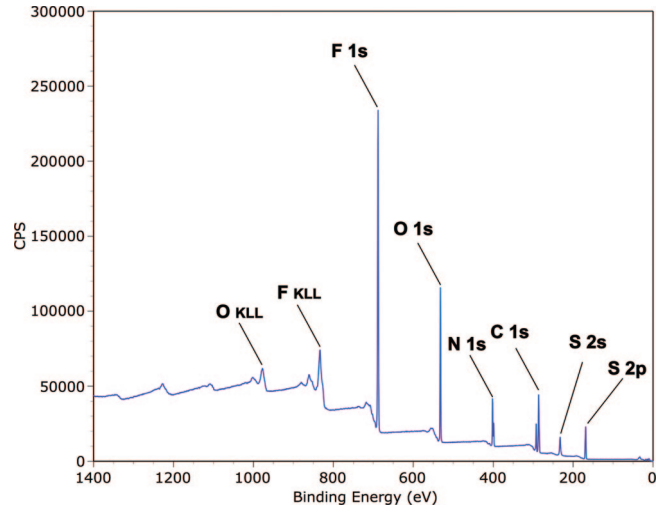

Figure 1. Wide-scan XP spectrum of $[C_2C_1Im][Tf_2N]$. Reprinted with permission from ref 119. Copyright 2006 American Chemical Society.

Many groups have used the aliphatic carbon signal (normally referenced to a value close to 285.0 eV) to charge correct their spectra.[113,123−127] It has been shown in the case of $[C_nC_1Im][Tf_2N]$ ILs (where $n = 2-16$) that the BE peak separation between carbon C 1s signals from the positive imidazolium ring, called C_{hetero}, and the aliphatic chain carbon, C_{alkyl} (see also next section), increases from $n = 2$ to $n = 8$ by 0.4 eV.[116] From the observation that C_{alkyl} shifts to higher BE as n decreases from 8 to 2, the authors conclude that alkyl carbons closer to the ring are more affected by the positive charge of the ring. Consequently, using C_{alkyl} as a reference for ILs with shorter alkyl chains is unlikely to be a valid method for all ILs. However, for $n \geq 8$, using C_{alkyl} as an internal reference standard seems to be a valid method of charge correction. Kolbeck et al. recently showed that, for $[C_8C_1Im][X]$ ILs with [X] being anions of different size, the BE separation for C_{hetero} and C_{alkyl} is shifted; therefore, C_{hetero} is also not a valid reference (C_{alkyl} is unlikely to be affected by changing the anion and so was used as the reference in these studies).[120] The use of nitrogen from the imidazolium ring was also investigated by Smith et al. and Chiappe et al. as an internal standard;[119,121] however, differences have since been observed in the N 1s spectra of the imidazolium ring that show sensitivity toward the nature of the anion,[120] making this method less general.

One problem with charge correction using an internal standard is simply that the internal standard will not be

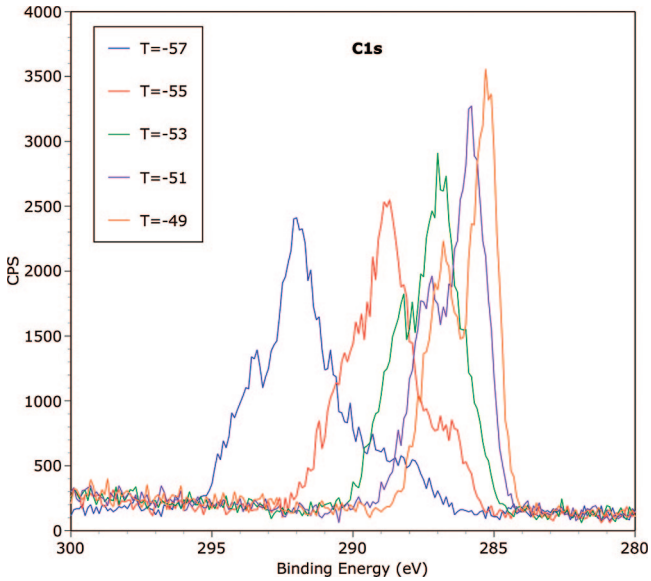

Figure 2. High resolution XPS spectra of $[C_2C_1Im][EtOSO_3]$ showing the measured binding energy of the C 1s photoemission as a function of temperature. At lower temperatures, when the sample becomes frozen, surface charging occurs, and the band is observed to shift to a higher energy. Reprinted with permission from ref 119. Copyright 2006 American Chemical Society.

present in all ILs studied, particularly functionalized ILs. For example, $[C_1C_1Im][Tf_2N]$ contains no distinct C_{alkyl} carbons and, consequently, gives an almost Gaussian peak shape for the C 1s region due to the single cationic environment (due to C_{hetero} only). In this case, C 1s aliphatic cannot be used for charge correction and another internal reference standard is required. For such ILs, other elements could possibly be used for internal standard charge correction. For example, for ILs containing the widely studied $[Tf_2N]^-$ anion, an element such as fluorine could be used as an internal standard, especially as most of the negative charge is not located on the CF_3 groups.[128] At this stage, no clear charge correction procedure is available for ILs at the IL−vacuum interface. Care must therefore be taken in reporting BEs and also in conclusions drawn.

An example where charge correction using an internal standard was required was highlighted in the work of Neaţu et al., who investigated $[C_6C_1Im][AuCl_4]$ dissolved in $[C_6C_1Im]Cl$. They reported BEs for Au 4f and derived conclusions on the gold oxidation state by comparison to literature gold BE values, but no details of charge correction, if used, were given.[129] Furthermore, no details of other elements measured, i.e., C 1s, were reported. As a consequence, other researchers active in the field cannot compare the validity of the reported values and develop confidence in the data. It is highly recommended that researchers give full details of charge correction methods used and report spectroscopic data for significant regions, particularly those which can be used in comparison to other measured systems, i.e., C 1s, N 1s, and F 1s.

When ILs are cooled to below their glass transition temperatures, they solidify into glasses/crystals. Such glasses/crystals are poorly conducting; consequently, during XPS analysis, the sample charges positively, as a result of the net loss of exiting photoelectrons. This loss leads to a shift in PES envelopes to a higher apparent BE, as shown in Figure 2 for a monochromated source.[119,130] The change on reducing the temperature from −49 to −57 °C is very large, as the surface is differentially charging, leading to broad peaks; see Figure 2. This result confirms that when ILs are in their liquid state, they are sufficiently conducting such that sample charging on the order of 5−10 eV is avoided. However, sample charging on a more subtle level required for BE deductions is a problem, as explained previously. Poorly conducting samples are typically studied with the aid of a charge compensation filament, which compensates for the emitted photoelectrons by bathing the sample surface with a flow of low energy electrons. However, this technique often overcompensates the surface such that the sample surface becomes slightly negatively charged. Overcompensation is not a problem as long as a suitable internal reference is available to enable charge correction.

2.1.1.2. Energy Resolution. A vital aspect of any PES system is the energy resolution, which depends on the bandwidth of the radiation used for excitation (e.g., monochromated vs nonmonochromated X-ray or gas discharge sources) and the analyzer setup (electron optics, pass energies, slit settings, etc.). In general, energy resolution is not crucial for simple elemental identification in XPS, and thus, many researchers do not give the resolution of their system. However, it becomes particularly important for XPS with respect to peak decomposition, e.g. using fitting procedures. The best peak resolution used thus far for XPS of ILs yielded 0.56 eV for the Ag $3d_{5/2}$ fwhm in a study by Licence and co-workers.[111,119,130,131] Krischok and co-workers[132] reported <0.6 eV, Caporali and co-workers 1.2 eV fwhm[112,121] for the Ag $3d_{5/2}$, and Fortunato et al. reported 1.16 eV for the Au $4f_{7/2}$ fwhm.[113] Maier and co-workers do not give a particular line width but report 0.9 eV as the overall energy resolution.[85,115,116,120,133−136] It is clear that higher resolution allows superior peak decomposition and electronic state identification. To date, no higher resolution synchrotron PES studies of ILs have been reported. For UPS studies, Yoshimura et al. gave 150 meV (at $h\nu = 40$ eV), estimated from the Fermi edge of Au.[114] Krischok and co-workers gave <150 meV,[132] and Iwahashi et al. gave ∼0.1 eV at 300 K.[137]

2.1.1.3. Chemical State Analysis: Carbon (C 1s). By far the most important core level for XPS of ILs is the C 1s, as all ILs studied thus far contain carbon. Unfortunately, XPS is not as sensitive to different carbon environments as other techniques, principally ^{13}C NMR. Therefore, it is necessary to develop fitting procedures to decompose C 1s spectra into different components. Such peak decomposition normally requires assumptions based on chemical structure.

Two different models have been proposed for fitting C 1s for imidazolium-containing ILs; here we refer to those models as the Licence model and the Maier model, after the groups who developed them.[116,119,120,122] Both models refer to $[C_nC_1Im]^+$, where $n = 2-16$; however, the XPS instruments employed by the two groups are very different. The Kratos system used by Licence and co-workers has a monochromated source and a resolution of 0.56 eV, and consequently, the C 1s spectra obtained can be decomposed to a greater extent than those obtained from the system used by Maier and co-workers, which has a resolution of 0.9 eV. The Licence model was proposed in 2006 and has been successfully used by a number of research groups.[123,138] The Maier model is newer and has not yet been applied by others, although it does involve fewer assumptions and is therefore simpler to use.

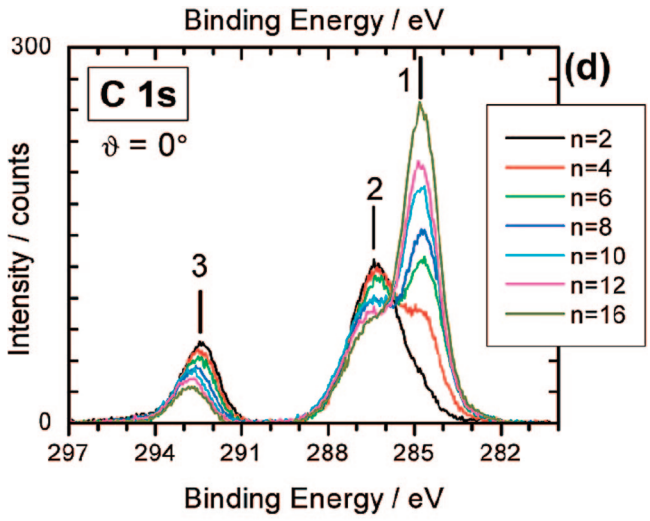

Figure 3. C 1s XP spectra of of $[C_nC_1Im][Tf_2N]$ (where $n = 2-16$), recorded at a 0° electron emission angle using nonmonochromatized Al Kα radiation. As the chain length increases, the intensity of the corresponding C 1s peak (1) increases, as expected from the increased number of alkyl carbons, C_{alkyl}, present. The intensity of the peaks due to C_{anion} (3) and C_{hetero} (2) both decrease with increasing n, due to the decrease in overall molar density with increasing size of the cation. Reprinted with permission from ref 116. Copyright 2009 American Chemical Society.

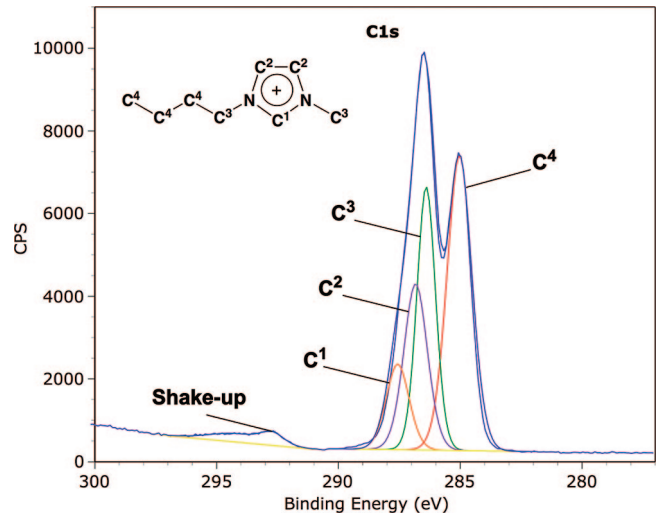

Figure 4. C 1s XP spectrum of $[C_4C_1Im][BF_4]$, detailing the C 1s photoemission. The experimental data (blue) are compared to a simulated fit where each nonequivalent carbon atom had a distinct shift in binding energy. Reprinted with permission from ref 119. Copyright 2006 American Chemical Society.

The Maier model will be introduced first as it relies on fewer intuitive assumptions, it will also be used to explain the shape of C 1s peak. For ILs containing $[C_nC_1Im]^+$ (where $n > 2$) there are generally two well-resolved cation related components.[120] These peaks are labeled C_{alkyl} (C^a) and C_{hetero} (C^h) (annotated as peaks 1 and 2 in Figure 3), where C_{alkyl} are aliphatic carbons and C_{hetero} are carbons bonded to at least one heteroatom, in the case of this model, nitrogen or oxygen. The peak due to C_{alkyl} is at a lower *BE* than the peak due to C_{hetero}. This analysis is supported by the fact that the C_{alkyl} peak increases proportionally in intensity as n increases from 2 to 16, whereas the C_{hetero} peak does not increase in intensity.[116] The C 1s signal of the $[Tf_2N]^-$ anion (peak 3, at 292 eV in Figure 3) is well separated from the cation associated carbons and thus does not interfere with the analysis.

The only assumption used in the Maier model is an empirically developed constraint on the ratio of the fwhm of the two C_{alkyl} and C_{hetero} components of the C 1s spectra taken at 0° emission angle (i.e., recorded along the surface normal, and thus, spectra are dominated by bulk signals). This constraint was developed by fitting C 1s spectra (after linear background subtraction) with Gaussian line shapes for a large set of different imidazolium-based ILs. By a systematic variation of the fwhm(C_{hetero})/fwhm(C_{alkyl}) ratio, consistent peak areas are obtained that match the stoichiometric composition of all ILs when a ratio of 1.11:1 is employed; that is, fwhm(C_{hetero}) is 1.11 times larger than fwhm(C_{alkyl}). Since the first application, this constraint has been successfully used to fit C 1s spectra recorded at different collection angles and also spectra from functionalized ILs, such as polyethylene glycol (PEG)-containing ILs.[116,120,136]

However, if one considers the structure of imidazolium-based ILs, it is possible to identify at least four different carbon chemical environments. The component at low BE has been identified by all authors as the signal coming from the aliphatic carbon atoms (C^4, the same as C^a).[120] The feature at higher BE corresponds to carbons C^1, C^2, and C^3, which were fitted as a single component in the Maier model. With monochromated sources such as that employed by Licence and co-workers, it is possible to identify an additional component, observed as a shoulder at higher BE and attributed to C^1; see Figure 4.[119]

Constraints were placed on the fitting system based upon chemical intuition: the binding energy positions of the three components C^1-C^3 were initially fixed relative to each other. The peak areas for C^1-C^3 were fixed in the ratio 0.8:1.6:2.0. This ratio recognizes losses due to shake-up/shake-off events from the intensities of the aromatic ring carbons (C^1 and C^2). Shake-up features are a consequence of the excitation of a valence electron from a π orbital into an unoccupied π^* just after the photoionization event. Shake-up satellites are frequently observed in atoms involved in multiple bonds and are characteristic of delocalized systems with multiple bonding and aromatic compounds.[139−143] Invariably, a phenomenon called shake-off occurs parallel to the shake-up and in a similar intensity.[140,142] In the case of shake-off, valence band electrons are excited into the continuum and do not produce a defined signal, as the energy of this transition is disperse. Electrons involved in shake-up and shake-off processes do not contribute to the main photoelectron signal, which, therefore, appears weaker than expected. Both shake-up and shake-off lead to loss in intensity from the main peak of around 20%.[141,143] This loss in the signal intensity of the main peak should be taken into account for quantification purposes. Shake-up peaks can be clearly seen in Figure 4; their combined intensity is approximately 10% that of the ring carbons. An equivalent loss was assumed for shake-off,[139] leading to the ratios reported above. This fitting protocol has been successfully applied across a wide range of ILs measured by at least two separate groups.[111,119,123,138] For all components, a Gaussian−Lorentzian product function with 30% Lorentzian was used to model the peak shape with the fwhms constrained to 0.9−1.1 eV. It has to be taken into account that the model highlighted above is simplified with respect to the peak shape that is applied to each of the synthetic components used in the construction of the model. In particular, the saturated alkyl chain carbons will give rise to a vibrationally broadened, nonsymmetric peak shape.[144] This effect should become more

significant as the relative proportion of this contribution increases.[145] As a general comment, XPS users should ensure that the spectral window recorded is sufficiently wide to capture all PE features, including shake-up and shake-off.

For cations other than 1-alkyl-3-methylimidazolium, XPS studies are not common. XPS has been successfully carried out on pyrrolidinium-containing ILs; however, C 1s spectra were only shown by Shigeyasu et al.[146−148] Shigeyasu proposed a model for fitting the C 1s region based upon measurements carried out on a single IL, $[C_4C_1Pyrr][Tf_2N]$.[148] An interesting comment regarding this model was that the BE of some C_{hetero} was identified at a lower BE than accepted values for C_{alkyl}, questioning the validity of the model. fwhms were all constrained to 1.0 eV, and no details are given as to BE constraints used to develop this model. As a general point, when fitting models are proposed, it is absolutely critical that all parameters and constraints are noted, thereby allowing other active researchers to employ and amend as required.

For the cyclic sulfonium cation of the form $[S(CH_2)_4C_4H_9]^+$, a single carbon peak due to the cation is observed at 285.0 eV.[117] This single peak shows that carbons bonded to S are not as shifted to as high a BE as those bonded to N in imidazolium cations. This observation is expected based upon C−S and C−N reference spectra of organics.[1]

In many cases, not only the cation but also the anion contains carbon atoms that can be investigated by XPS. For the ILs studied thus far, the carbon atoms on the anion exhibit two distinct types of C 1s signals: (1) peaks around and above 290 eV which are attributed to CF_x-moieties in the anion and (2) peaks closer to the C_{alkyl} and C_{hetero} position of the imidazolium cation. Typical examples of the latter are $[EtOSO_3]^-$,[111,133] $[OcOSO_3]^-$,[116] $[B(CN)_4]^-$,[120] and $[N(CN)_2]^-$,[122,149] where differentiation between the carbon atoms of the imidazolium cation and the anion becomes very difficult. Therefore, satisfactory fitting assumptions are required in these cases, particularly for the peak position.[111,133] $[C_2C_1Im][EtOSO_3]$ has been satisfactorily fitted using the Licence model.[119,138] Other ILs containing C_{hetero} and C_{alkyl} in the anion have been successfully fitted using the Maier model also, although difficulties are encountered when investigating the surface composition of ILs, as will be explained in section 2.1.3.[120] One way around this problem is to study ILs with small sulfonium cations, which have essentially one carbon environment only, to allow easier identification of anion carbons peaks than for ILs with imidazolium cations.[117] Anions containing CF_x-type moieties have been widely studied with XPS, and in particular the $[Tf_2N]^-$-containing ILs.[112,116,117,119,132,150] All such carbon atoms give peaks at BEs higher than 290 eV due to the electron-withdrawing nature of the fluorine atoms.[120] For $[TfO]^-$- and $[Tf_2N]^-$-containing ILs, a single CF_3 peak was observed, and an example is shown in Figure 3 (peak 3).[120] For $[FAP]^-$- and $[Pf_2N]^-$-containing ILs, two peaks were observed: CF_2 at ∼3 eV lower than for CF_3, due to different number of attached fluorine atoms.[120]

Thus far, the study of functionalized ILs with XPS has been limited to ILs containing PEG groups on the imidazolium cation, in place of the aliphatic alkyl chain present in nonfunctionalized imidazolium ILs.[115,116,136] It has been found that any carbon attached to an oxygen atom appears at a BE similar to that of a C−N carbon atom, and hence, such atoms were labeled C_{hetero}, as the carbons are bonded to heteroatoms.

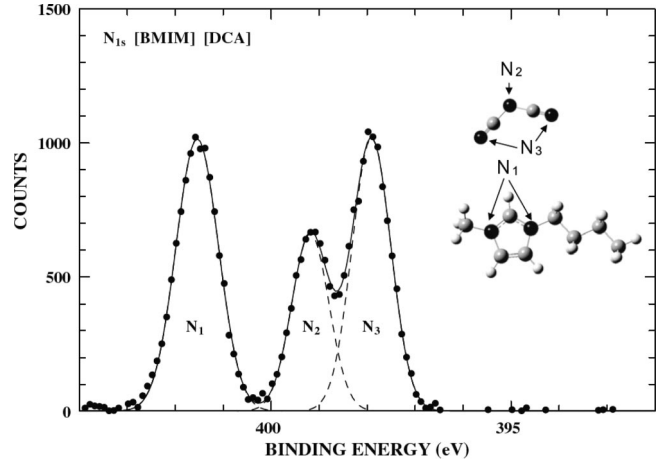

Figure 5. XPS spectrum of N 1s for $[C_4C_1Im][N(CN)_2]$. The spectrum consists of three peaks. The relation between the individual peaks and the N atoms in $[C_4C_1Im][N(CN)_2]$ is indicated. The intensity ratio of these peaks is exactly in agreement with the stoichiometric ratio, [DCA] = $[N(CN)_2]$ = dicyanamide anion. Reprinted with permission from ref 149. Copyright 2010 Elsevier.

However, it has subsequently been shown that C−S carbons, which could also be known as C_{hetero}, appear at BEs more representative of C_{alkyl}. Hence, trying to classify carbon atoms on cations into groups is difficult, and great care is required when fitting. It should be noted that the PEG-containing ILs investigated by Maier and co-workers are troublesome for charge correction purposes, as they contain little or no C_{alkyl} carbons; hence, development of an internal charge reference for anions as well as cations is required.

The study of the IL−vapor interface of functionalized ILs is of particular relevance to studies of ILs at the solid−IL interface, as comparisons to the electronic environment and surface composition of the pure IL are a great help. A very good example of how studying the IL−vacuum interface can benefit studies at the solid−IL interface is the work of Chang and co-workers[147,151,152] (also see section 2.4.2). In this work, the pseudocapacitive mechanism of manganese oxide in a variety of ILs was investigated, in part using the N 1s region of ILs at the IL−vapor interface and comparing to the relative ratio of N 1s peaks due to the anion and cation after electrochemical measurements.

2.1.1.4. Chemical State Analysis: Nitrogen (N 1s). Another element that is vital for ILs is nitrogen. Nitrogen is present in most IL cations, i.e. imidazolium, pyridinium, pyrrolidinium, and ammonium, and is also present in many anions, e.g. $[Tf_2N]^-$, $[Pf_2N]^-$, $[N(CN)_2]^-$, and $[SCN]^-$. To date XPS has been applied almost exclusively to imidazolium and pyrrolidinium containing ILs. Consequently, most studies have included an analysis of the N 1s region. A good example to show that differentiation between oxidation states for nitrogen is possible is that of $[C_nC_1Im][Tf_2N]$, where $2 < n < 16$.[112,116,119,132,150] N_{cation} is ∼2.6 eV higher in N 1s BE than N_{anion},[116] confirming that the nitrogen on the cation is more positively charged than the nitrogen on the anion. The N 1s spectra for nitrile-containing ILs (such as $[C_2C_1Im][SCN]$ and $[C_4C_1Pyrr][N(CN)_2]$) similarly contain components that originate in both the anion and the cation;[147,149,152] see Figure 5 for $[C_4C_1Im][N(CN)_2]$. The peak at BE ∼401.5 eV is attributed to N_{cation}, the peak at BE ∼399.2 eV to N_{C-N-C}, and the peak at BE ∼397.9 eV to N_{CN}. These observations confirm that the N_{cation} is more positively charged than N_{anion}. The ratio of these peaks can

be qualitatively confirmed as 2:1:2, as expected by visual inspection. More quantitative ratios are achievable and will be explained in section 2.1.3.

Shake-up/shake-off features are also observed in the N 1s spectra of ILs which are based upon resonance stabilized heteroaromatics, i.e. 1-alkyl-3-methylimidazolium and alkylpyridinium: these components originate from the nitrogen atoms present within the delocalized aromatic system. The shape of the shake-up/shake-off components is broad and less well-defined than is the case for the equivalent C 1s feature, partly because the intensity is lower. The intensity of the main shake-up component is typically around 6% of the total N 1s signal intensity.[119] Shake-up features can be observed in the N 1s high resolution scan for $[C_2C_1Im][Tf_2N]$. The ratio of the intensity of the two main N 1s components is slightly less than the nominal stoichiometric ratio of 2:1; this is attributed to shake-up reducing the contribution toward the N component of the cation.[119] It is worth noting that in the case of $[C_4C_1Pyrr][Tf_2N]$, where the heteroatom containing pyrrolidinium does not involve delocalization, i.e., when N is sp^3 hybridized as opposed to sp^2 hybridized in $[C_nC_1Im]^+$, shake-up/shake-off is not observed and the ratio N_{anion}/N_{cation} is 1:1, as expected.[148]

2.1.1.5. Chemical State Analysis: Oxygen (O 1s) and Fluorine (F 1s). Oxygen is common to a wide variety of IL components, particularly anions, including $[EtOSO_3]^-$,[111,119,133] $[OcOSO_3]^-$,[116] $[Tf_2N]^-$,[116,119] $[TfO]^-$,[120] and $[ClC_4H_8SO_3]^-$,[85] and cations that are modified with ether,[115,116,136] hydroxyl, or carboxylate functionalities. From an XPS standpoint, the most interesting oxygenated anions are those of the general form $[ROSO_3]^-$, where R is typically Et (C_2H_5) but can also include other chain lengths of varying molecular mass and functionality. If we consider the generic structure, it is quite obvious that there are four oxygen atoms that are present in two distinct environments with a ratio of 1:3 (O_{S-O-C}/O_{SO3}), with the larger, more negative O_{SO3} component being observed at the lower BE and with the BE separation between the two components being 1.4 eV.[116] The most commonly studied anions by XPS, $[Tf_2N]^-$ and $[TfO]^-$, are characterized by a single-component signal; this indicates that all oxygen atoms in each case are in identical environments.

Maier and co-workers have also studied ILs containing PEG-functionalized cations.[115,116,136] In terms of XPS, each oxygen atom in the polyether chain exhibits identical connectivity; as a result, they can be viewed as "identical" and, hence, exhibit the same BE. It should be noted that the BEs of the polyether O atoms are very similar to the O atoms of $[Tf_2N]^-$, emphasizing that atoms on the cation and the anion do not necessarily give BEs that match the overall charge on the parent ion; that is, atoms on the anion can be more positively charged than those on the cation, and vice versa, due to their local environment.

Along with oxygen, fluorine is a common component in polyatomic anions, including $[BF_4]^-$,[120] $[PF_6]^-$,[120] $[Tf_2N]^-$,[116,119] $[TfO]^-$,[120] and $[FAP]^-$.[120] The F 1s spectra published to date contain relatively little chemical information, as the fluorine atoms do not appear to be influenced greatly by the presence of different cations; that is, the reported BE appears to be insensitive to the nature of the cation.[116] However, fluorine may well become an important element in charge correction as an internal reference standard.

2.1.1.6. Chemical State Analysis: Spin−Orbit Coupling. There are elements present in many ILs for which the commonly studied orbital is not an s-type orbital. Due to spin orbit coupling, high resolution scans of p-, d-, and f-type orbitals are normally composed of two distinguishable contributions. For example, for the 2p levels, two peaks, $2p_{1/2}$ and $2p_{3/2}$, are observed in the XP spectra. According to the degeneracy of the magnetic quantum numbers for $j = {}^1/_2$ ($m_j = -{}^1/_2, +{}^1/_2$) and $j = {}^3/_2$ ($m_j = -{}^3/_2, -{}^1/_2, +{}^1/_2, +{}^3/_2$), the intensity ratio is 1:2. For d- and f-type orbitals, the according intensity ratios are 2:3 ($d_{3/2}/d_{5/2}$) and 3:4 ($f_{5/2}/f_{7/2}$), respectively. The BE peak splitting between the two photoemission peaks is characteristic of each orbital type and element, as shown in Table 3. As a general rule of thumb, the magnitude of the splitting increases with increasing binding energy; that is, for core levels with high binding energy, a clear separation of the two peaks is found, whereas, for core levels with low binding energy, the two peaks can often hardly be resolved, if at all. During the fitting of p-, d-, or f-type orbitals, users should ensure that appropriate constraints are applied to take spin−orbit coupling into account. BE separation and the relative peak areas should be constrained to the appropriate literature values;[1] the fwhm for each peak should also be identical.[153] It should be noted that the latter constraint is only valid if the decay of the corresponding core hole follows a normal Auger decay and not a Coster−Kronig decay.[154] Otherwise, the core hole lifetime is significantly reduced, leading to an increased fwhm.

Table 3. BE Peak Splittings due to Spin Orbit Coupling for Selected Elements Often Present in ILs[a]

element	orbital	BE splitting/eV	peak area ratio	BE region/eV
P	$2p_{1/2}/2p_{3/2}$	0.84	1:2	128.5−135.5
S	$2p_{1/2}/2p_{3/2}$	1.18	1:2	160−177
Cl	$2p_{1/2}/2p_{3/2}$	1.60	1:2	198−209
Br	$3d_{3/2}/3d_{5/2}$	1.05	2:3	68−69.5
I	$3d_{3/2}/3d_{5/2}$	11.5	2:3	618−624
Au	$4f_{5/2}/4f_{7/2}$	3.67	3:4	84−87.5

[a] BE regions are taken for the most intense peak. All peak splittings and BE regions are taken from ref 1.

Unfortunately, in some of the XPS studies of ILs published to date, the phenomenon of spin orbit coupling has been completely ignored and the corresponding contributions were erroneously assigned to additional species, leading to the incorrect interpretation of data.[148,155] As can be seen in Table 3, the BE separations are often smaller than the resolution of the experimental setup. Consequently, individual contributions due to spin−orbit coupling cannot be satisfactorily resolved, even when measured at the highest possible resolution; see Figure 6.[119] In such cases, the investigation of multiple core levels for the same element is necessary; for example, in the case of P, S, and Cl, recording the XP spectra for the 2s and the 2p photoemissions will provide additional information on the chemical environments present.

Sulfur is omnipresent in a broad range of anions, including $[EtOSO_3]^-$,[111,119,133] $[OcOSO_3]^-$,[116] $[Tf_2N]^-$,[116,119] $[TfO]^-$,[120] and $[ClC_4H_8SO_3]^-$.[85] Sulfur is also present in a number of cations, including sulfonium, and more commonly in task specific ILs. A further example where spin orbit coupling is relevant is Cl: Paape et al. reported one environment only for both Cl^- and $[ClC_4H_8SO_3]^-$, and hence, two peaks (Cl $2p_{1/2}$ and $2p_{3/2}$) are observed.[85] There is a shift of ~3 eV to higher BE for the Cl peaks in $[ClC_4H_8SO_3]^-$ than in Cl^-, showing that the Cl is more positively charged in $[ClC_4H_8SO_3]^-$ than in Cl^-, as would be expected by intuition.

2.1.1.7. Chemical State Analysis: Metal-Containing ILs. In some cases, high-resolution spectra of transition metals

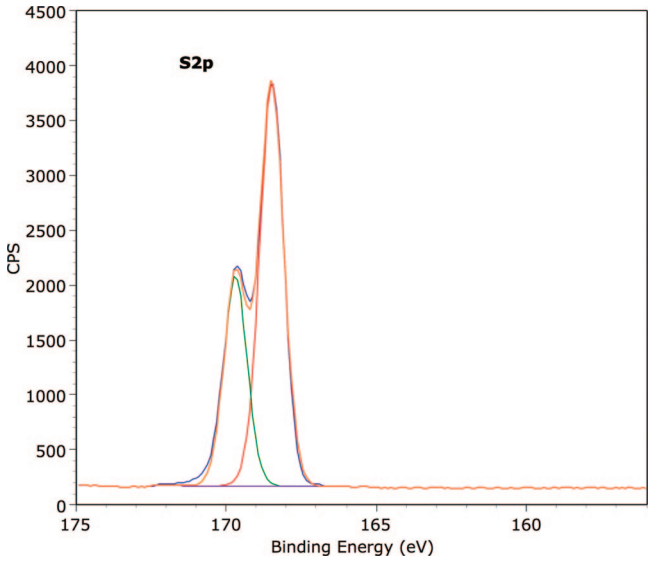

Figure 6. High-resolution XP spectra of the S 2p region for the IL $[C_2C_1Im][NTf_2]$. The spectrum is observed as a partially resolved doublet ($2p_{1/2}/2p_{3/2}$ with a relative intensity of 1:2). Reprinted with permission from ref 119. Copyright 2006 American Chemical Society.

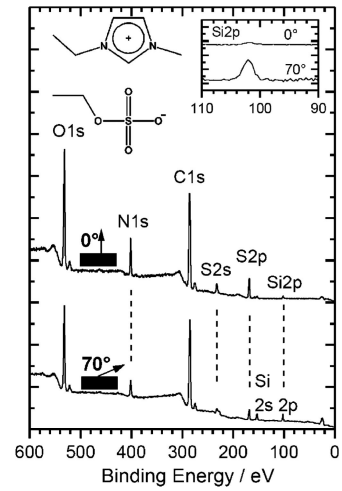

Figure 7. Wide scan XP spectrum of $[C_2C_1Im][EtOSO_3]$; the inset shows evidence of surface segregated Si containing impurities; recorded using nonmonochromatized Al Kα radiation. Reprinted with permission from ref 133. Copyright 2006 Oldenbourg Wissenschaftsverlag.

can appear quite complicated for some oxidation states. Multiplet splitting of the signal can occur due to the core−valence exchange interactions involving unpaired valence electrons. However, multiplet splitting patterns can be theoretically generated, as for the case of some iron compounds (for both $[C_4C_1Im][FeCl_4]$ and $[C_4C_1Im]_2[FeCl_4]$) using the Gupta-Sen (GS) components,[156,157] as previously demonstrated by Grosvenor et al. for iron halide compounds.[158] These components can be used to fit the spectra, although the best way to identify if the signal is coming from a certain substance is to compare it to a previously measured sample. The fittings by Grosvenor et al. were, for example, a good starting point for the analysis made by Taylor et al., and the same number of contributions was chosen to fit mixtures of $[C_4C_1Im][FeCl_4]$ and $[C_4C_1Im]_2[FeCl_4]$, but the relative percentages of the components attributed to each of the differing oxidation states of Fe observed, i.e. Fe^{2+} and Fe^{3+}, was determined by analysis of pure reference samples.[131] Nguyen et al. have also investigated Fe-containing ILs dissolved in other ILs.[155,159] XPS was also reported by Neaţu et al. in their investigation of $[C_6C_1Im][AuCl_4]$ dissolved in $[C_6C_1Im]Cl$, BEs were reported for Au 4f,[129] although no peak deconstruction and fitting of the Au spectrum was included.

2.1.1.8. Chemical State Analysis: Detection of Impurities. The ability to identify specific chemical elements and oxidation states allows one not only to check that the expected elements are present but also to check for impurities and dissolved species. The area of mixtures of ILs and deliberately dissolved species, such as metal complexes, will be examined further in section 2.2.2. Of the three major categories of IL impurities (water, halides, and "chromophores"), only two are really relevant for PES, as most of the water present in an IL is likely to desorb at UHV pressures, even at room temperature.[83,84] Halide detection is possible for relatively low concentrations; however, this is dependent upon the sensitivity of the XPS instrumentation employed.[146] Chromophores are more difficult to detect, primarily due to their very low concentration, but also because they are generally composed of carbon, hydrogen, nitrogen, and oxygen atoms, which are omnipresent in most ILs.

One of the most common problems associated with XPS is the observation of hydrocarbon-based impurities on the sample surface. In the case of IL-based measurements, this is most likely due to surface contamination as a result of silicone impurities (Si 2p)[115,116,119,120,130,133] and simple organics (C 1s and generally O 1s),[115,117,119,149] which can be attributed to either synthetic or storage protocols. The amount of Si present has been estimated to be approximately 2 atom %. It is worth commenting here that if such an amount of impurity was present in the bulk, it would be possible to detect it using conventional bulk solution techniques, including NMR. However, bulk Si contamination has never been reported as a problem in ILs, suggesting that the Si contamination is minor. The data published to date suggests that the Si is preferentially segregated toward the surface of the sample, as has been unambiguously demonstrated by Gottfried et al. in an elegant angle resolved XPS (ARXPS) study; see Figure 7.[133] The exact identity and origin of this commonly observed contamination has not been determined yet. However, it has been shown that silicone grease brought into contact with clean ILs gives rise to similar contamination signals in XPS.[133] When using ARXPS to check for surface segregated impurities, and similarly for the detection of low concentrations in general, great care has to be taken, because solute elements may have relatively low photoemission cross sections.[1] Consequently, they may yield relatively small peaks compared to other elements; Si is an excellent example of such an element. Hashimoto et al. recently used XPS in combination with high-resolution Rutherford backscattering (HRBS) spectroscopy to investigate $[C_4C_1Im][N(CN)_2]$.[149] It was found that a carboxylate-type contaminant was present at the outer surface of the IL.

Surface segregated impurities can be removed from the surface by *in situ* sputtering with Ar^+, a technique that is well-established for cleaning solid samples in a UHV environment. It has been shown for a number of ILs that sputtering can remove surface impurities to yield a surface that agrees with the expected stoichiometric composition of the IL.[115,116,120,123,130] Typical conditions used for Ar^+ sput-

tering are 500 eV, 5 μA, 10 min.[115] It has been shown that surface impurities removed by Ar^+ sputtering may return over time, indicating slow segregation of these low-concentration impurities from the bulk to the surface.[115]

Finally, it should be noted that many of the other surface sensitive techniques applied to the study of ILs are not as element specific as XPS and are consequently not capable of identifying impurities such as Si. Therefore, XPS provides a unique opportunity to characterize surface chemistry and confirm that sample surfaces are clean. As a result, experimentalists can have high confidence levels in sample integrity and physical properties measured thereupon.

2.1.1.9. Chemical State Analysis: Beam Damage. In metallic conductors such as gold, which are routinely studied with PES, the diffusion rate of the atoms within the depth probed by PES is very small, at room temperature. By contrast, in the case of IL samples, the diffusion rate is much higher. Consequently, degradation products could diffuse away from the PES analysis volume. The penetration depth of a typical incident X-ray photon is of the order of micrometers (μm); however, the escape depth of the emitted photoelectrons, when detected at 0°, is between ~7 and 9 nm for organic samples, such as ILs. Therefore, any degradation products that are produced by the X-ray beam will be present in the analysis volume, unless the degradation products desorb or diffuse away from the analysis volume.

In solid state samples, it has been observed that an electron beam can cause damage, whereas photons were less likely to cause damage in general.[107] Many organic molecules decompose when irradiated by intense X-ray sources as bonds are excited and break, mainly induced by the created secondary electrons. Samples affected by severe beam damage are observed to get visibly darker, and C 1s scans change to reflect differences in bonding.[160] This damage is an acknowledged problem with organic-based systems including polymers and can limit the analysis time dramatically.[161,162]

In the case of IL-based PES, reports on damage due to irradiation can be broken down into two discrete categories: those initiated by monochromated X-ray sources and those caused by nonmonochromated X-ray sources. Villar-Garcia reported prolonged XPS analysis of the same region of a range of liquid IL samples using a monochromated X-ray source. Samples were continuously irradiated for periods of up to 24 h without any sign of degradation; that is, no detectable changes in the spectra or physical appearance of the sample were observed.[122] Using the same instrument, solid $[C_8C_1Im][BF_4]$ was irradiated for several hours (at ~175 K);[130] again, no evidence of damage was observed while the IL remained frozen. However, as the sample was melted, damage products were observed in N 1s spectra at a lower BE than that for the original imidazolium-based N component; see Figure 8. The chemical shift of the nitrogen damage peak corresponds to uncharged nitrogen. It was proposed that, when the IL was frozen, the damage products were produced but were below the detection limits of the instrument. However, upon melting of the IL, the damage products were able to diffuse, allowing them to segregate toward the surface. Further to the published work, Jones et al. have confirmed that the observed damage was initiated by the X-ray source; nonirradiated areas of the sample did not show any evidence of damage.

Similar studies, carried out with a nonmonochromated X-ray source, showed that extended exposure to X-rays during XPS can lead to spectral changes.[120] Evidence of

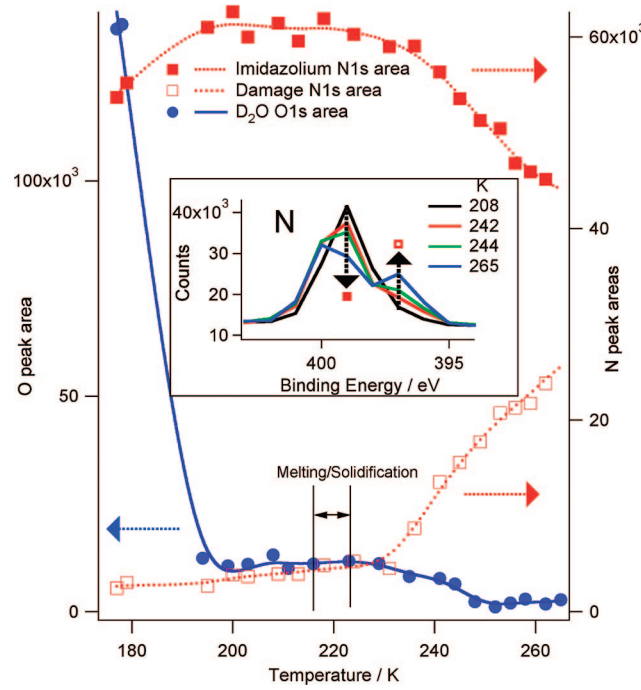

Figure 8. $[C_8C_1Im][BF_4]$, XPS peak areas of O 1s, N 1s imidazolium, and N 1s damage peaks as a function of temperature, with smooth curves to guide the eye. The inset shows the N 1s peak, illustrating the decrease/increase of the imidazolium/damage components with temperature. Reprinted with permission from ref 130. Copyright 2007 The Royal Society of Chemistry.

damage was observed in N 1s spectra for a series of nine $[C_8C_1Im]^+$-based ILs. The most significant damage occurred for $[C_8C_1Im][BF_4]$ and $[C_8C_1Im][FAP]$, both of which contain significant amounts of fluorine; however, it should be noted that $[C_8C_1Im][PF_6]$ appeared to be remarkably stable with little, or no, sign of damage after 12 h of exposure. Samples typically could be studied for a maximum of 4 h with a standard nonmonochromated X-ray source (power 150 W) before damage (5% of the total N 1s intensity) was noted. The data presented by Kolbeck et al.[120] were collected at lower X-ray exposure times (<4 h).

Krischok et al. minimized the irradiation time to minimize the risk of photon-induced damage.[150] For UPS, the applied flux was kept low; also, spectra recorded at low temperature and then at room temperature were virtually identical. Auxiliary experiments showed that metastable atoms, low-energy photons, and electrons with a kinetic energy of ~10 eV cause, in contrast to high-energy photons and electrons (>1 keV), only minor changes in the valence band and vibrational spectra, even if comparably high fluxes were applied.

Since there are no general rules that allow the user to predict beam damage for a particular IL, one has to carefully consider the individual chemistries and decomposition pathways associated with IL components and investigate the experimental parameters with great care. As the liquid is, by definition, mobile, it can mix, and consequently, the analysis volume can continually renew itself. Paradoxically, this can both eliminate and indeed cause problems regarding the detection of both contaminants and decomposition products. It is clear from the studies published to date that there are a number of examples where solute species segregate toward the near surface region of the analysis volume, leading to enrichment in the associated PES signals. However, it must also be acknowledged that the same mass

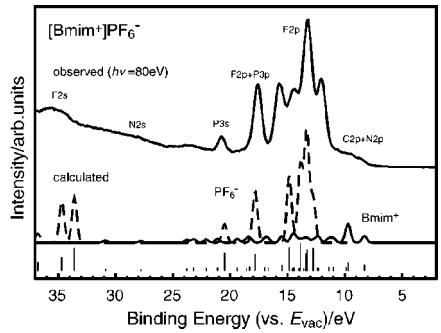

Figure 9. Experimental and simulated UPS spectra for $[C_4C_1Im][PF_6]$. Reprinted with permission from ref 114. Copyright 2005 Elsevier.

transport mechanisms can, in principle, lead to the diffusion of solutes away from the analysis volume. Furthermore, volatile decomposition products can also desorb into the vacuum. Consequently, great care should be taken before concluding that decomposition is not occurring.

2.1.2. Valence Band Structure

The valence electronic structure of ILs is of pivotal importance for the understanding of the chemical properties and the interactions between the constituents of ILs. One important and central aspect is how the electronic structures of the cation and the anion combine to form the electronic structure of the IL. Here, obviously, the strong electrostatic interaction between the partners and the specific character of the top region of the occupied states and the bottom region of the unoccupied states are most important. The question arises, can the concepts known for "ordinary" inorganic ionic solids such as NaCl, where the top of the occupied states is derived from the anion and the bottom of the unoccupied states comes from the cation,[163] be transferred to ILs. The investigation of the origin of the top part of the occupied states and the bottom part of the unoccupied states for ILs thus is of great interest.

Ultraviolet photoemission spectroscopy (UPS), inverse photoemission spectroscopy (IPES), metastable impact electron spectroscopy (MIES) (also known as MAES, metastable atom electron spectroscopy), and XPS are powerful methods that allow the experimentalist to probe the valence electronic structure of materials. Interestingly, sample charging was not observed (or noted) in any of the studies highlighted below.

The first UPS study on ILs was reported by Yoshimura et al. in 2005,[114] who investigated the electronic structures of ILs by UPS with synchrotron radiation. They studied $[C_4C_1Im][BF_4]$, $[C_4C_1Im][PF_6]$, and $[C_4C_1Im][Tf_2N]$. By comparison to molecular orbital (MO) calculations, they concluded that the top of the occupied states in these ILs was derived from the $[C_4C_1Im]^+$ cation. This result seemed surprising at first, since the calculated energies of the highest occupied molecular orbitals (HOMOs) of the isolated anions were higher than those of the isolated cation, presumably because it is easier to emit an electron from the isolated anions due to strong electron repulsion, while the "hole" in the cation lowers the energies of electrons.

The authors regarded the observed spectra (e.g., for $[C_4C_1Im][PF_6]$ in Figure 9) as the superposition of the contributions from the cation and anion. To reproduce the experimental spectra, they therefore added the calculated density of states (DOS) of the isolated ions. Prior to superposition, however, the calculated spectra of the anions

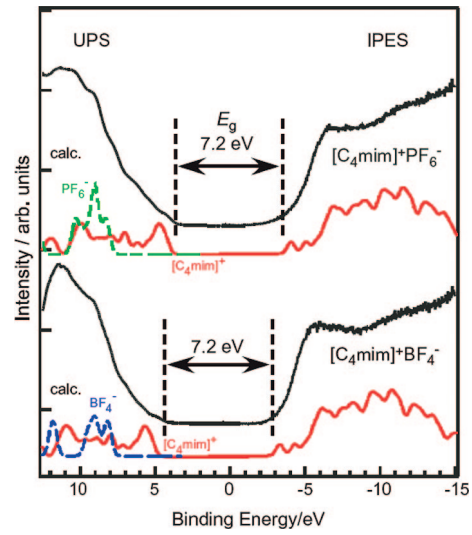

Figure 10. UPS and IPES spectra of $[C_4C_1Im][BF_4]$ and $[C_4C_1Im][PF_6]$. The origin of the abscissa is the Fermi level of the Au substrate. Simulated UPS spectra based on DFT calculations are also shown. Red and blue broken lines show the DOS of cations and anions, respectively. E_g denotes the energy gap. Reprinted with permission from ref 165. Copyright 2008 Elsevier.

and cations had to be differentially shifted on the binding energy scale to account for the effect of the surrounding ions in the ILs. For the $[C_4C_1Im]^+$ ion, a shift toward lower energy is needed while the direction is reversed for the inorganic anions, suggesting that the orbital energies of the cation are destabilized while those of anions are stabilized in the IL.[114] This effect of the surrounding ions and the resulting change in the order of the MO energies was ascribed to the effect of the Madelung potential, V_M,[164] which was estimated to be between 5.0 and 6.2 eV for the investigated ILs.[114]

This reversal of the order of the molecular orbitals of anions and cations is in contrast to the case of usual ionic salts, such as NaCl, where the top of the valence band is due to Cl^- anion. In NaCl, the energy separation between the Na 3s and 2p states is large, and the 3s level of Na neutral atom is only singly occupied. Thus, the highest occupied state of the Na^+ ion becomes the Na 2p state, which is deeper than the Cl 4s level, even after the lifting by the Madelung potential.[164] In contrast, for $[C_4C_1Im]^+$ the separation between the HOMO and the next occupied states is small, since the top of the valence states consists of many MOs. Thus, the topmost occupied states are not derived from the anion but from the $[C_4C_1Im]^+$ cation.

Using inverse photoelectron spectroscopy (IPES), the same group also studied the unoccupied states $[C_nC_1Im][BF_4]$ and $[C_nC_1Im][PF_6]$, when $n = 4$, 8, 10, with fluorine-containing anions (Figure 10).[165] They found that not only the top of the occupied states but also the bottom of the unoccupied states of $[C_nC_1Im][BF_4]$ and $[C_nC_1Im][PF_6]$ are both derived from the cation. Therefore, the energy gaps of these ILs are determined by cations only, in sharp contrast to the case of alkali halides, where the energy gap is defined by the top of the occupied states formed by the anion and the bottom of the unoccupied states formed by the cation. From the dependence on the alkyl chain length of the $[C_nC_1Im]^+$ cation, the HOMOs of the $[C_8C_1Im]^+$ and $[C_{10}C_1Im]^+$ ions are found to be the σ orbitals in the alkyl chains, whereas that of $[C_4C_1Im]^+$ is the π orbital distributed on the imidazolium ring. This marked difference in the HOMO character is made responsible for the difference in the

observed energy gaps of $[C_8C_1Im][BF_4]$ and $[C_{10}C_1Im][BF_4]$ from that of $[C_4C_1Im][BF_4]$.

In a separate study, Krischok and co-workers investigated $[C_2C_1Im][Tf_2N]$, a comparable imidazolium-based IL, but with a significantly larger, sulfur containing anion.[132] Based on their UPS data, combined with XPS and MIES, they showed that the composition of the outer surface region shows no significant deviation from the bulk composition. From temperature dependent measurements, they conclude that volatilization of $[C_2C_1Im][Tf_2N]$ starts around 350 K.[150] Furthermore, by comparison of the spectroscopic data to density functional calculations, they propose for this specific system that the valence band maximum is to be attributed to the HOMO of the $[Tf_2N]^-$ anion within the $[C_2C_1Im][Tf_2N]$ complex,[150] in contrast to what is found by simple combination of the DOS of the separated cation and anion.

Additional insight in the contributions of anions and cations to the upper valence can be obtained from soft X-ray emission spectroscopy (SXES), which locally probes the valence structure at the position of different atoms within a molecule, i.e. at the cation or the anion.[166] In two recent papers,[167,168] Kanai and co-workers studied a variety of imidazolium-based ILs, $[C_4C_1Im]^+$ or $[C_8C_1Im]^+$ combined with Br^-, $[BF_4]^-$, $[PF_6]^-$, $[Tf_2N]^-$, or $[TfO]^-$. From UPS data combined with SXES, IPES, and MO calculations, the authors derive conclusions on the origin of the uppermost occupied electronic states, which provided further evidence that the molecular orbital energies of these ILs are indeed significantly affected by the electrostatic Madelung potential among the ions. In particular, they showed that the contributions of cations and/or anions to the topmost electronic states differ depending on the nature of the anion: For $[BF_4]^-$ and $[PF_6]^-$, they found that both the highest occupied (HOMO) and the lowest unoccupied states (LUMO) are derived from the imidazolium cation, which means that the band gap is solely determined by the cation. On the other hand, for larger anion molecules such as $[Tf_2N]^-$ and $[TfO]^-$, both cation and anions contribute to the topmost occupied states (see Figure 11). Furthermore, for Br^- the highest occupied state is the Br 4p level, so that the topmost electronic states are only due to the anion. These results suggest that, with careful design of the anion and/or cation components, the IL's energy gap may be controlled and new classes of the ionic materials developed in terms of electronic structure.

To conclude the discussion concerning the electronic structure, Table 4 summarizes the available information on the valence electronic structure of the investigated ILs along with the corresponding references. Apart from the contribution of the cations (C) and anions (A) to the HOMO and LUMO, the HOMO−LUMO gaps, E_G, and the Madelung potentials, V_M, are denoted. The observed values of the energy gap (7.2 eV) differ substantially from the electrochemical window estimated from the oxidation and reduction potentials measured by cyclic voltammetry (CV) (e.g., 7.2 eV in Table 4 for $[C_4C_1Im][BF_4]$ as compared to 4.9 eV obtained by CV[169]). Nishi et al. argue[165] that, in CV measurements, anions are always collected by the applied voltage to the anode and are oxidized, while cations are collected to the cathode and are reduced, which may not be truly representative of the bulk. Furthermore, the Madelung energy of ILs near the electrode can be different from that in the bulk or the free surface. It is thus probable that the electrochemical window measured by CV does not reflect the actual energy gap for ILs.[165] It is also worth noting that, in the first vapor-phase photoelectron spectroscopy study of ILs by Strasser et al., the ionization energy of the subject of the study, $[C_2C_1Im][Tf_2N]$, was determined to be 8.9 ± 2 eV.[51]

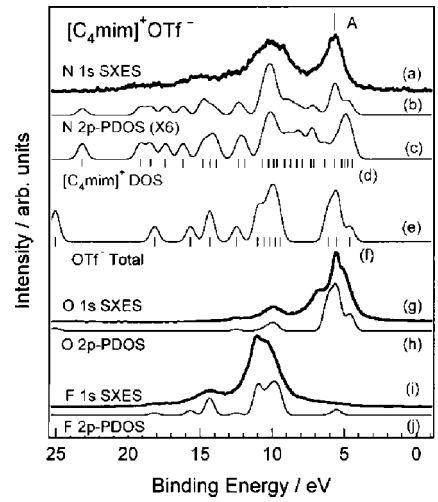

Figure 11. SXES measurements above the N 1s, O 1s, and F 1s edges of $[C_4C_1Im][TfO]$ compared with the simulated DOS and PDOS. The N 1s SXES spectrum (a) is compared with the simulated N 2p-PDOS (b) of $[C_4C_1Im]^+$ and the DOS of isolated $[C_4C_1Im]^+$ (c). Part d represents the result of the calculated MOs of $[C_4C_1Im]^+$. The O 1s SXES spectrum (g) is compared with the simulated O 2p-PDOS of the isolated $[TfO]^-$ (h). The F 1s SXES spectrum (i) is compared with the simulated F 2p-PDOS of $[TfO]^-$ (j). Parts e and f represent the simulated DOS and the calculated MOs of the isolated $[TfO]^-$, respectively. The simulated DOS and PDOS were obtained by broadening the calculated MOs with 0.6 eV fwhm to reproduce the observed spectra. The structure labeled "A" in the UPS spectrum is composed of the mixture of N, C valence states of the cation and O valence states of the anion. Reprinted with permission from ref 167. Copyright 2008 American Institute of Physics.

Table 4. Overview of the Imidazolium-Based ILs Studied, Including the Contributions of the Cations (C) and the Anions (A) to the HOMO and LUMO, the Energy Gap E_G between the HOMO and the LUMO, and the Madelung Potential, as Derived from the Differential Shifts of Simulated Spectra in Order To Find Agreement with the Experimental Spectra (for Procedure, See Ref 114)

cation	anion	HOMO[a]	LUMO[a]	E_G[b]	V_M[d]	ref
$[C_2C_1Im]^+$	$[Tf_2N]^-$	A				170
$[C_4C_1Im]^+$	$[BF_4]^-$	C (π)	C	7.2	5.3	114, 165
	$[PF_6]^-$	C (π)	C	7.2	5.0	114, 165, 167
				(6.9)	(4.78)	
	$[Tf_2N]^-$	A + C		8.3	6.2	114, 165, 167
	$[TfO]^-$	A + C		8.1	(4.36)	167, 168
$[C_8C_1Im]^+$	$[BF_4]^-$	C (σ)	C	8.1[c]		165, 168
				9.1[c]		
	Br^-	A	C	5.3		168
$[C_{10}C_1Im]^+$	$[BF_4]^-$	C (σ)	C	8.1		165

[a] A, anion; C, cation. [b] Determined from UPS/IPES. [c] Two different values found by same group.[167,168] [d] Values determined from UPS data; value in parentheses from SXES data.

Finally, we want to mention a recent more structure oriented study by Iwahashi et al., who investigated $[C_nC_1Im][X]$ (where n = 4, 8, and 10 and X = $[BF_4]^-$, $[TfO]^-$, $[Tf_2N]^-$) using MIES, UPS, and DOS calculations.[137] The MIES spectra show that for the ILs with the shorter alkyl chain (n = 4) the anions and cations share the surface. For the ILs with longer alkyl chains (n = 8, 10), the outermost surfaces tend to be covered by an alkyl chain layer

which conceals the anions. This coverage effect depends upon the size of the anion; that is, a larger size anion $[Tf_2N]^-$ is less effectively shaded by the alkyl chain. Comparison of UPS and MIES spectra indicates that the nonpolar groups, such as the alkyl chain and the CF_3 group, point toward the vacuum, while the polar groups such as the SO_3 and SO_2 groups face toward the bulk. From their study, the authors propose a plausible surface structural model in which the alkyl chains are pointing away from the bulk into the air (or vacuum) with local clustering and layering of alkyl chains, with the imidazolium rings and the anions forming a polar layer beneath the surface. This preferential enrichment of the longer alkyl chains at the surface and the derived model are consistent with results reported recently by Kolbeck et al.[120] The surface composition of ILs investigated using PES will be explained further in section 2.1.3.

2.1.3. Surface Composition

As highlighted in the earlier sections of this document, and indeed in earlier reviews and perspectives articles,[45,101−103,171] an intimate knowledge of the interfacial regions of ionic liquid-based systems is essential to the future development of multiphasic, multicomponent devices and reaction systems. UHV dependent surface sensitive techniques including photoelectron spectroscopies can reveal this critical knowledge. It has been shown that elements can be identified and spectra fitted and decomposed into different components. The areas of these peaks from different elements are not directly comparable due to different photoionization cross sections. Relative sensitivity factors (RSFs) have been developed to account for these differences in cross sections, allowing direct comparison of areas and relative elemental composition to be obtained. It is vital to emphasize that a realistic fwhm must be used (generally between 1 and 1.5 eV) and where necessary quoted (or at least any constraints used should be quoted). Also, if any constraints on BE are used, then they should be detailed. As a general rule, raw data should be shown when more than one component is present, so readers can judge the quality of any fits obtained as well as the quality of the material, particularly as impurity detection is important in ILs and XPS of ILs is a relatively new unchartered field.

There are two methods of obtaining RSFs. First, an RSF set empirically determined on a specific XPS system can be used; Wagner et al.[12] supplied an RSF set that is very widely used today, and his RSFs are provided in a number of analysis packages. In this case, the transmission characteristics (i.e., changes in intensity as a function of kinetic energy) of ones own instrument may be different from those of the reference system, leading to considerable errors. The second method of obtaining an RSF set is to develop one using data recorded on ones own system. This method has been used by a number of groups.[112,115,119,120] For example, Maier and co-workers used a selection of small ILs at a collection angle (θ) of 0° and varied the RSFs until the compositions matched calculated stoichiometric values. The RSFs obtained have been shown to give good agreement, when $\theta = 0°$, between measured and theoretical surface compositions for a range of ILs not in the original training set (i.e., not among those used to determine the RSFs).

Early papers published on the IL−vapor interface gave details at 0° of the surface composition. For example, Höfft et al. showed for $[C_2C_1Im][Tf_2N]$ that the surface composition at 0° using XPS (estimated probe depth of ∼7−9 nm) is the same as that of the bulk.[132] As explained in section 1.2.2, the depth probed for 0° for organic samples is ∼7−9 nm, which is not particularly surface sensitive. However, by increasing the angle from 0° to greater than 70°, the surface sensitivity is greatly increased; at 80°, the depth probed is ∼1−1.5 nm. The first example of using angle resolved XPS (ARXPS) to investigate the surface composition of ILs was by Maier and co-workers.[133,134] This group showed for a surface clean $[C_2C_1Im][EtOSO_3]$ that at 0° and 70° there was no difference in composition, indicating a homogeneous distribution of IL cations and anions in the near-surface region at a depth of ∼2−3 nm.[133] Subsequently, Lockett et al. showed for $[C_nC_1Im][BF_4]$, where $n = 4−8$, that there is more alkyl chain present at the surface than imidazolium ring or anion.[123] This effect was greater for longer alkyl chains, leading to the conclusion that the alkyl chain is oriented away from the IL surface. Maier and co-workers built upon these results by studying a wide range of different IL systems using ARXPS.[85,115,116,120] It was shown that for $[C_nC_1Im][Tf_2N]$, where $n = 2−16$, there is more alkyl chain present in the near-surface region than expected by stoichiometry, agreeing with the conclusions of Lockett et al.[116] Furthermore, investigations for $[C_2C_1Im][OcOSO_3]$ showed that there is more alkyl chain in the near-surface region, whether the alkyl chain is located on the cation or the anion, agreeing with results for sum frequency generation (SFG),[116,172,173] X-ray reflectivity,[173] MIES,[137] and simulations.[174] Nine different ILs with the same cation and different anions, $[C_8C_1Im][X]$, where X ranged in size from Cl^- to $[FAP]^-$, were also investigated with ARXPS.[120] It was shown that more alkyl chain is present in the near-surface region for those ILs containing smaller anions such as halides and $[BF_4]^-$ than those containing larger anions such as $[Tf_2N]^-$, $[FAP]^-$, and $[Pf_2N]^-$, as shown in Figure 12. ILs containing PEG-functionalized cations were also investigated and showed, even at a probe depth of 1−1.5 nm, a very similar composition to the bulk stoichiometric composition, strongly suggesting that the O-atoms in the EG chains interact, most likely, with the H atoms in the cation and, therefore, the alkyl chains are not at the outermost of the surface, as for nonfunctionalized ILs.[115,116] Metal complexes dissolved in ILs have also been investigated by ARXPS and will be discussed in section 2.2.2. Recently, the surface composition of a mixture of two ILs has been investigated using ARXPS; this work will be commented upon in section 2.2.1.

2.1.4. Phase Change Detection

As described in section 2.1.1.1, as ILs are cooled through their glass transition temperature and as glass formation and potentially crystallization occurs, the result in terms of PES is that the sample becomes poorly conducting.[130,150] As a result, surface charging of the sample can occur, peaks are observed to shift to a range of higher apparent BEs, and the peak appears to become broader (see Figure 2). This observable drop in conductivity can be used to monitor the solid−liquid phase transition of ILs in the absence of volatile contaminants, including dissolved gases and water.[83,84] A key problem with this approach is accurate and precise measurement of the sample temperature when in the UHV chamber.

The liquid−vapor transition of ILs has also been monitored using PES.[150] As discussed in section 1.4.2.2, many aprotic ILs can be successfully vaporized as neutral ion pairs.[52,53] The two methods used are slightly different. The first method involved vaporizing $[C_2C_1Im][Tf_2N]$ and monitoring the

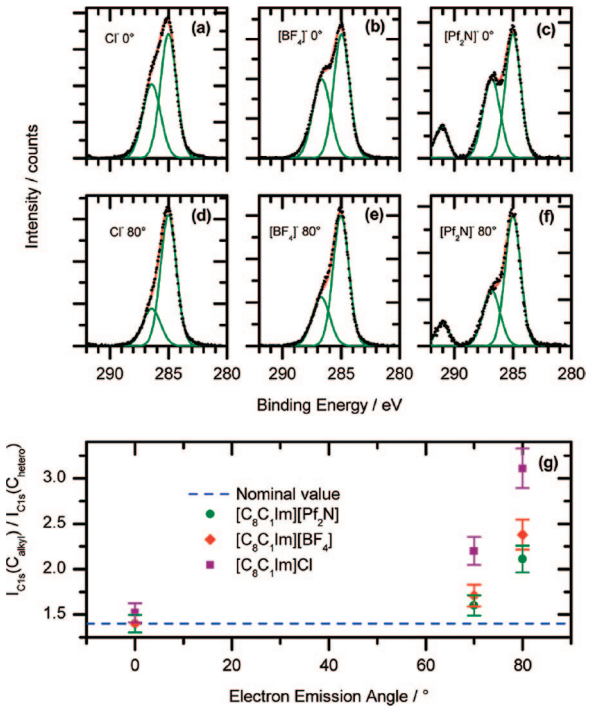

Figure 12. ARXP spectra of the C 1s region for $[C_8C_1Im]Cl$ at (a) 0 and (d) 80°, $[C_8C_1Im][BF_4]$ at (b) 0 and (e) 80°, and $[C_8C_1Im][Pf_2N]$ at (c) 0 and (f) 80°. (g) Ratio of the C_{alkyl}/C_{hetero} intensities for the three ILs as a function of emission angle. At 0°, the measured intensity ratios C_{alkyl}/C_{hetero} for all three ILs approximately match the nominal ratio, 7:5 = 1.4, as shown in part g, suggesting a homogeneous distribution of all components within the i.d. of 7−9 nm. At 80° (i.d. of 1.0−1.5 nm), C_{hetero} decreases relative to C_{alkyl}, indicating more alkyl carbons than ring carbon present in the near-surface region atoms. C_{alkyl}/C_{hetero} at 80°, i.e., the degree of enrichment of the alkyl chains decreases with increasing anion size, from Cl^- to $[BF_4]^-$ to $[Pf_2N]^-$, as evident from part g. Reprinted with permission from ref 120. Copyright 2009 American Chemical Society.

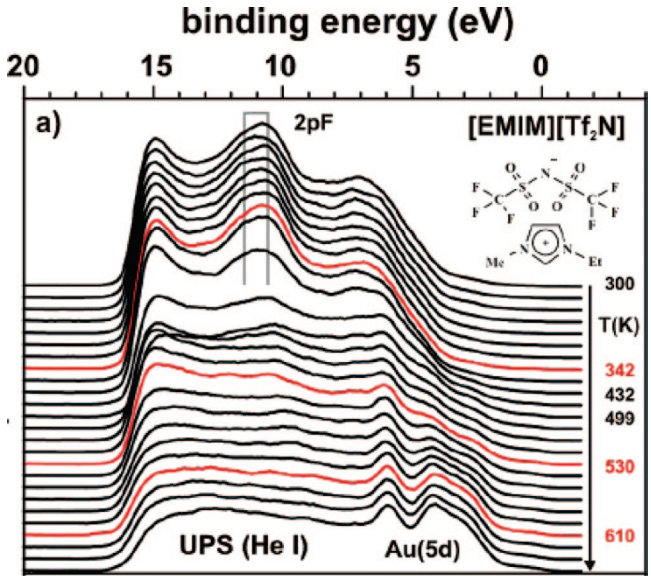

Figure 13. UP spectra of $[C_2C_1Im][Tf_2N]$. Reprinted with permission from ref 150. Copyright 2007 American Chemical Society.

decrease in IL signals and concurrent increase in gold substrate signals with respect to temperature using UPS, as shown in Figure 13.[150] The second method involves vaporizing $[C_2C_1Im][Tf_2N]$ and monitoring IL layer growth using XPS.[135] This method will be explained in detail in section 2.1.1, as this method is very useful for investigating the solid−liquid interface. The lowest vaporization temperature detected using PES is approximately 320−350 K, which is lower than those of most other published vaporization studies.[55] The reasons are that, first, PES is very sensitive to changes in composition and, second, the vapor phase was not detected directly, which is far more experimentally challenging than detecting at a surface. As mentioned in section 2.1.2, the vapor phase photoelectron spectrum has also been recorded.[51]

The investigation of phase changes under UHV conditions offers many potential advantages over more traditional laboratory-based techniques and calorimetric methods. Maintaining the UHV environment, typically using pumping systems with very high pumping speeds, ensures that volatile impurities are removed. Such impurities often have a significant impact on the physical properties of ILs, even at incredibly low concentrations. Thus far, XPS[119] and ToF-SIMS[175,176] have been successfully employed in the detection of changes in state, most notably liquid−solid and glassy-crystalline. In principle, a wide range of UHV techniques could be developed to investigate phase transitions; however, the accurate and reliable measurement of real sample temperatures on interchangeable low temperature stages is a challenge that must be overcome before the true potentials of this area of research can be fulfilled.

2.2. Supported Ionic Liquid Layers

Currently, the preparation of supported ionic liquid layers on solid support materials is a very diverse field of research. The materials afforded by this work offer contributions to applications as far reaching as electrochemical sensors and large-scale industrial catalytic systems. Full characterization of these designer materials, including the systematic investigation of potential ionic liquid layer contamination originating from the substrate (see section 2.1.1.8), is absolutely critical if functionality is to be retained throughout device fabrication and controlled scale-up stages. For the sake of simplicity within the context of this review, we have characterized solid supported ionic liquid-based systems as a function of the interaction that takes place between the support and the ionic liquid components themselves, i.e. via either physisorption or the formation of a formal covalent bond, chemisorption; each case is discussed in turn.

2.2.1. Physisorbed Ionic Liquid Layers (PhILL)

A physisorbed ionic liquid layer (PhILL) is, quite simply, a thin layer of an ionic liquid that is physisorbed onto the surface of a solid matrix that can be either organic or inorganic in nature. This type of material is becoming increasingly common, as it is characteristic of a wide variety of materials employed in applications ranging from SILP catalysis to functionalized electrodes and the lubrication of load bearing surfaces.[48,101,177] The thickness of the ionic liquid layer studied, in the case of PhILLs, is a topic that requires a brief comment. The ionic liquid layer must be thin, such that the sample does not adopt bulk type properties as described in the earlier sections of this review. However, the layer must be thick enough such that only the IL−vacuum interface is observed; that is, the surface of the support (substrate) is not observed through the ionic liquid layer. In summary, PhILL samples must be thin enough to ensure that

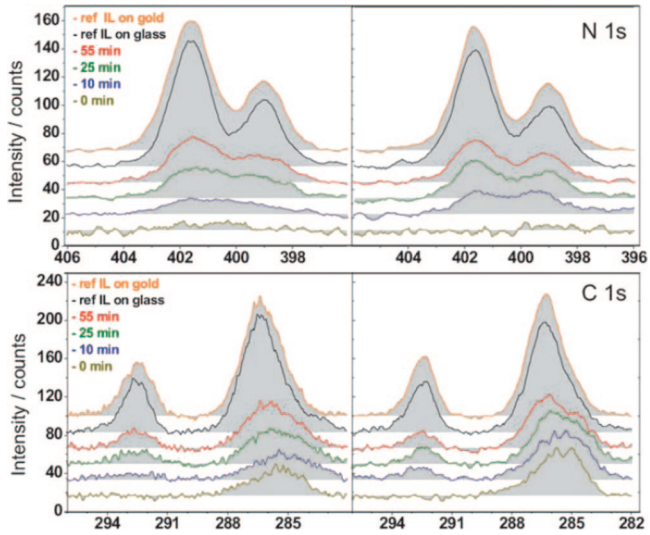

Figure 14. N 1s and C 1s XP spectra of $[C_2C_1Im][Tf2N]$ deposited on a glass substrate, at emission angles of 0° (left) and 70° (right). Spectra are shown for deposition times of 0, 10, 25, and 55 min and for a thick layer ("ref IL on glass"). Also shown are the corresponding spectra of the IL in the reservoir ("ref IL on gold"). In the case of the IL films on the glass substrate, charging was observed. To compensate for this, and to allow a comparison of the different layers, the spectra were shifted uniformly to lower binding energies (with maximum deviations of 0.5 eV) by the following values (0°/70°): 0 min, 9.2/6.9 eV; 10 min, 8.7/7.0 eV; 25 min, 9.2/7.1 eV; 55 min, 8.5/6.6 eV; thick, 0.5/0.4 eV. Note that the N 1s and C 1s spectra have been smoothed. Adapted with permission from ref 135. Copyright 2008 Wiley.

properties are dominated by interfacial anisotropic behavior as opposed to bulk type properties.

As a general comment, there are two main methods that are used in the production of PhILLs. The first method, using a volatile cosolvent, is the most commonly used, as it requires no specific instrumentation or equipment. Briefly, a solution of the material to be adsorbed onto the surface in a solvent (with a relatively high vapor pressure) is coated onto the substrate and the solvent evaporated, leaving the IL on the surface. This relatively simple method is used to produce thin IL films, although the thickness of the physisorbed layer is difficult to control. The second, more challenging, method is direct vaporization deposition of the IL under UHV conditions. Many aprotic ILs can be successfully vaporized as neutral ion pairs (NIPs) at reduced chamber background pressures ($<10^{-5}$ mbar) and elevated temperatures (>273 K).[52,53] Direct deposition can, in principle, occur via the deposition of NIPs onto the sample surface or via the deposition of larger mass ion aggregates at the surface; both methods allow a greater level of control over layer thickness and uniformity.

The preferred method of production, in terms of sample quality, is direct vapor deposition; however, this method is also the most experimentally challenging, as vaporization without decomposition of aprotic ILs is best achieved at reduced pressures.[52,53] The amount of IL vaporized onto the substrate can be varied, giving rise to films of tunable thickness (see Figure 14). Increased control of thickness is also possible; indeed, submonolayer coverage of intact $[C_2C_1Im][Tf_2N]$ was reported by Cremer et al.[135] Cremer et al. also used ARXPS to show that the cation is located nearer to the glass substrate than the $[Tf_2N]^-$. Intact layers of $[C_2C_1Im][Tf_2N]$, produced by direct deposition, have also been studied using time-of-flight secondary ion mass spectrometry (ToF-SIMS).[178−180]

A combined XPS and infrared reflection absorption spectroscopy (IRAS) in combination with density functional theory (DFT) study was performed to investigate the growth of ionic liquid (IL) thin films on and the interaction with oxide supports.[181] Thin films of $[C_4C_1Im][Tf_2N]$ are grown on an atomically flat, well-ordered alumina film on NiAl(110) using physical vapor deposition. By XPS the purity of the used IL was verified. Time-resolved IRAS measured during the growth and subsequent thermal desorption points toward reversible molecular adsorption and desorption. There was no indication of decomposition. The vibrational bands are assigned with the help of DFT calculations. Strong relative intensity changes in individual $[Tf_2N]^-$ bands are observed in the monolayer region. This indicates pronounced orientation effects for the anion. The adsorption geometry of $[Tf_2N]^-$ is determined on the basis of a detailed comparison with DFT. The results suggest that $[Tf_2N]^-$ anions adopt a cis-conformation in the submonolayer region. They adsorb in a slightly tilted orientation with respect to the surface, mainly interacting with the support via the sulfonyl groups.

There is a tremendous scope for investigations of fundamental systems using vaporized films: Direct deposition via vaporization has a huge advantage over spin coating/solvent evaporation by allowing control of layer thickness; nondestructive *in situ* monitoring of the process can also be conducted using a range of UHV analysis techniques, including PES and optical methods.

Direct deposition, in this case via the sputtering of IL aggregates, was employed by Shigeyasu et al., who successfully prepared PhILL-based samples employing $[C_4C_1Pyrr][NTf_2]$ on alumina.[148] Based upon XPS, the authors deduced the presence of ionic liquid-based nanoparticles on the substrate surface. It is conceivable that these spectra could also indicate PhILL formation (this scenario is far more likely than the IL nanoparticles remaining as such on the surface).

Bovio et al. produced thin $[C_4C_1Im][Tf_2N]$ films on mica via evaporation of a volatile cosolvent.[182] XPS was used to analyze the composition of the thin film, confirming that there were no side reactions between the pure IL, $[C_4C_1Im][Tf_2N]$, the cosolvent (methanol) and the mica substrate itself. A quantitative evaluation of the surface composition of pure $[C_4C_1Im][Tf_2N]$ provided the following ratios: F/O/N/C/S = 6:4:3.5:11.2:2, in good agreement with the nominal stoichiometry of F/O/N/C/S = 6:4:3:10:2. A more quantitative evaluation of the surface composition of $[C_4C_1Im][Tf_2N]$ microdroplets deposited from a $[C_4C_1Im][Tf_2N]$/methanol solution yielded the following ratios: F/O/N/C/S = 6:4:3:11:2, again in good agreement with the nominal stoichiometry (contributions of oxygen bound to Si, in native SiO_2, were subtracted in order to obtain the reported ratios).

Du et al. deposited $[C_4C_1Im][BF_4]$ onto single walled carbon nanotubes (SWNTs), leading to an interesting series of PhILLs.[183] XPS was used to confirm that an IL layer had indeed been created; however, the authors relied entirely upon the appearance of a signal corresponding to N 1s as justification that physisorption had occurred; see Figure 15. No other PE regions were reported or commented upon; consequently, the stoichiometry of the PhILL could not be confirmed. Similarly, true chemical reaction or ChILL formation could not be eliminated either.

The preparation of multicomponent adsorbed layers of ILs was investigated by Kocharova et al., who adsorbed two

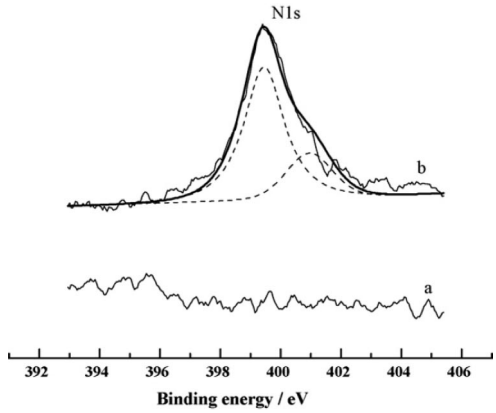

Figure 15. XPS spectra of the SWNTs (a) and $[C_4C_1Im][BF_4]$-SWNTs composite (b) in the N 1s region. The dashed line in curve b is the nonlinear regression results of the N 1s spectrum of the $[C_4C_1Im][BF_4]$−SWNT composite. Note that the BE axis is reversed as compared to the other figures. Reprinted with permission from ref 183. Copyright 2007 Elsevier.

distinct ILs, $[C_{12}C_1Im]Br$ and $[HS\text{-}C_{12}C_1Im]Br$, onto carbon nanotubes.[184,185] In their earlier publication,[184] S 2p, C 1s, and N 1s spectra were reported, suggesting the successful deposition of the IL film. However, some of the fitting procedures used were not thoroughly discussed, and spin−orbit coupling peaks were commented upon but not presented. In their later work,[185] synchrotron radiation was used to obtain high-resolution XP spectra. Only C 1s spectra were given, and again fitting procedures were not discussed. An important point to note was that a C 1s spectrum of "pure" nanotubes was presented; the authors claimed that this spectrum was composed of a single component; however, inspection of the published data clearly reveals that the peak is composed of two components. The presence of this second component in the spectra suggests the presence of some kind of contamination that leads one to doubt the veracity of conclusions drawn for the functionalized nanotubes, as sample contamination has clearly not been considered at all.

Zhang et al. used PhILL architectures to produce some elegantly tethered metal nanoparticles.[186] Their process was elegant, as they used a preassembled PhILL composed of functionalized or task specific ILs, as a stabilizing reaction environment in which the reduction of nanoparticle precursors could be carried out. The resulting composite material was investigated by XPS, confirming the presence of both the nanoparticle and the functionalized PhILL layer itself. Most crucially, they compared their composite XPS spectra to those of neat ILs, and charge correction to C 1s at 284.6 eV was employed; consequently, the data is easily compared to future experiments and stands as an excellent reference piece. Pt nanoparticles were stabilized by carboxylic acid-functionalized ILs which showed, in the O 1s spectrum, that metal oxide was present on the Pt nanoparticle surface. Similarly, subtle differences were noted between the C 1s and N 1s spectra of the pure IL and the PhILL composite material. XPS was also used to confirm the complete removal of chemical reducing agent ($NaBH_4$); that is, there was no evidence of either Na 1s or B 1s in XP spectra, although a lower limit for detection was not given. Using the same methodology, Au nanoparticles were stabilized by amine-functionalized ILs, and a Au $4f_{7/2}$ BE of 84.0 eV revealed that the Au was indeed metallic. The N 1s spectrum showed a 2:1 ratio, as expected based upon the stoichiometric ratio of imidazolium ring to amine present in each IL moiety. It was not possible to determine if reductant remained after nanoparticle synthesis for this system, as the reductant also contained carbon, and hence peaks would overlap with those from the IL; this difficulty also complicated analysis of the IL carbon component also. It was speculated that XPS showed an interaction between the nanoparticles and the IL, although more evidence is required for definitive conclusions to be drawn.

2.2.2. Chemisorbed Ionic Liquid Layers (ChILL)

IL moieties can be covalently attached to surfaces and thus can be seen as chemisorbed IL layers (ChILL). The best known and most studied example of covalent attachment to a surface is self-assembled monolayers (SAMs). There are two methods of covalently attaching IL moieties to a surface. The first, single-step method is achieved by simply reacting a suitably functionalized IL with an appropriate surface. The second, multistep method is achieved by first functionalizing a surface with a suitable reactive group that can then undergo reaction with a suitable reagent such as 1-methylimidazole, thereby forming charged IL moieties at the surface. These two synthetic strategies are highlighted in Figure 16. In both cases, the surface supported ionic moiety can undergo metathesis to yield the anion substituent of choice. In principle, both routes are capable of producing ordered surfaces that are functionalized by the desired IL fragments. Direct ChILL formation is favored, quite simply because the reaction of the functionalized IL with the surface gives rise to surfaces with more homogeneous composition, allowing the investigation of subtle variations in sample surface coverage and orientation. The archetypal SAM is composed of *n*-alkanethiol molecules attached to a gold surface, where a gold−thiolate bond is formed and the alkyl chains self-assemble to form an ordered overlayer. It is important to note that not all monolayers are as ordered as gold−thiolate *n*-alkane SAMs; indeed, many are disordered.[187]

2.2.2.1. Gold−Thiolate ChILLs. Lee and co-workers investigated the formation of ChILLs using gold surfaces and thiol-functionalized ILs with XPS. The thiol-terminated IL $[HSC_{12}H_{24}C_1Im]Br$, 1-(12-mercaptododecyl)-3-alkylimidazolium bromide, was reacted directly with a polycrystalline gold surface.[188−190] Peaks characteristic of the IL were positively observed in the N 1s and Br 3d spectra. It is difficult from XPS alone to determine if the IL is covalently attached to the gold surface, rather than simply physisorbed, or a combination of both chemisorption and physisorption. No clean gold spectra were given for comparison, so it is not possible to determine the thickness of the layer from damping of the Au signals. The C 1s spectrum shows the approximately expected shape for the cation; that is, the C_{alkyl} peak is about twice the intensity of the C_{hetero} peak. The Au-$[SC_{12}H_{24}C_1Im]Br$ surface was subsequently reacted by direct anion exchange with salts of the form MX, where X = $[BF_4]^-$, $[PF_6]^-$, $[NO_3]^-$, $[ClO_4]^-$, $[TfO]^-$, and $[Tf_2N]^-$ (and M = Li^+ or Na^+). For the Au-$[SC_{12}H_{24}C_1Im][BF_4]$ surface, peaks were observed, as expected, due to N, C, and Au (no S region was reported). Single peaks were also observed for B 1s and F 1s, but no contributions were observed for Br 3d. This observation strongly indicated that Br^- had been successfully exchanged for $[BF_4]^-$. It is important to note at this point that if XPS is to be used to comment upon the efficiency of ion exchange processes, experimental details and notes regarding minimum detection limits of each species of interest should be given such that confidence can be

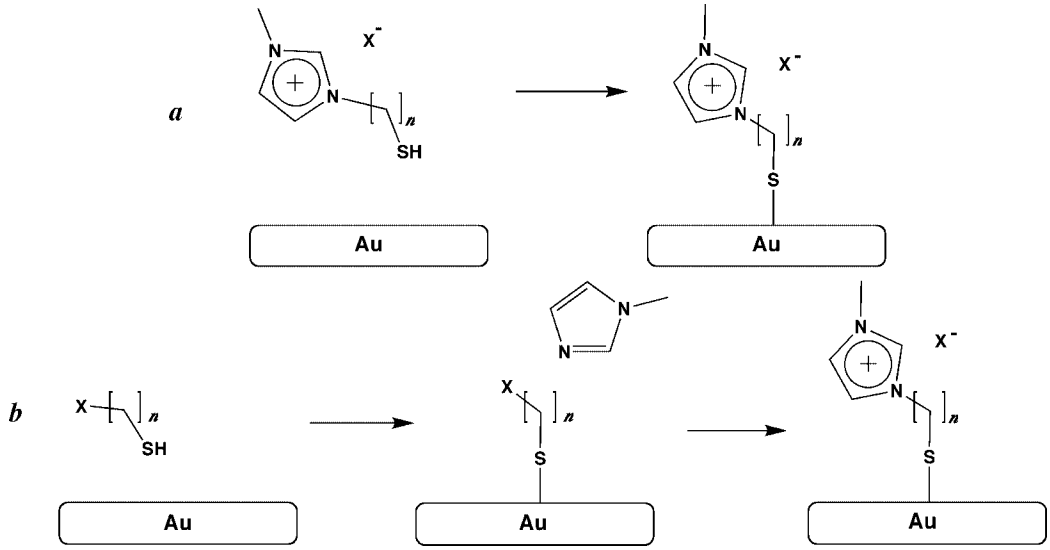

Figure 16. Diagrammatic representation of alternative synthetic strategies that are typically employed in the formation of chemisorbed IL layers (ChILLs) via (a) direct and (b) indirect methods.

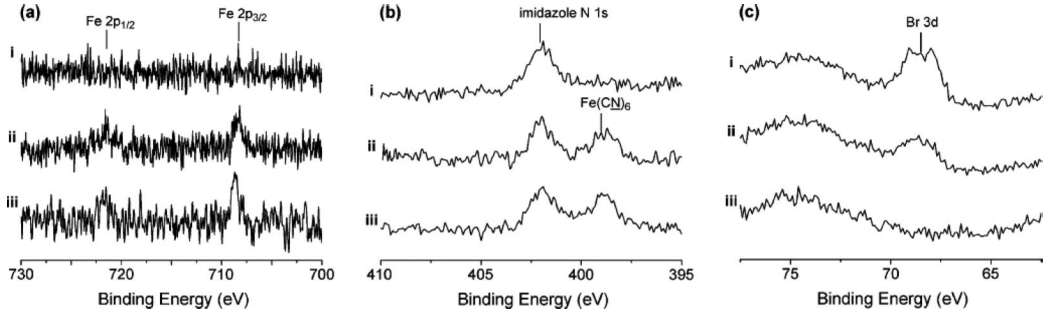

Figure 17. High resolution XP scans of the (a) Fe 2p, (b) N 1s, and (c) Br 3d regions of the self-assembled monolayer Au-$[SC_{12}H_{24}C_1Im]Br$. Before electrochemistry (i), after electrochemistry (ii), and after pretreatment with $K_3Fe(CN)_6$. Reprinted with permission from ref 188. Copyright 2005 American Chemical Society.

established in this approach to quantification. Direct comparisons of the intensity of key components (in both the anion and cation) should also be included to establish the experimental stoichiometry of the sample of interest; the simplest procedure would be to compare the ratio of N (from the imidazolium ring) to the appropriate atoms from the anion, e.g. F, particularly in the case of $[BF_4]^-$, $[PF_6]^-$, $[TfO]^-$, and $[Tf_2N]^-$, simply because F 1s has a relatively large photoemission cross section at $h\nu = 1253.6$ and 1486.6 eV. As a general comment, photon energies should be supplied, or referred to, in all XPS studies.

Further *in situ* ion exchange of the Au-$[SC_{12}H_{24}C_1Im]X$ surface (where $X = Br^-$, $[PF_6]^-$, $[Tf_2N]^-$) has been carried out and used to prepare electroactive surface layers. XPS was used to show the presence of particular elements both before and after electrochemical investigations of redox active switches; see Figure 17.[188] Anion exchange from Br^- to $[Fe(CN)_6]^{3-}$ was confirmed by consideration of the Fe 2p, N 1s, and Br 3d regions. Similarly, exchange from $[Fe(CN)_6]^{3-}$ to $[SCN]^-$ or $[OCN]^-$ was also confirmed by XPS. Cyclic voltammetry was later used to show how anion variation affected the redox properties of the Au surface, demonstrating the potential for tuning electrode surfaces with respect to electrochemistry. Very similar experiments were carried out by Hwang et al., employing an analogous series of protic IL starting materials.[191] It is important to note that both cations and anions studied herein contain nitrogen atoms; hence, study of the IL−vacuum interface would give additional details and allow investigation of whether adsorption to the gold surface affects the $N_{cation}-N_{anion}$ BE separation. In fact, it would be greatly advantageous to build up an "XPS library" of IL cations and anions, which would allow researchers, particularly those investigating the solid−IL interface, to make comparisons to the IL−vacuum interface where only interactions between ions are present and no interactions to solid surfaces.

2.2.2.2. SiO_2−Siloxane-Based ChILLs. The functionalization of nonconducting silicon-based (Si/SiO_2) surfaces via soft, sol−gel type methods was reported by Lee and coworkers; employing siloxane-functionalized ILs, they prepared a series of ChILLS and used XPS to analyze the surface composition.[192] The presence of Cl^- was confirmed by the observation of a Cl 2p signal at 198.7 eV. However, as no charge correction details were given, it is difficult to draw conclusions regarding the environment of the Cl^- in this system based solely upon the reported BE. The BE of Cl 2p in $[C_8C_1Im]Cl$ is reported at 197.0 eV (employing $C_{alkyl} = 285.0$ eV as reference).[120] The imidazolium chloride-functionalized surface was then anion exchanged to yield $[BF_4]^-$ and $[PF_6]^-$ functionalized surfaces. After the exchange, the Cl 2p photoemission was no longer observed and new XP signals corresponding to the $[BF_4]^-$, B 1s at 193.1 eV and F 1s at 686.5 eV, or $[PF_6]^-$, P 2p at 136.9 eV and F 1s at 687.1 eV, were observed. The observed BE differences between the F 1s peaks for $[BF_4]^-$ and $[PF_6]^-$, 0.6 eV, are comparable to that reported by Kolbeck et al. for F 1s in XP spectra recorded for $[C_8C_1Im][BF_4]$ and $[C_8C_1Im][PF_6]$, respectively.[120] Contact angle measurements

were also used to confirm the influence of the anion exchange on the surface properties.

Coman, Pârvulescu and co-workers presented two further studies based upon siloxane IL functionalized surfaces.[193] XPS was used to confirm the preparation of IL layers prepared via both 1 and 2 step strategies and also to evidence an anion exchange process at the supported ChILL. However, no spectra are presented, either in the article or in the Supporting Information. Thus, it is difficult for the reader to trust their interpretations, as only peak positions and atomic ratios are presented.

2.2.2.3. Functionalized Nanotubes. As described earlier in section 2.1.2, there are two main methods of covalently attaching IL moieties to a surface: directly by using a functionalized IL and indirectly by forming the IL using a prefunctionalized surface. Both approaches have been used to attach IL moieties to carbon nanotubes. Two groups used acid chloride functionalized carbon nanotubes to attach IL moieties. Park et al. used XPS to identify the indirect attachment of an amine functionalized IL moiety to nanotubes, and they confirm the successful exchange of anions on the ChILL.[194] A strong point of this contribution was the fact that all relevant spectra are published either in the paper or in the Supporting Information; this approach is recommended highly. N 1s spectra, in particular, were used to confirm successful IL moiety attachment, and then peaks due to the anions (e.g. F 1s, B 1s, Br 3d, P 2p) were used to validate the successful anion exchange. Physisorbed IL moieties were also successfully removed using aqueous HCl; this observation was again confirmed by N 1s spectra. Yu et al. used direct attachment of a hydroxylated IL to acid chloride functionalized nanotubes.[195] As the reported XP signals are very small, extraction of data is nontrivial, and consequently, developing independent conclusions is not easy. In simple cases such as this, BE charge correction is not so vital, as XPS is used for element identification rather than oxidation state identification. Wang et al. used a similar method to produce NT-IL-NP hybrids.[196] In this case, carboxylic acid-functionalized nanotubes were reacted with an amine-functionalized IL to form a covalent bond. Then $[AuCl_4]^-$ was added, without the addition of further reducing agents, to form Au nanoparticles on the surface of the nanotubes. The main conclusion from the XP spectra is that the Au 4f BEs were ~0.5 eV higher than those of bulk metallic gold, indicating a possible interaction between the IL and the nanoparticle.

More recently, Wang et al. covalently attached a carboxylic acid-functionalized IL to an oxidized boron-doped diamond surface. N 1s XP spectra revealed that the ratio between contributions from the cation $[(COOH)C_1C_8Im]^+$ and anion $[Tf_2N]^-$ agreed with the expected stoichiometry, confirming ion pair adsorption to the diamond surface.[197]

2.3. Mixtures and Solutions

2.3.1. Ionic Liquid Mixtures

One of the most interesting characteristics of ILs is their tunability. Every pair of ions can give rise to a new primary IL, which consequently has its own set of physicochemical properties. The number of combinations can be expanded to the order of billions of binary mixtures (mixtures of three different ions) or even trillions if ternary mixtures (four different ions) of ILs are considered.[198] If the properties of these combinations were known, they would constitute an invaluable database from where to select the most suitable IL to meet the specifications of a given application. Despite the endless possibilities, there are not many publications investigating IL mixtures. Just in the past few years, some studies have started to appear.[31,199] Detailed studies are required in order to understand the properties of IL mixtures, especially when specific properties are enhanced because of the mixture. An understanding of these mixtures at a molecular level is lacking.[31,84,199] Thus, far studies of mixtures of ILs using PES have been limited.[122,146] Silvester et al. used XPS to determine the amount of Br^- dissolved in $[C_4C_1Pyrr][Tf_2N]$ using $[C_4C_1Pyrr]Cl$ as the solute,[146] and Villar-Garcia investigated a range of IL mixtures and the effect on BE.[122]

Recently, Maier et al. investigated a 9:1 mixture of $[C_2C_1Im][Tf_2N]/[C_{12}C_1Im][Tf_2N]$ using ARXPS.[136] At 0° the C 1s spectrum approximately matches that of $[C_3C_1Im][Tf_2N]$, as expected for the 9:1 ratio used (the ratio 9:1 was chosen such that the stoichiometric composition contained two C_{alkyl} on average, as for $[C_3C_1Im][Tf_2N]$). At high surface sensitivity (i.e. 70° and 80° emission angles), the C 1s spectra still approximately matched that of $[C_3C_1Im][Tf_2N]$, rather than that of $[C_{12}C_1Im][Tf_2N]$ (as would be expected if the outer surface was composed mainly of $[C_{12}C_1Im][Tf_2N]$). These results show that the surface composition of the mixture approximately matches that of the nominal composition of the mixture, indicating that the alkyl chain being located at the outer surface is not the primary driving force for surface formation; hence, the interaction of the charged headgroup is likely to be the driving force for surface formation. This result has implications for many fields, such as SILP catalysis and gas absorption, and strongly suggests that many more mixtures of ILs need to be studied, both with PES and also with other techniques. Thus far, the use of PES to investigate mixtures of ILs is a greatly underused method, as many insights can potentially be drawn on both electronic structure and surface composition.

2.3.2. Metal Catalysts/Complex Solutions

The application of ILs as solvents for metal catalysis opens up a range of exciting new experimental possibilities in terms of both XPS and indeed characterization of solution chemistry. Prior to the application of UHV techniques, examination of isolated metal ions or complexes in solution was almost impossible, with clustering effects and bulk property characteristics dominating. ILs provide an ideal opportunity to probe quite fundamental scientific questions; do ILs interact with solutes, or are they mere spectators? Does this situation change as the concentration of solutes, contaminants, or even cosolvents is varied? Can ILs have an active role in catalysis? On a more practical note, ILs, on account of their unique combination of physical properties (see section 1.4.2), offer tremendous opportunity as an immobilization medium for homogeneous catalysts. These drivers, among others, have led to the investigation of a wide variety of solvent/solute systems that are highlighted below.

The importance of correct BE correction is particularly vital when studying solutes dissolved in ILs. One of the most significant goals of XPS studies in ILs has been the investigation of the influence an IL may have on the electronic environment of the solute (catalyst). The first attempt at such an investigation was reported Smith et al., who investigated $[Pd(OAc)_2(PPh_3)_2]$ dissolved in $[C_2C_1Im][EtOSO_3]$.[111] They showed that, as a function of

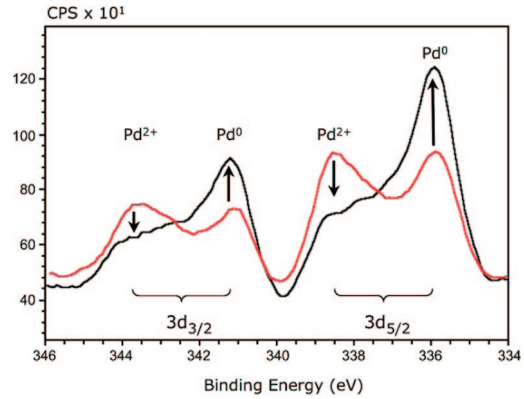

Figure 18. Pd 3d XP spectrum of a solution of $Pd(OAc)_2(PPh_3)_2$ in $[C_2C_1Im][EtOSO_3]$. The plot illustrates the facile reduction of the Pd^{2+}. The red line shows data recorded at the start of the XPS experiment, minutes after the solution was prepared; note Pd^0 is already observed. The black line presents data recorded 6 h later. 300 data sets were recorded between these points. Note, the Pd 3d photoemission is observed as a $3d_{3/2}/3d_{5/2}$ doublet with intensities 2:3 due to spin−orbit coupling. Reprinted with permission from ref 111. Copyright 2005 The Royal Society of Chemistry.

time, the intensity of the observed Pd^{2+} peak decreased, with a concomitant increase in the intensity of the new Pd^0 peak; see Figure 18.

Later Maier et al.[134] published an ARXPS analysis of a platinum salt $[Pt(NH_3)_4]Cl_2$ dissolved in $[C_2C_1Im][EtOSO_3]$ (up to its maximum concentration by using an inhomogeneous solution). ARXPS data revealed that the metal complex was highly enriched at the surface and that Cl^- was not observed at the surface by means of XPS. These findings were attributed to the different polarizabilities (mainly size) of the two ions. However, in the case of a homogeneous solution (i.e., without residual undissolved salt), the XPS intensity of the metal complex rapidly decreased over exposure time, indicating beam damage effects.

Mikkola et al. determined the chemical state of a Pd^{2+} catalyst, $Pd(acac)_2$, dissolved in a supported IL catalytic system;[200] a more detailed study was published in 2007 by the same group.[201] According to the XPS results, the oxidation state of Pd varied, depending on the IL and whether an *ex situ* hydrogenation reaction on an aldehyde had been carried out. Somewhat surprisingly, in fresh samples with dissolved $Pd(acac)_2$, the Pd oxidation state was Pd^{4+} after dissolution, suggesting immediate reaction of the $Pd(acac)_2$ with the IL. For reduced samples, the Pd oxidation state was found to be Pd^0 in the case of $[C_4C_1Im][BF_4]$, indicating decomposition of the transition metal complex and formation of nanoparticles. However, for $[C_4C_1Im][PF_6]$, by contrast, the results indicated a reduction state of Pd^+, suggesting formation of complexes with the IL.

Ruta et al. investigated the reduction, by hydrogenation, of $Pd(acac)_2$ in two ILs, $[C_4C_1Im][PF_6]$ and $[(HOC_4H_8)C_1Im][Tf_2N]$.[202] They showed that a mixture of Pd^{2+} and Pd^0 (as Pd nanoparticles) was obtained; for complete reduction of the Pd precursor to be achieved, a higher pressure of H_2 was required. Recently, Tao et al.[203] used XPS analysis to prove the existence of palladium as Pd^0 nanoparticles in their IL-based catalytic systems immobilized on sepiolite.

A very important point was raised by Ruta et al., namely that a poor signal-to-noise ratio in the Pd 3d region was obtained due to the scarcity of the Pd phase on the surface of the material.[202] For a solute to be detected in XPS, either the solute must surface segregate, as observed by Maier et al., or it must be in high enough concentration that if there is no surface segregation, the solute can still be detected.[134]

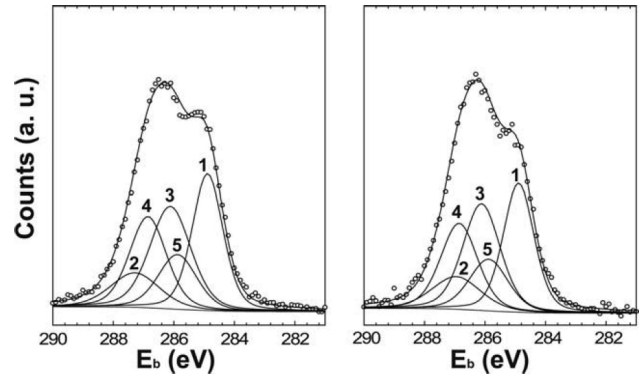

Figure 19. X-ray photoelectron spectra showing the C 1s region with the fitting results for pure IL $[C_2C_1Im][EtOSO_3]$ (left) and with dispersed Ir^0 nanoparticles (right). Reprinted with permission from ref 138. Copyright 2009 Elsevier.

One method of obtaining higher metal content in IL solutions is to use solutes with ions common to the IL, thus giving higher concentrations. This approach has been used by a number of groups.[121,131,155,159] In 2008, Au 4f spectra were used by Neaţu et al.[129] to prove, in conjunction with EXAFS measurements, the presence of gold as Au^{3+} in mixtures of $[C_6C_1Im]Cl$ and $[C_6C_1Im][AuCl_4]$ that were used as catalytic media for cycloisomerization reactions. Nguyen et al.[155,159] analyzed Fe-containing IL catalytic systems by XPS and were able to detect the reduction of iron in $[C_4C_1Im][FeCl_4]$ and $[C_4C_1Im][Fe_2Cl_7]$ melts after treatment with diethylaluminium chloride. Taylor et al. also investigated $[C_4C_1Im][FeCl_4]$ dissolved in an IL; a more thorough discussion of this work will appear in section 2.3.2.[131] Recently, Chiappe et al. used solutes of the form $M[Tf_2N]$ and $M[NO_3]$, where M = a wide range of metals such as Ag, Ni, and Al.[121] ARXPS was used to investigate whether the metal cations were present in the near-surface region, although changing from a takeoff angle of 0° to 60° will not give very much greater surface sensitivity.

Bernardi et al. investigated the interaction of Ir nanoparticles dispersed in $[C_2C_1Im][EtOSO_3]$ using C 1s XPS (Figure 19).[138] The C 1s fitting procedure proposed by Smith et al. for $[C_2C_1Im][EtOSO_3]$ was used.[111] A shift of 0.3 eV to lower BE was observed for the C^2 carbon (the N−C−N carbon) on addition of the Ir nanoparticles. On addition of the nanoparticles, a change in the shape of the C 1s spectra is clearly seen; however, from the XPS data set provided, the proposed interaction of the nanoparticles with the C^2 carbon as a carbene formation seems to be arbitrary to some extent.

2.4. Reaction Monitoring

Reaction monitoring is recognized as a key development in modern chemical processing; it is critical to ensuring that reaction performance is maintained by manipulation of reaction conditions and tuning of reaction components, including catalysts and solvents. Monitoring methods can be characterized into many specific types, i.e., electrochemical, spectroscopic, etc. In the context of this review, monitoring by XPS or related PES techniques, we have broken reaction monitoring down into two sections:

(i) *Ex situ* analysis, which may be defined as analysis of a material postprocessing/reaction, i.e., carried out by

transferring the product into the UHV chamber after the process has concluded.

(ii) *In situ* analysis, which is defined as analysis carried out during the particular chemical process carried out inside the analytical UHV chamber.

It is clear that *ex situ* analysis is, in its broadest sense, very common indeed. Much of the work highlighted in the previous sections could, in principle, be defined as *ex situ* analysis; consequently, this topic will not be discussed in great detail here. We will focus our discussion on solution transformations carried out in IL-based systems.

2.4.1. Ex Situ Analysis

PES, as in the case of many analytical techniques, can be employed *ex situ* in the characterization of reaction products that may be formed in solution or in the solid state. There are numerous examples of the use of PES to characterize the functionalization of surfaces, both inorganic and, indeed, polymer-based.[1,2,11] Using these existing protocols, PES and related techniques can be used to characterize new materials and composites that are produced in IL-based systems. Kwon et al. characterized the product of an A_3 coupling reaction by XPS analysis;[124] the authors showed that they could monitor the formation of propargylamine by investigating a series of aliquots taken every 15 min from the reaction mixture and placed in the vacuum chamber. An increase in the intensity of the C_{alkyl} peak is clearly observed as the reaction proceeds toward completion; however, the reader must assume that no products of the reaction are removed when pumped down to UHV pressure, as this was not specifically commented upon. Although regular NMR experiments may be simpler to run, one significant advantage afforded by PES would be that it allows the simultaneous investigation of all elements in the sample.

A significant improvement would be to use ILs that have relatively few carbon atoms present, which would simplify any C 1s peak decomposition. For example, using the IL $[S(CH_2)_4C_4H_9][Tf_2N]$ would give greater simplicity, as this IL only contained C_{alkyl} carbons and no C_{hetero} carbons.[117] Nguyen et al. have investigated imidazolium-based Fe-containing ILs, obtained from the reaction of $[C_4C_1Im]Cl$ with $FeCl_3$ or $FeCl_2$, and the effect of adding diethylaluminium chloride on dimerization of 2,5-norbornadiene.[155,159] Again, the reaction products were monitored *ex situ*. It is important to note that fitting of the Cl 2p region was incorrectly carried out, as no spin−orbit coupling was included;[155] therefore, all conclusions drawn have to be treated with extreme caution. Also, no details are given as to whether multiplet splitting was included in the fitting of the Fe region.

2.4.2. In Situ Analysis

The monitoring of reactions *in situ* rather than *ex situ* is, of course, preferable for a number of reasons; most specifically, it allows the experimentalist to adjust reaction conditions when reactions are not performing as required, i.e. online optimization. A particular difficulty that must be overcome in the monitoring of reactions *in situ* using PES, or any other UHV technique, is sample evaporation. A wide variety of aprotic ILs and indeed catalysts have sufficiently low vapor pressures to be studied using PES at room temperature. However, the vast majority of reactants of interest will evaporate when exposed to UHV pressures at room temperature. There are two obvious approaches to overcoming this significant impasse: (i) the use of neutral compounds of sufficiently high molecular weight (and hence low vapor pressure) to reduce the probability of evaporation or (ii) the use of materials that are ionic in nature (hence, low vapor pressure).

A combined *in situ* XPS and time-resolved infrared reflection absorption spectroscopy (TR-IRAS) study was performed on supported noble metal catalysts modified by an IL film.[181,204] The model surface consists of Pd nanoparticles grown in UHV on an ordered alumina film on NiAl(110). Thin films of the room temperature IL $[C_4C_1Im][Tf_2N]$ are deposited onto this surface by means of physical vapor deposition (PVD). At 300 K, the IL adsorbs molecularly both onto the Pd particles and onto the alumina. The IR spectra suggest that the $[Tf_2N]^-$ anions interact with Pd sites preferentially via the sulfonyl groups. CO preadsorbed on the Pd particles is partially displaced by the IL, even at 300 K, and only the part of CO adsorbed onto hollow sites on (111) facets of the Pd particles remains in place. Upon heating to temperatures higher than the desorption temperature of the IL (>400 K), molecular desorption of the IL competes with decomposition. The combined XPS/IRAS analysis demonstrates that the decomposition products, atomic species and small fragments, remain preferentially adsorbed onto the Pd nanoparticles and strongly modify their surface properties. Most of the decomposition products originate from the $[C_4C_1Im]^+$ cations, whereas the $[Tf_2N]^-$ anions desorb for the most part.[204]

One area where it has recently been proven that reactions at UHV in ILs can be monitored *in situ* is using spectroelectrochemistry.[131,205] The intrinsic electrolytic capability and low volatility of ILs was utilized to run solution phase electrochemistry in an unmodified XPS analysis chamber. Neutral redox mediators such as ferrocene cannot be used for *in situ* UHV investigations, as even at room temperature such solutes evaporate.[206,207] The electrochemical reduction of Fe^{3+} to Fe^{2+} in the IL mixture of $[C_2C_1Im][EtOSO_3]$ and $[C_4C_1Im][FeCl_4]$ was successfully monitored *in situ* by XPS. Repeated high resolution scans of the Fe 2p region were taken during a coulometric experiment, as shown in Figure 20, to monitor the electrochemically driven change in oxidation state of Fe. Over time, the peaks due to Fe^{3+} were seen to decrease in intensity and the peaks due to Fe^{2+} to increase.

High vacuum spectroelectrochemistry has also been used to identify the *in situ* electrochemically generated Cu species and monitor their surface diffusion in a Cu dissolution experiment. Survey scans and high resolution XP spectra of each of the characteristic elements of the IL and solute (Cu) were performed before and during the dissolution process. Analysis of the Cu 2p spectrum in combination with the KLL Auger signal provided the positive identification of the Cu species as Cu^+. Moreover, the monitoring of the Cu 2p spectrum, as a function of time using the snapshot mode of the spectrometer, allowed a kinetic study of the diffusion of Cu^+ across the sample surface. The experimental data were compared to a theoretical diffusion model to obtain the surface diffusion coefficient, which is 4 orders of magnitude higher than that calculated for radial diffusion through the bulk.[205]

Adsorption studies at the IL−gas interface are vital for many applications of ILs, such as heterogeneous catalysis, gas absorption, and separation.[101] IL surfaces can also be

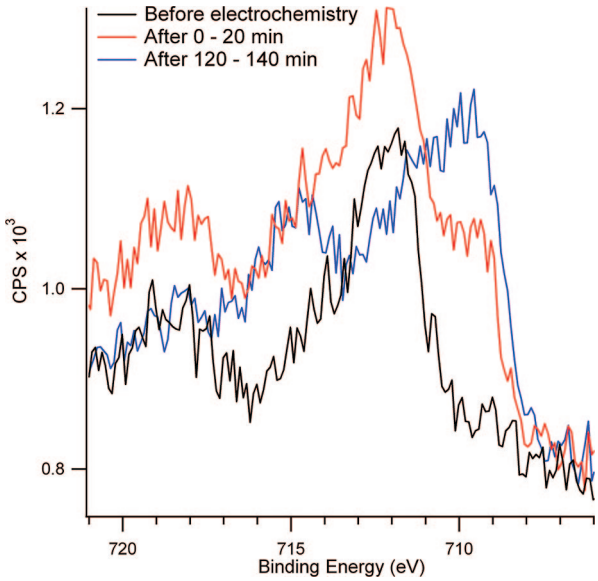

Figure 20. High resolution scans of the Fe 2p3/2 region taken at 0, 20, and 120 min of the coulometric experiment, showing the decrease in peaks corresponding to Fe^{3+} and subsequent increase in peaks corresponding to Fe^{2+}. Reprinted with permission from ref 131. Copyright 2009 The Royal Society of Chemistry.

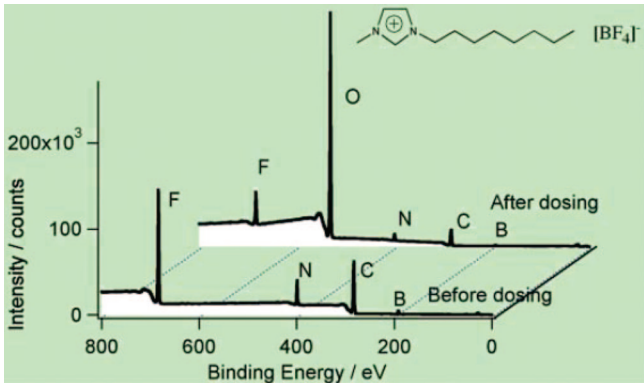

Figure 21. Wide scan XP spectra taken at 175 K before and after adsorbing multilayers of D_2O onto the solid surface of $[C_8C_1Im][BF_4]$. Reprinted with permission from ref 130. Copyright 2007 The Royal Society of Chemistry.

used as model hydrophobic surfaces when cooled.[208] By far the most interesting adsorbate with respect to ILs is water, as water impacts on almost all applications of ILs to a greater or lesser extent. The only example thus far of adsorption studies of ILs using PES is by Lovelock et al., using water and monitoring the O 1s signal *in situ*, as shown in Figure 21.[130] Water was adsorbed onto frozen $[C_8C_1Im][BF_4]$, and temperature-programmed XPS was used to heat the IL until the O 1s signal had disappeared. The water signal disappeared at ~245 K, after $[C_8C_1Im][BF_4]$ had melted. Based on Henry's constants, it was assumed that the water had desorbed into the vacuum rather than absorbed into the bulk IL. However, further work is required to confirm this finding. Kinetics of desorption/adsorption can also be determined using XPS.[130]

There is plenty of scope for further investigations into this area, particularly with different adsorbates. One difficulty is that the orbital of the adsorbate being investigated must not coincide with orbitals from the IL; otherwise, peak decomposition is difficult. For example, studying the adsorption of water onto an oxygen-containing IL such as $[C_nC_1Im][Tf_2N]$ is far more problematic than for $[C_8C_1Im][BF_4]$. Other adsorbates of great interest will be CO_2, SO_2, CO, H_2, and low molecular weight hydrocarbons. Another area with many possibilities is using a high pressure XPS system.[16] These systems are capable of operating at background pressures up to 1 mbar, and hence, adsorbates can be dosed at much higher pressures than the ones employed by Lovelock et al. It may even be possible to study gas−IL reactions *in situ*, although this work would pose many difficulties.

2.5. Materials-Based Applications

The unusual combination of physico/chemical properties offered by ILs alongside the almost limitless degree of tunability offered upon combination of just a modest series of ions renders them ideal as solvents and, indeed, materials for a very broad range of applications. ILs, although often thought of as replacement solvents, are starting to make a significant impact upon the broader scientific and materials-based communities. Materials scientists are now experimenting with these interesting new materials, and significant contributions and potential scale-up applications are being developed. This exciting new area of development was recently highlighted in the excellent review from Kuwabata and co-workers titled "New Frontiers in Materials Science Opened by Ionic Liquids".[209] In the following sections, we highlight key contributions where PES has given additional data to new end exciting materials-based studies.

2.5.1. Metal Nanoparticles

Stable, zerovalent metal nanoparticles have been formed using a variety of methods in ILs.[210] A range of different synthetic methods were used, ranging from reduction by molecular hydrogen of metal precursors,[138,203,211−214] plasma electrochemical deposition, and sputter deposition.[215] After removal from excess IL, typically by centrifugation, interactions between metal nanoparticles and ILs have been investigated using XPS (after being mounted on a suitable solid substrate). The metal nanoparticles studied include the following: Pd,[108] Ir,[138,213] Pt,[212,216,217] Au,[186,196,218−220] and Cu.[221]

ILs were found to remain attached to the surface of nanoparticles, even after washing and then drying under vacuum.[210] It was concluded by many authors that the ILs provided stabilization for the nanoparticles, generally by physisorption, leading to a protective layer. Generally, peaks due to the anion were used to identify the presence of IL, as identification is unambiguous; for example, Fonseca et al. used F 1s to identify the presence of fluorine-containing ILs, as shown in Figure 22. Ir nanoparticles were synthesized using $[Ir(1,5\text{-cyclooctadiene})Cl]_2$ as pre-cursor in $[C_4C_1Im][BF_4]$, $[C_4C_1Im][PF_6]$, and $[C_4C_1Im][TfO]$, and the Ir 4f spectra showed multiple peaks for all ILs investigated, strongly indicating that interactions occur between the nanoparticles and the IL.[213] Synthesizing Pd nanoparticles from $Pd(Cl)_2$ in an aqueous solution in combination with a protic IL, Tao et al., stated in their XPS analysis that no Cl^- from the pre-cursor remained in the obtained Pd nanoparticles, without giving an approximate lower detection limit.[203] The oxidation state of the nanoparticles can also be checked using XPS, although a suitable energy reference level is required.[196,220] In another study of Au nanoparticles formed in $[C_4C_1Im][PF_6]$, Khatri et al. employed XPS to monitor the successful cleansing of residual IL from the surface of

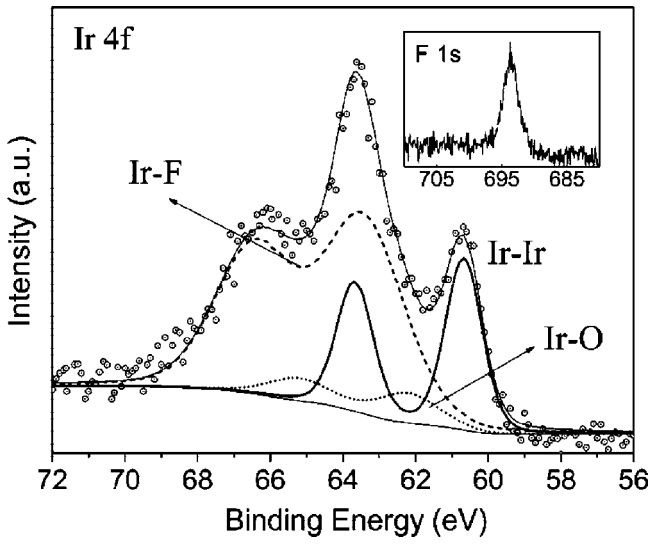

Figure 22. X-ray photoelectron spectra of Ir(0) nanoparticles prepared with $[C_4C_1Im][PF_6]$, showing the Ir 4f region with the fitting results. The Ir 4f doublet presents up to three components corresponding to Ir−Ir (thick line), Ir−O (dotted curve), and Ir−F bonds (dashed curve). The inset shows the F 1s signal observed. Reprinted with permission from ref 213. Copyright 2006 Elsevier.

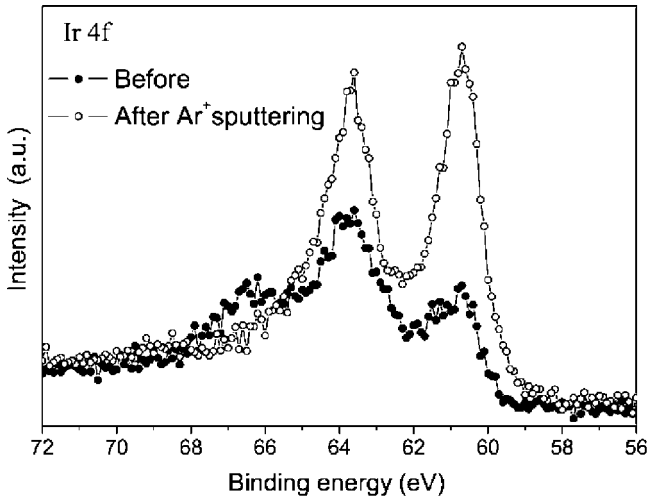

Figure 23. X-ray photoelectron spectra of the Ir 4f region for Ir(0) nanoparticles prepared in $[C_4C_1Im][PF_6]$ before and after Ar^+ sputtering. The Ar^+ sputtering eliminates the outmost layers of the particles, resulting in the Ir 4f region being dominated by the $4f_{5/2}$ and $4f_{7/2}$ levels of metallic Ir. Reprinted with permission from ref 213. Copyright 2006 Elsevier.

the particles in an ultrasonic acetone bath: whereas physisorbed IL was readily removed, a further decrease in intensity of the F 1s peak after successive sonications indicated that $[PF_6]^-$ hydrolysis was also occurring.[215]

To confirm that the IL was located solely at the outer surface of the nanoparticles and not involved in the bulk composition, Fonseca et al. used Ar^+ bombardment/sputtering in combination with XPS as a depth profiling tool.[213] Ir nanoparticles before sputtering with Ar^+ ions showed peaks due to Ir−F and Ir−O components, as well as the main Ir−Ir component; after sputtering, the Ir−Ir component increased greatly in intensity and the Ir−F and Ir−O components decreased greatly in intensity; see Figure 23. The very believable conclusion drawn was that the IL was located solely at the surface of the nanoparticles.

2.5.2. Electrodes

XPS can be used to investigate the interaction of ILs with electrodes, normally *ex situ* after the electrochemical experiments have been carried out. Sun and co-workers have investigated the pseudocapacitive behavior of Mn oxide electrodes in ILs using XPS. Using electrochemical methods, ILs containing nitrile-functionality in the anion, i.e. $[SCN]^-$- and $[N(CN)_2]^-$-containing ILs, were found to give better pseudocapacitive behavior than traditional aqueous electrolytes. The electrochemical charge storage mechanism was determined for a number of different ILs using chemical state analysis and surface composition analysis via depth profiling (ARXPS was not used but would complement these studies very well). As discussed in section 1.2.4, the liquid/gas interfaces of pure ILs $[C_2C_1Im][N(CN)_2]$,[151] $[C_4C_1Pyrr][N(CN)_2]$,[147] and $[C_2C_1Im][SCN]$[152] were investigated, and thus, comparisons were possible between the pure ILs and the Mn oxide/IL electrodes. For all three ILs listed above, the N 1s region contains peaks due to both the cation and the anion, making this region excellent for comparisons, both for BE shifts caused by the oxide and also for composition. For $[C_2C_1Im][N(CN)_2]$, the anionic component of the N 1s peak shifts to a higher BE, when in the Mn oxide, when compared to the neat IL, suggesting that the anion is more positively charged while interacting with the Mn oxide. For all cations, the BE acquired for the N 1s peak was the same for both the pure IL and the Mn oxide/IL electrode, strongly suggesting that the cation does not interact with the Mn oxide surface. For the pure ILs investigated, the different relative ratios of N_{cation}/N_{anion} were close to stoichiometry (2:1 and 2:3 for $[SCN]^-$- and $[N(CN)_2]^-$-containing ILs, respectively). For the electrodes, peaks due to the anion for each IL investigated were monitored as the depth profiled was increased from 0 to 50 nm. For example, for $[C_2C_1Im][SCN]$, the N 1s peak was monitored, as shown in Figure 24. At both polarizations used (−0.3 and −1.8 V), the peak due to the cation (BE ∼ 401.6 eV) was not observed after ∼5 nm depth, indicating surface adsorption only, whereas the peak due to the anion (BE ∼ 397.6 eV) was observed at depths up to ∼50 nm, showing that the anion penetrated into the bulk of the electrode. Based on these results, it was shown for all nitrile-containing ILs that the anion compensated for the change in valence of Mn, and not the cation. Sugimoto et al. also used Ar^+ sputtering to depth profile electrodes and show the effect of using $[C_2C_1Im][Tf_2N]$ as an additive to the electrolyte.[222]

2.5.3. Membranes

Fortunato et al. have investigated the stability of supported IL membranes using XPS.[113] In their work, simple ILs $[C_nC_1Im][PF_6]$ ($n = 4, 8$) and $[C_{10}C_1Im][BF_4]$ were studied and compared to the supported IL membrane. Good charge correction was carried out, and also sample irradiation was kept to a maximum of 15 min to avoid possible X-ray damage. The results indicate that the entire membrane surface is covered with IL; based upon the elemental ratios, such as F/N, F/B, and F/P, fluorine is present in both the IL and the membrane, whereas nitrogen, boron, and phosphorus are only present in the ILs. The membranes were also analyzed with XPS after being stored in water for a week.

Mistry et al. investigated the interfacial interactions in aprotic IL-based protonic membranes using XPS.[223] Upon addition of $[C_4C_1Im][Tf_2N]$ to membranes, a new O 1s peak

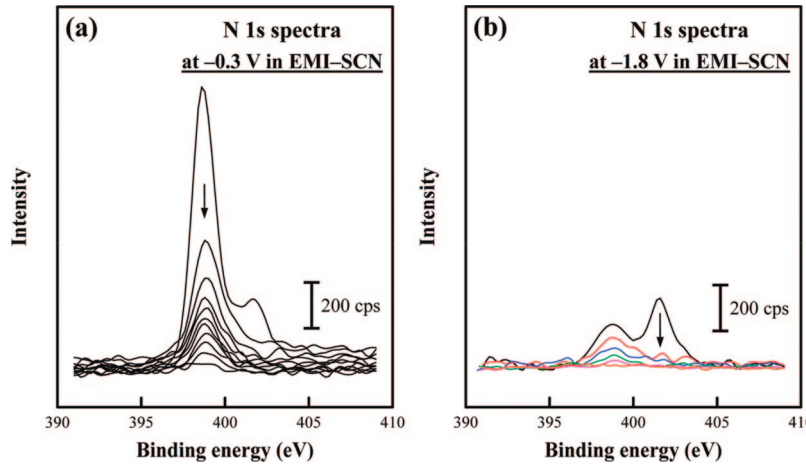

Figure 24. XPS N 1s depth-profiling spectra taken from the Mn oxide electrodes previously polarized at (a) −0.3 V and (b) −1.8 V in EMI-SCN, $[C_2C_1Im][SCN]$. Reprinted with permission from ref 152. Copyright 2009 American Chemical Society.

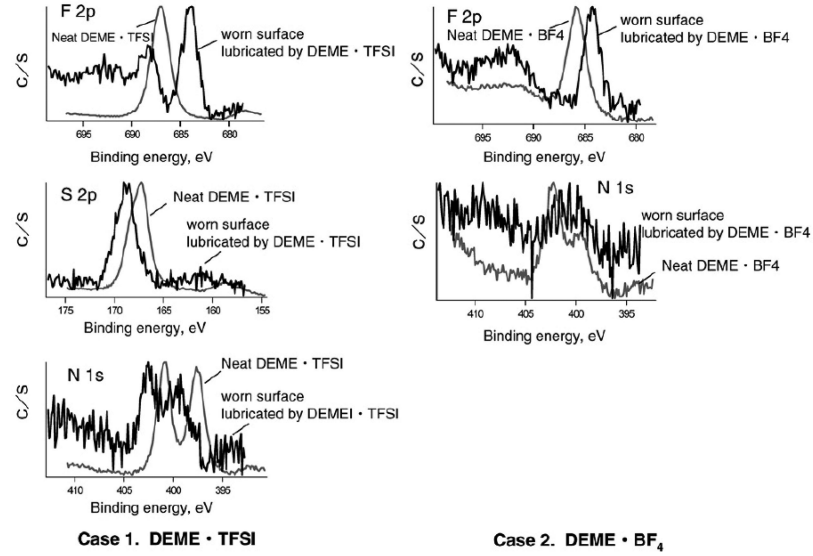

Figure 25. XPS spectra of a worn steel surface lubricated by the ILs *N*,*N*-diethyl-*N*-methyl-*N*-(2-methoxyethyl)ammonium bis(trifluoromethanesulfonyl) imide ([DEME]TFSI) and *N*,*N*-diethyl-*N*-methyl-*N*-(2-methoxyethyl)ammonium tetrafluoroborate ([DEME][BF_4]). Note, the figure published in the original article is incorrectly annotated, the data in the top two panels is due to F 1s photoemission and not F 2p as stated. Reprinted with permission from ref 127. Copyright 2007 Elsevier.

was observed at a relatively high BE of 536 eV. This new peak is not due to the IL, as XPS of neat $[C_4C_1Im][Tf_2N]$ shows a single peak at ~532.5 eV.[115,116] It was concluded that the new peak is due to an SO_3−IL interaction.

2.5.4. Lubricants

Since their proposal as high performance synthetic lubricants,[46] ILs have been extensively studied with respect to their remarkable lubrication and antiwear properties; at the time of writing, there were more than 100 publications available on this topic alone.[177] Much of the research in this field has focused on the use of ILs as neat base oil lubricants. In these cases, the analysis of worn surfaces by XPS revealed the occurrence of complicated tribochemical reactions during friction at boundary conditions that produced surface protective films that helped reduce friction and wear. These tribochemical reactions between active elements in ionic liquids such as P, O, F, B, or O and contacts are quite complicated, and their mechanisms have not been disclosed satisfactorily yet. However, XPS analysis can add information to aid in the identification of the products of these reactions. Being able to investigate ILs using XPS is a major advantage in lubrication research; many of the studies published to date have included analysis of pure ILs of interest[46,125−127,224−227] or used data from the literature in order to either confirm or discount the presence of ILs or IL degradation products on the surfaces analyzed. A good example of this type of study is the work by Kamimura et al.; worn steel−steel contacts were analyzed by XPS, and all high resolution spectra of relevance were compared to the characteristic XP spectra of the neat ILs employed.[127] As can be seen in Figure 25, only traces of the original IL could be observed in the XPS scans of the worn surfaces; at the same time, the scans show peaks characteristic of compounds, including iron sulfates and iron fluorides, which can only arise by direct reaction of the load surface with the IL. This data, in combination with ToF-SIMS analysis, helped the authors conclude that the good tribological performance observed was mainly due to the formation of a tribological layer based on the products of the reaction of the anion with the steel−steel contact.

Additional capabilities of standard XPS instruments can also be used to analyze lubricated surfaces. Minami et al. performed XPS analysis both before and after surface etching

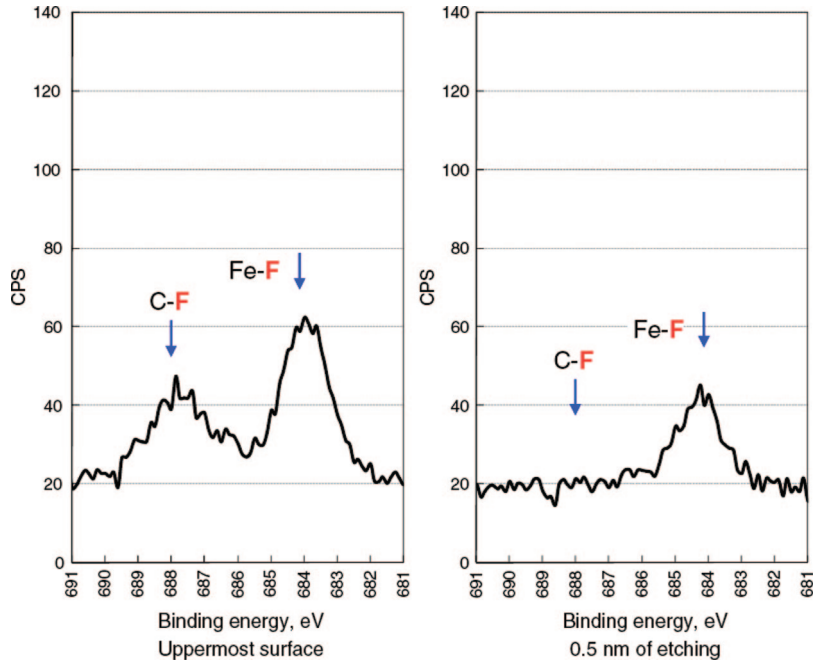

Figure 26. F 1s XPS spectra of flat steel samples rubbed with $[C_2C_1Im][FAP]$ at 10 N, before and after surface etching to 0.5 nm depth. Reprinted with permission from ref 228. Copyright 2008 Springer.

of prerubbed steel surfaces that were lubricated by $[FAP]^-$-based ILs.[228] They observed peaks characteristic of the ILs before etching and those characteristic of metal fluorides after 0.5 nm of etching; see Figure 26. These findings again prompted the authors to suggest that the boundary film was composed of adsorbed anions on the uppermost layers and reacted anion-based species on lower subsurfaces.

Many different metal contacts have been studied by XPS after lubrication with ILs either neat or as lubrication additives.[46,125−127,177,224−226,229−241] ILs have also been used for thin film lubrication of nano- and microelectromechanical systems (NEMS and MEMS), and it is probably in these applications where XPS becomes most useful. First, XPS can be used to check for the successful formation of IL films (PhILLs) on surfaces by comparing the XPS scans of the coated surfaces to those of the pure IL precursor and the clean substrate. Moreover, XPS can be used to look for chemical changes in the film after friction experiments. Mo et al. observed IL peaks on the surface of their successfully dip coated single-crystal silicon surfaces and observed similar spectra of the thin film coated surfaces after friction experiments; see Figure 27.[242] It was subsequently claimed that no chemical modifications have been effected on the film and, therefore, that the lubrication properties of the film were not due to the formation of new compounds after tribochemical reactions. However, their XPS analysis only included wide scans, and high resolution scans of the targeted elements would have given much more information and provided more conclusive evidence. A similar case is observed by Zhu et al.[243]

Kondo et al. use XPS to investigate the coverage of magnetic thin media by protic ILs;[244] they also employed ARXPS to determine the thickness and uniformity of the IL film. By comparing their ARXPS results to an island model, they concluded that their IL films covered the surface of the substrate uniformly. However, as no XP spectra were included in the publication, the reader has no opportunity to consider or question the primary data for himself.

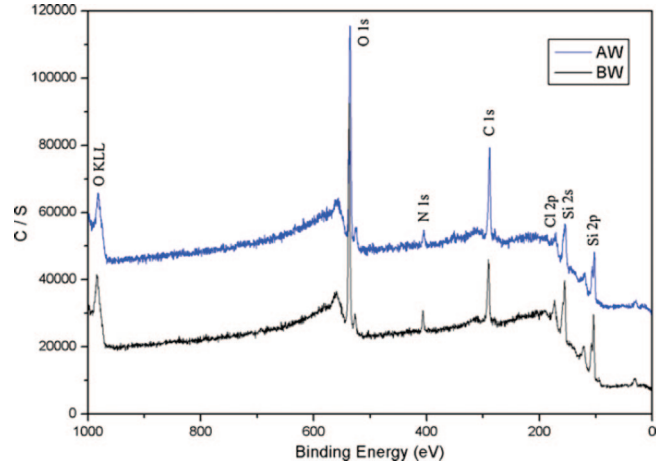

Figure 27. XPS survey spectra of 1-alkyl-3-ethylcarboxylic acid imidazolium chloride, [AEImi]Cl, films on a silicon surface both before and after a wear test (BW, before wear test; AW, after wear test). Reprinted with permission from ref 242. Copyright 2008 Elsevier.

3. Conclusions and Recommendations

In this review we have presented a detailed account on the physical and chemical properties of ILs and IL-based interfaces, based upon results obtained by photoelectron spectroscopies (PES) under UHV conditions. It was realized only some years ago that, due to their very low vapor pressure, ILs do not readily evaporate at room temperature under UHV conditions and also do not contaminate the sensitive UHV systems typically used in Surface Science. Therefore, the field of "Ionic Liquid Surface Science" is very young and strongly expanding. Nowadays, the complete toolbox of UHV-based surface science methods is increasingly applied to investigate IL surfaces with atomic-level accuracy. In this context, XPS, also denoted as electron spectroscopy for chemical analysis (ESCA), is the most prominent UHV-based method. XPS is generally accepted as the most common and powerful tool to analyze the

chemical composition of the near-surface region of condensed matter. It not only allows the quantitative determination of the elemental composition of a sample, but it is also sensitive to the local chemical environment, allowing the identification of chemical states (e.g., oxidation state) of each atom. Furthermore, XPS is inherently surface sensitive; it can be employed to determine composition depth profiles of the near-surface region using angle-resolved XPS (ARXPS), i.e., employing different electron emission angles with different surface sensitivities.

Despite the great achievements so far, IL surface science, particularly the application of XPS as a state-of-the art analytical method to investigate IL surfaces, is still is a strongly growing field. There are an ever increasing number of groups applying such techniques that were not working in surface science before. We were motivated by the impression that the field now requires a comprehensive review article to present what has already been achieved and to allow key strengths and also weaknesses to be highlighted for the healthy development of the field. As mentioned above, the potential is incredible and we believe that the entire IL field can benefit from this review, as many applications could potentially profit from XPS analysis capabilities. Our hope is that this review will have the effect of consolidating the excellent progress made in this research field over the past 5 years and minimize the potential barriers that new researchers would encounter when entering the field.

In the introduction, section 1, we discussed the fundamental principles of photoelectron spectroscopy in general, followed by sections addressing PES of liquids and thereafter the properties and applications of ILs. We thereby put special emphasis on topics that should be considered when studying IL surfaces by PES.

In the main results section, section 2, we addressed the current status of the study of IL interfaces with XPS and also UPS. The data presented demonstrate that the characterization and investigation of the surface properties, at an atomic level of accuracy, is of pivotal importance for ILs, similar in many aspects to the situation for solids. Surface termination, the orientation of the outermost species, segregation effects, surface contaminations, etc. are just some of the most relevant scientific challenges that have been addressed thus far. After these very fundamental studies on simple primary ILs, we addressed more complex IL-based systems, such as supported ionic liquid layers (PhILLs and ChILLs), IL mixtures and solutions, the monitoring of chemical reactions, and finally also materials-based applications. Most of the studies provide very reliable, detailed, and thorough insight into physical and chemical properties. Many studies are only on the exploratory level, and others do not lead to truly unequivocal conclusions, partly because of missing information and/or over-interpretation of available data. These aspects have been commented upon throughout the manuscript.

One of the primary goals, and indeed a motivation for summarizing this rapidly emerging field, was the aim to define recommended standards for both data collection and presentation of future contributions. The analysis of the available literature shows that despite the fact that many spectra have been accumulated, the conclusive power of a significant proportion of the data is severely hampered by two key factors:

(i) important experimental conditions are typically not well-defined and

(ii) background theory and limitations are not so well understood. These factors not only impact upon the quality of conclusions made as a result of experimentation but also hinder the independent reproduction of experiments for verification and method development. In closing, we would like to suggest the following key points, which should be considered when including PES-based data in the presentation of future scientific studies.

(I) A very important point, which is certainly not only restricted to the field of IL surface science, is the inclusion of all relevant information regarding the experimental system in publications or in the associated Supporting Information. Such critical data includes simple and obvious things, including energy resolution, details of charge correction methods, sample temperature, vacuum conditions, applied parameters when sputtering (voltage, current, time, ...), fit parameters, etc. Quite generally, this data is required such that other scientists can use published data for direct comparison to new measurements and, more fundamentally, to increase the credibility of analysis or of derived conclusions. It is critical that all such data is provided for the reader, rather than showing no spectra at all and/or only giving quantification tables. Complete reporting of the experimental parameters employed, such as the photon energy of the applied radiation (e.g., Al Kα vs Mg Kα, He I, He II or synchrotron radiation), angle of photon incidence, angle of electron emission, and experimental resolution, is required for all analysis.

(II) XPS is well suited for quantitative analysis, but this application relies on thorough calibration of the spectrometer; simply using relative sensitivity factors (RSFs, sometimes referred to as ASFs) from the literature often leads to unreliable results. Consequently, when used, it is absolutely critical that the full details of all RSFs employed during analysis should be included in the experimental section. Here, ultrapure ILs containing a large number of different elements (with PE peaks spread over the entire kinetic energy range) open a new and very efficient route for the calibration of PES spectrometers.

(III) Careful calibration of the BE scale, which is also called charge referencing or charge correction, is essential for all analysis. This is particularly important, as ILs do not have a well-defined Fermi "edge" that is commonly used for that purpose in metal substrates. Thus, appropriate internal reference levels must be chosen and, equally important, recorded in all publications. Charge correction is especially required, if small shifts on the order of only several tenths of an electronvolt are used to derive, or support, far reaching conclusions. As a general comment, shifts can only be considered to be real if they are larger than the error bars associated with the determination of the BE.

(IV) The detection limits of the method must to be considered; note that it differs for a simple elemental identification and the much more complex analysis of the chemical environment.

(V) One has to be aware of the fact that, as with all other surfaces, IL surfaces are also prone to contamination. In particular, segregation of bulk contamination (which may be present at concentrations as low as ppm!) can lead to concentrated layers of contamination at the surface. XPS and ARXPS are particularly well suited to verify the cleanness of a surface. An important aspect to note is that IL surfaces, to some extent, can also be cleaned using sputtering with

Ar^+ ions. This procedure can even be used for depth profiling. ARXPS yields significant additional information, from surface termination, orientation of the outermost species, segregation effects, and surface contaminations to nondestructive depth profiling.

(VI) Beam damage is an omnipresent challenge in XPS of molecular systems. Appropriate measures have to be chosen to identify and minimize related changes.

(VII) For complex XPS signals with more than one contribution from the same element, appropriate fitting procedures and according protocols must be developed, thereby allowing comparable and unequivocal peak assignments or species identification. The corresponding parameters and applied constraints employed must be reported alongside the data. It is also strongly recommended that all spectra are given, either in the main body of the paper or in the Supporting Information.

(VIII) Traditional surface science of solid complex surfaces has been particularly successful, especially if more that one experimental method has been employed on the same sample system. This comment also holds for IL surfaces, and thus, the combination of XPS with other methods, such as UPS, MIES, HREELS, RBS, or SFG, is highly recommended.

4. Acknowledgments

P.L., I.J.V., and K.R.J.L. thank the U.K. Engineering and Physical Sciences Research Council (EPSRC) for funding via the Science and Innovation Award (EP/D501229/1). P.L. is currently holder of an EPSRC Advanced Research Fellowship (EP/D073014/1). H.-P.S. and F.M. acknowledge financial support of the Deutsche Forschungsgemeinschaft within the priority program SPP 1191 (Ionic liquids) and the Erlangen Cluster of Excellence "Engineering of Advanced Materials". We are grateful to R. G. Jones, P. Wasserceid, and E. F. Smith for helpful discussion and constructive advice and to Tom Huddle for the design of the cover image.

5. References

(1) Moulder, J. F.; Stickle, W. F.; Sobol, P. E.; Bomben, K. D. *Handbook of X-ray photoelectron spectroscopy: a reference book of standard spectra for identification and interpretation of XPS data*; Physical Electronics: Eden Prairie, MN, 1995.
(2) *Surface Analysis by Auger and X-ray Photoelectron Spectroscopy*; Briggs, D., Grant, J. T., Eds.; IM Publications: Chichester, 2003.
(3) Woodruff, D. P.; Bradshaw, A. M. *Rep. Prog. Phys.* **1994**, *57*, 1029–1080.
(4) Kelly, M. A. In *Surface Analysis by Auger and X-ray Photoelectron Spectroscopy*; Briggs, D., Grant, J. T., Eds.; IM Publications: Chichester, 2003.
(5) Sherwood, P. M. A. *J. Electron Spectrosc. Relat. Phenom.* **2010**, *176*, 2–4.
(6) Kelly, M. A. *J. Electron Spectrosc. Relat. Phenom.* **2010**, *176*, 5–7.
(7) Suzer, S.; Sezen, H.; Ertas, G.; Dana, A. *J. Electron Spectrosc. Relat. Phenom.* **2010**, *176*, 52–57.
(8) Seah, M. P. In *Surface Analysis by Auger and X-ray Photoelectron Spectroscopy*; Briggs, D., Grant, J. T., Eds.; IM Publications: Chichester, 2003.
(9) Siegbahn, K. *Philos. Trans. R. Soc., A: Math. Phys. Eng. Sci.* **1970**, *268*, 33–57.
(10) Hüfner, S. *Photoelectron Spectroscopy: Principles and Applications*, 3rd ed.; Springer-Verlag: Berlin, 2003.
(11) *Practical Surface Analysis*; Briggs, D., Seah, M. P., Eds.; John Wiley and Sons: Chichester, 1994; Vol. 1 (Auger and X-Ray Photoelectron Spectroscopy).
(12) Wagner, C. D.; Davis, L. E.; Zeller, M. V.; Taylor, J. A.; Raymond, R. H.; Gale, L. H. *Surf. Interface Anal.* **1981**, *3*, 211–225.
(13) *Surface Analysis: The Principle Techniques*; Vickerman, J. C., Ed.; John Wiley & Sons: Chichester, 1997.
(14) Morgner, H.; Oberbrodhage, J.; Richter, K.; Roth, K. *J. Phys.: Condens. Matter* **1991**, *3*, 5639–5655.
(15) Ogletree, D. F.; Bluhm, H.; Lebedev, G.; Fadley, C. S.; Hussain, Z.; Salmeron, M. *Rev. Sci. Instrum.* **2002**, *73*, 3872–3877.
(16) Pantförder, J.; Pöllmann, S.; Zhu, J. F.; Borgmann, D.; Denecke, R.; Steinrück, H.-P. *Rev. Sci. Instrum.* **2005**, *76*, 014102.
(17) Tostmann, H.; DiMasi, E.; Pershan, P. S.; Ocko, B. M.; Shpyrko, O. G.; Deutsch, M. *Phys. Rev. B* **2000**, *61*, 7284–7287.
(18) Köhler, S. P. K.; Allan, M.; Kelso, H.; Henderson, D. A.; McKendrick, K. G. *J. Chem. Phys.* **2005**, *122*.
(19) Winter, B.; Faubel, M. *Chem. Rev.* **2006**, *106*, 1176–1211.
(20) Fairbrother, D. H.; Somorjai, G. A. *J. Phys. Chem. B* **2000**, *104*, 4649–4652.
(21) Fellnerfeldegg, H.; Siegbahn, H.; Asplund, L.; Kelfve, P.; Siegbahn, K. *J. Electron Spectrosc. Relat. Phenom.* **1975**, *7*, 421–428.
(22) Siegbahn, H.; Svensson, S.; Lundholm, M. *J. Electron Spectrosc. Relat. Phenom.* **1981**, *24*, 205–213.
(23) Wilson, K. R.; Rude, B. S.; Catalano, T.; Schaller, R. D.; Tobin, J. G.; Co, D. T.; Saykally, R. J. *J. Phys. Chem. B* **2001**, *105*, 3346–3349.
(24) Freiwald, M.; Cramm, S.; Eberhardt, W.; Eisebitt, S. *J. Electron Spectrosc. Relat. Phenom.* **2004**, *137*, 413–416.
(25) de Boer, J. H. *The Dynamical Character of Adsorption*; Clarendon Press: Oxford, 1968.
(26) Kondow, T.; Mafune, F. *Annu. Rev. Phys. Chem.* **2000**, *51*, 731–761.
(27) Faubel, M. In *Photoionization and photodetachment*; Cheuk-Yiu, N. G., Ed.; World Scientific Publishing: Singapore, 2000.
(28) *Ionic Liquids in Synthesis*, 2nd ed.; Wasserscheid, P., Welton, T., Eds.; Wiley-VCH: Weinheim, 2008.
(29) Every, H. A.; Bishop, A. G.; MacFarlane, D. R.; Oradd, G.; Forsyth, M. *Phys. Chem. Chem. Phys.* **2004**, *6*, 1758–1765.
(30) Annat, G.; MacFarlane, D. R.; Forsyth, M. *J. Phys. Chem. B* **2007**, *111*, 9018–9024.
(31) Lopes, J. N. C.; Cordeiro, T. C.; Esperança, J. M. S. S.; Guedes, H. J. R.; Huq, S.; Rebelo, L. P. N.; Seddon, K. R. *J. Phys. Chem. B* **2005**, *109*, 3519–3525.
(32) Plechkova, N. V.; Seddon, K. R. *Chem. Soc. Rev.* **2008**, *37*, 123–150.
(33) MacFarlane, D. R.; Seddon, K. R. *Aust. J. Chem.* **2007**, *60*, 3–5.
(34) Mantz, R. A. In *Ionic liquids in synthesis*; Wasserscheid, P., Welton, T., Eds.; Wiley-VCH: Weinheim, 2008.
(35) Stark, A.; Seddon, K. R. In *Kirk-Othmer Encyclopaedia of Chemical Technology*, 5th ed.; Seidel, A., Ed.; John Wiley & Sons: New Jersey, Wienheim, 2007; Vol. 26.
(36) Wilkes, J. S. *Green Chem.* **2002**, *4*, 73–80.
(37) Anthony, J. L.; Brennecke, J. F.; Holbrey, J. D.; Maginn, E. J.; Mantz, R. A.; Rogers, R. D.; Trulove, P. C.; Visser, A. E.; Welton, T. In *Ionic liquids in synthesis*, 2nd ed.; Wasserscheid, P., Welton, T., Eds.; Wiley-VCH: Weinheim, 2008.
(38) Wasserscheid, P.; Schulz, P. In *Ionic liquids in synthesis*, 2nd ed.; Wasserscheid, P., Welton, T., Eds.; Wiley-VCH: Weinheim, 2008.
(39) Weingärtner, H. *Angew. Chem., Int. Ed.* **2008**, *47*, 654–670.
(40) Chiappe, C.; Pieraccini, D. *J. Phys. Org. Chem.* **2005**, *18*, 275–297.
(41) Endres, F.; El Abedin, S. Z. *Phys. Chem. Chem. Phys.* **2006**, *8*, 2101–2116.
(42) Tokuda, H.; Hayamizu, K.; Ishii, K.; Susan, M.; Watanabe, M. *J. Phys. Chem. B* **2005**, *109*, 6103–6110.
(43) Krossing, I.; Slattery, J. M.; Daguenet, C.; Dyson, P. J.; Oleinikova, A.; Weingärtner, H. *J. Am. Chem. Soc.* **2006**, *128*, 13427–13434.
(44) Baranyai, K. J.; Deacon, G. B.; MacFarlane, D. R.; Pringle, J. M.; Scott, J. L. *Aust. J. Chem.* **2004**, *57*, 145–147.
(45) Wasserscheid, P. *Nature* **2006**, *439*, 797–797.
(46) Ye, C. F.; Liu, W. M.; Chen, Y. X.; Yu, L. G. *Chem. Commun.* **2001**, 2244–2245.
(47) Han, X.; Armstrong, D. W. *Acc. Chem. Res.* **2007**, *40*, 1079–1086.
(48) Riisager, A.; Fehrmann, R.; Haumann, M.; Wasserscheid, P. *Eur. J. Inorg. Chem.* **2006**, 695–706.
(49) Rogers, R. D.; Seddon, K. R. *Science* **2003**, *302*, 792–793.
(50) Earle, M. J.; Esperança, J. M. S. S.; Gilea, M. A.; Lopes, J. N. C.; Rebelo, L. P. N.; Magee, J. W.; Seddon, K. R.; Widegren, J. A. *Nature* **2006**, *439*, 831–834.
(51) Strasser, D.; Goulay, F.; Kelkar, M. S.; Maginn, E. J.; Leone, S. R. *J. Phys. Chem. A* **2007**, *111*, 3191–3195.
(52) Leal, J. P.; Esperança, J. M. S. S.; da Piedade, M. E. M.; Lopes, J. N. C.; Rebelo, L. P. N.; Seddon, K. R. *J. Phys. Chem. A* **2007**, *111*, 6176–6182.
(53) Armstrong, J. P.; Hurst, C.; Jones, R. G.; Licence, P.; Lovelock, K. R. J.; Satterley, C. J.; Villar-Garcia, I. J. *Phys. Chem. Chem. Phys.* **2007**, *9*, 982–990.
(54) Ludwig, R.; Kragl, U. *Angew. Chem., Int. Ed.* **2007**, *46*, 6582–6584.

(55) Esperança, J. M. S. S.; Lopes, J. N. C.; Tariq, M.; Santos, L. M. N. B. F.; Magee, J. W.; Rebelo, L. P. N. *J. Chem. Eng. Data* **2010**, *55*, 3–12.
(56) Deyko, A.; Lovelock, K. R. J.; Corfield, J.-A.; Taylor, A. W.; Gooden, P. N.; Villar-Garcia, I. J.; Licence, P.; Jones, R. G.; Krasovskiy, V. G.; Chernikova, E. A.; Kustov, L. M. *Phys. Chem. Chem. Phys.* **2009**, *11*, 8544–8555.
(57) Zaitsau, D. H.; Kabo, G. J.; Strechan, A. A.; Paulechka, Y. U.; Tschersich, A.; Verevkin, S. P.; Heintz, A. *J. Phys. Chem. A* **2006**, *110*, 7303–7306.
(58) Emel'yanenko, V. N.; Verevkin, S. P.; Heintz, A. *J. Am. Chem. Soc.* **2007**, *129*, 3930–3937.
(59) Seeberger, A.; Andresen, A. K.; Jess, A. *Phys. Chem. Chem. Phys.* **2009**, *11*, 9375–9381.
(60) *Handbook of Chemistry and Physics: a ready-reference book of chemical and physical data*, 87th ed.; Lide, D. R., Ed.; CRC Press: Boca Raton, FL, 2006.
(61) Yoshizawa, M.; Xu, W.; Angell, C. A. *J. Am. Chem. Soc.* **2003**, *125*, 15411–15419.
(62) Emel'yanenko, V. N.; Verevkin, S. P.; Heintz, A.; Voss, K.; Schulz, A. *J. Phys. Chem. B* **2009**, *113*, 9871–9876.
(63) Hagiwara, R.; Matsumoto, K.; Tsuda, T.; Kohara, S.; Suzuya, K.; Ito, Y. *Proc. 6th Int. Symp. Molten Salt Chem. Technol.* **2001**, 136–139.
(64) Hagiwara, R.; Matsumoto, K.; Nakamori, Y.; Tsuda, T.; Ito, Y.; Matsumoto, H.; Momota, K. *J. Electrochem. Soc.* **2003**, *150*, D195–D199.
(65) Vila, J.; Gines, P.; Rilo, E.; Cabeza, O.; Varela, L. M. *Fluid Phase Equilib.* **2006**, *247*, 32–39.
(66) Van Valkenburg, M. E.; Vaughn, R. L.; Williams, M.; Wilkes, J. S. *Thermochim. Acta* **2005**, *425*, 181–188.
(67) Xu, W.; Cooper, E. I.; Angell, C. A. *J. Phys. Chem. B* **2003**, *107*, 6170–6178.
(68) Tsuzuki, S.; Tokuda, H.; Hayamizu, K.; Watanabe, M. *J. Phys. Chem. B* **2005**, *109*, 16474–16481.
(69) Kanakubo, M.; Harris, K. R.; Tsuchihashi, N.; Ibuki, K.; Ueno, M. *J. Phys. Chem. B* **2007**, *111*, 2062–2069.
(70) Stolwijk, N. A.; Obeidi, S. *Electrochim. Acta* **2009**, *54*, 1645–1653.
(71) Every, H.; Bishop, A. G.; Forsyth, M.; MacFarlane, D. R. *Electrochim. Acta* **2000**, *45*, 1279–1284.
(72) Tokuda, H.; Ishii, K.; Susan, M.; Tsuzuki, S.; Hayamizu, K.; Watanabe, M. *J. Phys. Chem. B* **2006**, *110*, 2833–2839.
(73) Tokuda, H.; Hayamizu, K.; Ishii, K.; Abu Bin Hasan Susan, M.; Watanabe, M. *J. Phys. Chem. B* **2004**, *108*, 16593–16600.
(74) Hussey, C. L.; Sanders, J. R.; Oye, H. A. *J. Electrochem. Soc.* **1985**, *132*, 2156–2158.
(75) Leys, J.; Wübbenhorst, M.; Menon, C. P.; Rajesh, R.; Thoen, J.; Glorieux, C.; Nockemann, P.; Thijs, B.; Binnemans, K.; Longuemart, S. *J. Chem. Phys.* **2008**, *128*, 064509.
(76) Hardacre, C.; Holbrey, J. D.; Nieuwenhuyzen, M.; Youngs, T. G. A. *Acc. Chem. Res.* **2007**, *40*, 1146–1155.
(77) Seddon, K. R.; Stark, A.; Torres, M. J. *Pure Appl. Chem.* **2000**, *72*, 2275–2287.
(78) Scammells, P. J.; Scott, J. L.; Singer, R. D. *Aust. J. Chem.* **2005**, *58*, 155–169.
(79) Widegren, J. A.; Laesecke, A.; Magee, J. W. *Chem. Commun.* **2005**, 1610–1612.
(80) Earle, M. J.; Gordon, C. M.; Plechkova, N. V.; Seddon, K. R.; Welton, T. *Anal. Chem.* **2007**, *79*, 758–764.
(81) Widegren, J. A.; Saurer, E. M.; Marsh, K. N.; Magee, J. W. *J. Chem. Thermodyn.* **2005**, *37*, 569–575.
(82) Wilkes, J. S.; Zaworotko, M. J. *J. Chem. Soc., Chem. Commun.* **1992**, 965–967.
(83) Lovelock, K. R. J. Ph.D. Thesis, University of Nottingham, 2008.
(84) Taylor, A. W.; Lovelock, K. R. J.; Deyko, A.; Licence, P.; Jones, R. G. *Phys. Chem. Chem. Phys.* **2010**, *12*, 1772–1783.
(85) Paape, N.; Wei, W.; Bösmann, A.; Kolbeck, C.; Maier, F.; Steinrück, H.-P.; Wasserscheid, P.; Schulz, P. S. *Chem. Commun.* **2008**, 3867–3869.
(86) Earle, M. J.; Katdare, S. P.; Seddon, K. R. *Org. Lett.* **2004**, *6*, 707–710.
(87) Pârvulescu, V. I.; Hardacre, C. *Chem. Rev.* **2007**, *107*, 2615–2665.
(88) Seddon, K. R. *J. Chem. Technol. Biotechnol.* **1997**, *68*, 351–356.
(89) Earle, M. J.; Seddon, K. R. *Pure Appl. Chem.* **2000**, *72*, 1391–1398.
(90) Couling, D. J.; Bernot, R. J.; Docherty, K. M.; Dixon, J. K.; Maginn, E. J. *Green Chem.* **2006**, *8*, 82–90.
(91) Swatloski, R. P.; Holbrey, J. D.; Rogers, R. D. *Green Chem.* **2003**, *5*, 361–363.
(92) Coleman, D.; Gathergood, N. *Chem. Soc. Rev.* **2010**, *39*, 600–637.
(93) Kralisch, D.; Reinhardt, D.; Kreisel, G. *Green Chem.* **2007**, *9*, 1308–1318.
(94) Anastas, P. T.; Warner, J. C. *Green Chemistry Theory and Practice*; Oxford University Press: Oxford, 1998.
(95) Jastorff, B.; Störmann, R.; Ranke, J.; Mölter, K.; Stock, F.; Oberheitmann, B.; Hoffmann, W.; Hoffmann, J.; Nüchter, M.; Ondruschka, B.; Filser, J. *Green Chem.* **2003**, *5*, 136–142.
(96) Capello, C.; Fischer, U.; Hungerbühler, K. *Green Chem.* **2007**, *9*, 927–934.
(97) Davis, J. H. *Chem. Lett.* **2004**, *33*, 1072–1077.
(98) Lee, S. G. *Chem. Commun.* **2006**, 1049–1063.
(99) Anthony, J. L.; Anderson, J. L.; Maginn, E. J.; Brennecke, J. F. *J. Phys. Chem. B* **2005**, *109*, 6366–6374.
(100) Huang, J.; Riisager, A.; Berg, R. W.; Fehrmann, R. *J. Mol. Catal. A: Chem.* **2008**, *279*, 170–176.
(101) Aliaga, C.; Santos, C. S.; Baldelli, S. *Phys. Chem. Chem. Phys.* **2007**, *9*, 3683–3700.
(102) Santos, C. S.; Baldelli, S. *Chem. Soc. Rev.* **2010**, *39*, 2136–2145.
(103) Steinrück, H.-P. *Surf. Sci.* **2010**, *604*, 481–484.
(104) Escard, J.; Mavel, G.; Guerchai, Je; Kergoat, R. *Inorg. Chem.* **1974**, *13*, 695–701.
(105) Lindberg, B. J.; Hedman, J. *Chem. Scr.* **1975**, *7*, 155–166.
(106) Wagner, C. D. *J. Vac. Sci. Technol.* **1978**, *15*, 518–523.
(107) Wagner, C. D.; Zatko, D. A.; Raymond, R. H. *Anal. Chem.* **1980**, *52*, 1445–1451.
(108) Gniewek, A.; Trzeciak, A. M.; Ziółkowski, J. J.; Kępiński, L.; Wrzyszcz, J.; Tylus, W. *J. Catal.* **2005**, *229*, 332–343.
(109) Chen, Y. L.; Chen, S.; Frank, C.; Israelachvili, J. *J. Colloid Interface Sci.* **1992**, *153*, 244–265.
(110) Herder, P. C.; Claesson, P. M.; Herder, C. E. *J. Colloid Interface Sci.* **1987**, *119*, 155–167.
(111) Smith, E. F.; Villar Garcia, I. J.; Briggs, D.; Licence, P. *Chem. Commun.* **2005**, 5633–5635.
(112) Caporali, S.; Bardi, U.; Lavacchi, A. *J. Electron Spectrosc. Relat. Phenom.* **2006**, *151*, 4–8.
(113) Fortunato, R.; Afonso, C. A. M.; Benavente, J.; Rodríguez-Castellón, E.; Crespo, J. G. *J. Membr. Sci.* **2005**, *256*, 216–223.
(114) Yoshimura, D.; Yokoyama, T.; Nishi, T.; Ishii, H.; Ozawa, R.; Hamaguchi, H.; Seki, K. *J. Electron Spectrosc. Relat. Phenom.* **2005**, *144*, 319–322.
(115) Kolbeck, C.; Killian, M.; Maier, F.; Paape, N.; Wasserscheid, P.; Steinrück, H.-P. *Langmuir* **2008**, *24*, 9500–9507.
(116) Lovelock, K. R. J.; Kolbeck, C.; Cremer, T.; Paape, N.; Schulz, P. S.; Wasserscheid, P.; Maier, F.; Steinrück, H.-P. *J. Phys. Chem. B* **2009**, *113*, 2854–2864.
(117) Zhang, Q. H.; Liu, S. M.; Li, Z. P.; Li, J.; Chen, Z. J.; Wang, R. F.; Lu, L. J.; Deng, Y. Q. *Chem.—Eur. J.* **2009**, *15*, 765–778.
(118) Citrin, P. H.; Thomas, T. D. *J. Chem. Phys.* **1972**, *57*, 4446–4461.
(119) Smith, E. F.; Rutten, F. J. M.; Villar-Garcia, I. J.; Briggs, D.; Licence, P. *Langmuir* **2006**, *22*, 9386–9392.
(120) Kolbeck, C.; Cremer, T.; Lovelock, K. R. J.; Paape, N.; Schulz, P. S.; Wasserscheid, P.; Maier, F.; Steinrück, H.-P. *J. Phys. Chem. B* **2009**, *113*, 8682–8688.
(121) Chiappe, C.; Malvaldi, M.; Melai, B.; Fantini, S.; Bardi, U.; Caporali, S. *Green Chem.* **2010**, *12*, 77–80.
(122) Villar-Garcia, I. J. Ph.D. Thesis, University of Nottingham, 2009.
(123) Lockett, V.; Sedev, R.; Bassell, C.; Ralston, J. *Phys. Chem. Chem. Phys.* **2008**, *10*, 1330–1335.
(124) Kwon, J. H.; Youn, S. W.; Kang, Y. C. *Bull. Kor. Chem. Soc.* **2006**, *27*, 1851–1853.
(125) Lu, Q. M.; Wang, H. Z.; Ye, C. F.; Liu, W. M.; Xue, Q. J. *Tribol. Int.* **2004**, *37*, 547–552.
(126) Liu, W. M.; Ye, C. F.; Gong, Q. Y.; Wang, H. Z.; Wang, P. *Tribol. Lett.* **2002**, *13*, 81–85.
(127) Kamimura, H.; Kubo, T.; Minami, I.; Mori, S. *Tribol. Int.* **2007**, *40*, 620–625.
(128) Hunt, P. A.; Gould, I. R.; Kirchner, B. *Aust. J. Chem.* **2007**, *60*, 9–14.
(129) Neaţu, F.; Pârvulescu, V. I.; Michelet, V.; Gênet, J. P.; Goguet, A.; Hardacre, C. *New J. Chem.* **2009**, *33*, 102–106.
(130) Lovelock, K. R. J.; Smith, E. F.; Deyko, A.; Villar-Garcia, I. J.; Licence, P.; Jones, R. G. *Chem. Commun.* **2007**, 4866–4868.
(131) Taylor, A. W.; Qiu, F. L.; Villar-Garcia, I. J.; Licence, P. *Chem. Commun.* **2009**, 5817–5819.
(132) Höfft, O.; Bahr, S.; Himmerlich, M.; Krischok, S.; Schaefer, J. A.; Kempter, V. *Langmuir* **2006**, *22*, 7120–7123.
(133) Gottfried, J. M.; Maier, F.; Rossa, J.; Gerhard, D.; Schulz, P. S.; Wasserscheid, P.; Steinrück, H.-P. *Z. Phys. Chem.—Int. J. Res. Phys. Chem. Chem. Phys.* **2006**, *220*, 1439–1453.
(134) Maier, F.; Gottfried, J. M.; Rossa, J.; Gerhard, D.; Schulz, P. S.; Schwieger, W.; Wasserscheid, P.; Steinrück, H.-P. *Angew. Chem., Int. Ed.* **2006**, *45*, 7778–7780.
(135) Cremer, T.; Killian, M.; Gottfried, J. M.; Paape, N.; Wasserscheid, P.; Maier, F.; Steinrück, H.-P. *ChemPhysChem* **2008**, *9*, 2185–2190.
(136) Maier, F.; Cremer, T.; Kolbeck, C.; Lovelock, K. R. J.; Paape, N.; Schulz, P. S.; Wasserscheid, P.; Steinrück, H.-P. *Phys. Chem. Chem. Phys.* **2010**, *12*, 1905–1915.

(137) Iwahashi, T.; Nishi, T.; Yamane, H.; Miyamae, T.; Kanai, K.; Seki, K.; Kim, D.; Ouchi, Y. *J. Phys. Chem. C* **2009**, *113*, 19237–19243.
(138) Bernardi, F.; Scholten, J. D.; Fecher, G. H.; Dupont, J.; Morais, J. *Chem. Phys. Lett.* **2009**, *479*, 113–116.
(139) Beamson, G.; Briggs, D. *Mol. Phys.* **1992**, *76*, 919–936.
(140) Yarzhemsky, V.; Nefedov, V. I.; Trzhaskovskaya, M. B.; Band, I. M.; Szargan, R. *J. Electron Spectrosc. Relat. Phenom.* **2002**, *123*, 1–10.
(141) Briggs, D.; Beamson, G. *Anal. Chem.* **1993**, *65*, 1517–1523.
(142) Svensson, S.; Eriksson, B.; Martensson, N.; Wendin, G.; Gelius, U. *J. Electron Spectrosc. Relat. Phenom.* **1988**, *47*, 327–384.
(143) Sjogren, B.; Svensson, S.; Debrito, A. N.; Correia, N.; Keane, M. P.; Enkvist, C.; Lunell, S. *J. Chem. Phys.* **1992**, *96*, 6389–6398.
(144) Beamson, G.; Clark, D. T.; Kendrick, J.; Briggs, D. *J. Electron Spectrosc. Relat. Phenom.* **1991**, *57*, 79–90.
(145) Briggs, D.; Fairley, N. *Surf. Interface Anal.* **2002**, *33*, 283–290.
(146) Silvester, D. S.; Broder, T. L.; Aldous, L.; Hardacre, C.; Crossley, A.; Compton, R. G. *Analyst* **2007**, *132*, 196–198.
(147) Chang, J. K.; Lee, M. T.; Tsai, W. T.; Deng, M. J.; Sun, I. W. *Chem. Mater.* **2009**, *21*, 2688–2695.
(148) Shigeyasu, M.; Murayama, H.; Tanaka, H. *Chem. Phys. Lett.* **2008**, *463*, 373–377.
(149) Hashimoto, H.; Ohno, A.; Nakajima, K.; Suzuki, M.; Tsuji, H.; Kimura, K. *Surf. Sci.* **2010**, *604*, 464–469.
(150) Krischok, S.; Eremtchenko, M.; Himmerlich, M.; Lorenz, P.; Uhlig, J.; Neumann, A.; Öttking, R.; Beenken, W. J. D.; Höfft, O.; Bahr, S.; Kempter, V.; Schaefer, J. A. *J. Phys. Chem. B* **2007**, *111*, 4801–4806.
(151) Chang, J. K.; Lee, M. T.; Cheng, C. W.; Tsai, W. T.; Deng, M. J.; Hsieh, Y. C.; Sun, I. W. *J. Mater. Chem.* **2009**, *19*, 3732–3738.
(152) Chang, J. K.; Lee, M. T.; Tsai, W. T.; Deng, M. J.; Cheng, H. F.; Sun, I. W. *Langmuir* **2009**, *25*, 11955–11960.
(153) Nesbitt, H. W.; Bancroft, G. M.; Davidson, R.; McIntyre, N. S.; Pratt, A. R. *Am. Mineral.* **2004**, *89*, 878–882.
(154) Grant, J. T. In *Surface Analysis by Auger and X-ray Photoelectron Spectroscopy*; Briggs, D., Grant, J. T., Eds.; IM Publications: Chichester, 2003.
(155) Nguyen, M. D.; Nguyen, L. V.; Jeon, E. H.; Kim, J. H.; Cheong, M.; Kim, H. S.; Lee, J. S. *J. Catal.* **2008**, *258*, 5–13.
(156) Gupta, R. P.; Sen, S. K. *Phys. Rev. B* **1974**, *10*, 71–77.
(157) Gupta, R. P.; Sen, S. K. *Phys. Rev. B* **1975**, *12*, 15–19.
(158) Grosvenor, A. P.; Kobe, B. A.; Biesinger, M. C.; McIntyre, N. S. *Surf. Interface Anal.* **2004**, *36*, 1564–1574.
(159) Nguyen, M. D.; Nguyen, L. V.; Lee, J. S.; Han, J. S.; Jeong, B. H.; Cheong, M.; Kim, H. S.; Kang, H. J. *Bull. Kor. Chem. Soc.* **2008**, *29*, 1364–1368.
(160) Beamson, G.; Clark, D. T.; Law, D. S. L. *Surf. Interface Anal.* **1999**, *27*, 76–86.
(161) Briggs, D.; Beamson, G. *Surface Spectra*; Manchester, 2000.
(162) *High Resolution XPS of Organic Polymers: The Scienta ESCA300 Database*; Briggs, D., Beanson, G., Eds.; John Wiley and Sons: Chichester, 1992.
(163) Poole, R. T.; Jenkin, J. G.; Liesegang, J.; Leckey, R. C. G. *Phys. Rev. B* **1975**, *11*, 5179–5189.
(164) Mott, N. F.; Gurney, R. W. *Electronic Processes in Ionic Crystals*, 2nd ed.; Oxford University Press: Oxford, 1948.
(165) Nishi, T.; Iwahashi, T.; Yamane, H.; Ouchi, Y.; Kanai, K.; Seki, K. *Chem. Phys. Lett.* **2008**, *455*, 213–217.
(166) Kotani, A.; Shin, S. *Rev. Mod. Phys.* **2001**, *73*, 203–246.
(167) Kanai, K.; Nishi, T.; Iwahashi, T.; Ouchi, Y.; Seki, K.; Harada, Y.; Shin, S. *J. Chem. Phys.* **2008**, *129*.
(168) Kanai, K.; Nishi, T.; Iwahashi, T.; Ouchi, Y.; Seki, K.; Harada, Y.; Shin, S. *J. Electron Spectrosc. Relat. Phenom.* **2009**, *174*, 110–115.
(169) Xiao, L.; Johnson, K. E. *J. Electrochem. Soc.* **2003**, *150*, E307−E311.
(170) Krischok, S.; Öttking, R.; Beenken, W. J. D.; Himmerlich, M.; Lorenz, P.; Höfft, O.; Bahr, S.; Kempter, V.; Schaefer, J. A. *Z. Phys. Chem.*−*Int. J. Res. Phys. Chem. Chem. Phys.* **2006**, *220*, 1407–1416.
(171) Baldelli, S. *Acc. Chem. Res.* **2008**, *41*, 421–431.
(172) Santos, C. S.; Baldelli, S. *J. Phys. Chem. B* **2009**, *113*, 923–933.
(173) Jeon, Y.; Sung, J.; Bu, W.; Vaknin, D.; Ouchi, Y.; Kim, D. *J. Phys. Chem. C* **2008**, *112*, 19649–19654.
(174) Jiang, W.; Wang, Y. T.; Yan, T. Y.; Voth, G. A. *J. Phys. Chem. C* **2008**, *112*, 1132–1139.
(175) Souda, R. *J. Phys. Chem. B* **2008**, *112*, 15349–15354.
(176) Souda, R.; Günster, J. *J. Chem. Phys.* **2008**, *129*, 094707.
(177) Bermúdez, M. D.; Jiménez, A. E.; Sanes, J.; Carrión, F. J. *Molecules* **2009**, *14*, 2888–2908.
(178) Souda, R. *J. Chem. Phys.* **2009**, *130*, 244707.
(179) Souda, R. *J. Phys. Chem. B* **2009**, *113*, 12973–12977.
(180) Souda, R. *J. Chem. Phys.* **2009**, *131*, 084702.
(181) Sobota, M.; Nikiforidis, I.; Hieringer, W.; Paape, N.; Happel, M.; Steinrück, H.-P.; Wasserscheid, P.; Laurin, M.; Libuda, J. *Langmuir* **2010**, *26*, 7199–7207.
(182) Bovio, S.; Podesta, A.; Lenardi, C.; Milani, P. *J. Phys. Chem. B* **2009**, *113*, 6600–6603.
(183) Du, P.; Liu, S. N.; Wu, P.; Cai, C. X. *Electrochim. Acta* **2007**, *52*, 6534–6547.
(184) Kocharova, N.; Aaritalo, T.; Leiro, J.; Kankare, J.; Lukkari, J. *Langmuir* **2007**, *23*, 3363–3371.
(185) Kocharova, N.; Leiro, J.; Lukkari, J.; Heinonen, M.; Skala, T.; Sutara, F.; Skoda, M.; Vondracek, M. *Langmuir* **2008**, *24*, 3235–3243.
(186) Zhang, H.; Cui, H. *Langmuir* **2009**, *25*, 2604–2612.
(187) Dannenberger, O.; Weiss, K.; Himmel, H. J.; Jager, B.; Buck, M.; Woll, C. *Thin Solid Films* **1997**, *307*, 183–191.
(188) Chi, Y. S.; Hwang, S.; Lee, B. S.; Kwak, J.; Choi, I. S.; Lee, S. *Langmuir* **2005**, *21*, 4268–4271.
(189) Lee, B. S.; Chi, Y. S.; Lee, J. K.; Choi, I. S.; Song, C. E.; Namgoong, S. K.; Lee, S. G. *J. Am. Chem. Soc.* **2004**, *126*, 480–481.
(190) Lee, B. S.; Lee, S. *Bull. Kor. Chem. Soc.* **2004**, *25*, 1531–1537.
(191) Hwang, S.; Lee, B. S.; Chi, Y. S.; Kwak, J.; Choi, I. S.; Lee, S. G. *Electrochim. Acta* **2008**, *53*, 2630–2636.
(192) Chi, Y. S.; Lee, J. K.; Lee, S.; Choi, I. S. *Langmuir* **2004**, *20*, 3024–3027.
(193) Coman, S. M.; Florea, M.; Pârvulescu, V. I.; David, V.; Medvedovici, A.; De Vos, D.; Jacobs, P. A.; Poncelet, G.; Grange, P. *J. Catal.* **2007**, *249*, 359–369.
(194) Park, M. J.; Lee, J. K.; Lee, B. S.; Lee, Y. W.; Choi, I. S.; Lee, S. G. *Chem. Mater.* **2006**, *18*, 1546–1551.
(195) Yu, B.; Zhou, F.; Liu, G.; Liang, Y.; Huck, W. T. S.; Liu, W. M. *Chem. Commun.* **2006**, 2356–2358.
(196) Wang, Z. J.; Zhang, Q. X.; Kuehner, D.; Xu, X. Y.; Ivaska, A.; Niu, L. *Carbon* **2008**, *46*, 1687–1692.
(197) Wang, M.; Schneider, A.; Niedziółka-Jónsson, J.; Marcon, L.; Ghodbane, S.; Steinmüller-Nethl, D.; Li, M.; Boukherroub, R.; Szunerits, S. *Electrochim. Acta* **2010**, *55*, 1582–1587.
(198) Holbrey, J. D.; Seddon, K. R. *J. Chem. Soc., Dalton Trans.* **1999**, 2133–2139.
(199) Xiao, D.; Rajian, J. R.; Hines, L. G.; Li, S. F.; Bartsch, R. A.; Quitevis, E. L. *J. Phys. Chem. B* **2008**, *112*, 13316–13325.
(200) Mikkola, J. P.; Virtanen, P.; Karhu, H.; Salmi, T.; Murzin, D. Y. *Green Chem.* **2006**, *8*, 197–205.
(201) Mikkola, J. P. T.; Virtanen, P. P.; Kordas, K.; Karhu, H.; Salmi, T. O. *Appl. Catal. A: Gen.* **2007**, *328*, 68–76.
(202) Ruta, M.; Laurenczy, G.; Dyson, P. J.; Kiwi-Minsker, L. *J. Phys. Chem. C* **2008**, *112*, 17814–17819.
(203) Tao, R. T.; Miao, S. D.; Liu, Z. M.; Xie, Y.; Han, B. X.; An, G. M.; Ding, K. L. *Green Chem.* **2009**, *11*, 96–101.
(204) Sobota, M.; Schmid, M.; Happel, M.; Amende, M.; Maier, F.; Steinrück, H.-P.; Paape, N.; Wasserscheid, P.; Laurin, M.; Gottfried, J. M.; Libuda, J. *Phys. Chem. Chem. Phys.* **2010**, in press.
(205) Qiu, F. L.; Taylor, A. W.; Men, S.; Villar-Garcia, I. J.; Licence, P. *Phys. Chem. Chem. Phys.* **2010**, *12*, 1982–1990.
(206) Taylor, A. W.; Qiu, F. L.; Hu, J. P.; Licence, P.; Walsh, D. A. *J. Phys. Chem. B* **2008**, *112*, 13292–13299.
(207) Barrosse-Antle, L. E.; Aldous, L.; Hardacre, C.; Bond, A. M.; Compton, R. G. *J. Phys. Chem. C* **2009**, *113*, 7750–7754.
(208) Souda, R. *J. Chem. Phys.* **2008**, *129*, 124707.
(209) Torimoto, T.; Tsuda, T.; Okazaki, K.; Kuwabata, S. *Adv. Mater.* **2010**, *22*, 1196–1221.
(210) Dupont, J.; Scholten, J. D. *Chem. Soc. Rev.* **2010**, *39*, 1780–1804.
(211) Hu, Y.; Yang, H. M.; Zhang, Y. C.; Hou, Z. S.; Wang, X. R.; Qiao, Y. X.; Li, H.; Feng, B.; Huang, Q. F. *Catal. Commun.* **2009**, *10*, 1903–1907.
(212) Scheeren, C. W.; Machado, G.; Teixeira, S. R.; Morais, J.; Domingos, J. B.; Dupont, J. *J. Phys. Chem. B* **2006**, *110*, 13011–13020.
(213) Fonseca, G. S.; Machado, G.; Teixeira, S. R.; Fecher, G. H.; Morais, J.; Alves, M. C. M.; Dupont, J. *J. Colloid Interface Sci.* **2006**, *301*, 193–204.
(214) Umpierre, A. P.; Machado, G.; Fecher, G. H.; Morais, J.; Dupont, J. *Adv. Synth. Catal.* **2005**, *347*, 1404–1412.
(215) Khatri, O. P.; Adachi, K.; Murase, K.; Okazaki, K.; Torimoto, T.; Tanaka, N.; Kuwabata, S.; Sugimura, H. *Langmuir* **2008**, *24*, 7785–7792.
(216) Tsuda, T.; Kurihara, T.; Hoshino, Y.; Kiyama, T.; Okazaki, K.; Torimoto, T.; Kuwabata, S. *Electrochemistry* **2009**, *77*, 693–695.
(217) Wu, B. H.; Hu, D.; Kuang, Y. J.; Liu, B.; Zhang, X. H.; Chen, J. H. *Angew. Chem., Int. Ed.* **2009**, *48*, 4751–4754.
(218) Imanishi, A.; Tamura, M.; Kuwabata, S. *Chem. Commun.* **2009**, 1775–1777.
(219) Suzuki, T.; Okazaki, K.; Kiyama, T.; Kuwabata, S.; Torimoto, T. *Electrochemistry* **2009**, *77*, 636–638.
(220) Zhu, J. M.; Shen, Y. H.; Xie, A. J.; Qiu, L. G.; Zhang, Q.; Zhang, S. Y. *J. Phys. Chem. C* **2007**, *111*, 7629–7633.
(221) Brettholle, M.; Höfft, O.; Klarhofer, L.; Mathes, S.; Maus-Friedrichs, W.; El Abedin, S. Z.; Krischok, S.; Janek, J.; Endres, F. *Phys. Chem. Chem. Phys.* **2010**, *12*, 1750–1755.

(222) Sugimoto, T.; Kikuta, M.; Ishiko, E.; Kono, M.; Ishikawa, M. *J. Power Sources* **2008**, *183*, 436–440.
(223) Mistry, M. K.; Subianto, S.; Choudhury, N. R.; Dutta, N. K. *Langmuir* **2009**, *25*, 9240–9251.
(224) Mu, Z. G.; Wang, X. X.; Zhang, S. X.; Liang, Y. M.; Bao, M.; Liu, W. M. *J. Tribol.—Trans. ASME* **2008**, *130*, 034501.
(225) Wang, H. Z.; Lu, Q. M.; Ye, C. F.; Liu, W. M.; Cui, Z. J. *Wear* **2004**, *256*, 44–48.
(226) Liu, X. Q.; Zhou, F.; Liang, Y. M.; Liu, W. M. *Wear* **2006**, *261*, 1174–1179.
(227) Xia, Y. Q.; Sasaki, S.; Murakami, T.; Nakano, M.; Shi, L.; Wang, H. Z. *Wear* **2007**, *262*, 765–771.
(228) Minami, I.; Kita, M.; Kubo, T.; Nanao, H.; Mori, S. *Tribol. Lett.* **2008**, *30*, 215–223.
(229) Suzuki, A.; Shinka, Y.; Masuko, M. *Tribol. Lett.* **2007**, *27*, 307–313.
(230) Weng, L. J.; Liu, X. Q.; Liang, Y. M.; Xue, Q. J. *Tribol. Lett.* **2007**, *26*, 11–17.
(231) Lu, R. G.; Mori, S.; Kobayashi, K.; Nanao, H. *Appl. Surf. Sci.* **2009**, *255*, 8965–8971.
(232) Phillips, B. S.; John, G.; Zabinski, J. S. *Tribol. Lett.* **2007**, *26*, 85–91.
(233) Mu, Z. G.; Zhou, F.; Zhang, S. X.; Liang, Y. M.; Liu, W. M. *Tribol. Int.* **2005**, *38*, 725–731.
(234) Bermúdez, M. D.; Jiménez, A. E.; Martinez-Nicolas, G. *Appl. Surf. Sci.* **2007**, *253*, 7295–7302.
(235) Jiménez, A. E.; Bermúdez, M. D. *Tribol. Lett.* **2007**, *26*, 53–60.
(236) Jiménez, A. E.; Bermúdez, M. D. *Wear* **2008**, *265*, 787–798.
(237) Jiménez, A. E.; Bermúdez, M. D. *Tribol. Lett.* **2009**, *33*, 111–126.
(238) Jiménez, A. E.; Bermúdez, M. D.; Carrión, F. J.; Martinez-Nicolas, G. *Wear* **2006**, *261*, 347–359.
(239) Jimenez, A. E.; Bermudez, M. D.; Iglesias, P.; Carrion, F. J.; Martinez-Nicolas, G. *Wear* **2006**, *260*, 766–782.
(240) Patton, S. T.; Voevodin, A. A.; Vaia, R. A.; Pender, M.; Dianianti, S. J.; Phillips, B. *J. Microelectromech. Syst.* **2008**, *17*, 741–746.
(241) Phillips, B. S.; Zabinski, J. S. *Tribol. Lett.* **2004**, *17*, 533–541.
(242) Mo, Y. F.; Yu, B.; Zhao, W. J.; Bai, M. W. *Appl. Surf. Sci.* **2008**, *255*, 2276–2283.
(243) Zhu, M.; Yan, J.; Mo, Y.; Bai, M. *Tribol. Lett.* **2008**, *29*, 177–183.
(244) Kondo, H. *Tribol. Lett.* **2008**, *31*, 211–218.

CR100114T